Re-expression of MeCP2 in early adulthood recovers cortical function in Rett syndrome

Re-expression of MeCP2 in early adulthood recovers cortical function in Rett syndrome

A dissertation presented

by

Alex Joseph Simon

to

The Division of Medical Sciences

in partial fulfillment of the requirements

for the degree of

Doctor of Philosophy

in the subject of

Neurobiology

Harvard University

Cambridge, Massachusetts

August 2016

Dissertation Advisor: Dr. Michela Fagiolini Alex Joseph Simon

Re-expression of MeCP2

in early adulthood recovers cortical function in Rett syndrome

Abstract

Impacting 1 in 10,000 girls, Rett syndrome (RTT) is caused by *de novo* mutations in the X chromosome gene, *MECP2*. Girls with RTT initially appear normal and reach developmental milestones in their first 6 months; nevertheless, they soon succumb to a symptomatic regression defined by a loss of motor, cognitive, social, and language skills and the onset of epilepsy. No cure exists.

Remarkably, the re-expression of MeCP2 in adult *Mecp2*-mutant mice is sufficient to reverse motor and respiratory phenotypes, which provides hope for future interventions in RTT patients. One question that remains unanswered is whether abnormalities in sensory information processing—an essential component of language, emotion and cognition—are amenable to rescue in adulthood, and if so, to what degree. Distinctively, sensory circuits are most amenable to modification in early stages of development, rather than in adulthood.

Using the visual system as a model, we tested whether the lateral geniculate nucleus (LGN) and visual cortex (V1) were sensitive to both the loss and re-expression of MeCP2 in early adulthood. We found that post-natal deletion of MeCP2 disrupted

excitatory neuronal function in the cortex, but did not perturb inhibitory interneuron connectivity in V1 nor anatomical wiring of the retinogeniculate synapse. Re-expression of MeCP2 in early adulthood permitted the recovery of pyramidal neuron function and visually evoked potential responses; yet, it failed to fully rescue all pre-existing deficits in cortex.

Although cortical RTT phenotypes were not completely reversed, our results suggest that re-expressing MeCP2 in early adulthood significantly ameliorates the condition and function of abnormally wired cortical circuits. Consequently, with regards to future Rett syndrome therapeutics, we are optimistic about the possibility for some degree of recovery in sensory processing after patients have undergone regression.

Table of Contents

Acknowledgements

Without question, there's no "I" in PhD. My graduate school experience has been immeasurably enriched and enabled by the stellar members (past and present) of the Fagiolini and Hensch labs. Additionally, I was beyond fortunate to collaborate with two dynamic PIs outside of my lab: Judith Steen and Chinfei Chen. I would like to thank my dissertation advisory committee members, Tom Schwarz, Mark Andermann and Bernardo Sabatini for providing guidance throughout the last few years. Moreover, a special thank you to my dissertation exam committee members, David Ginty, Mustafa Sahin, James Eubanks, and Bernardo Sabatini for offering their feedback as I finish my thesis.

I'm much obliged to Janis Lochner at Lewis & Clark College for transforming me from a college student into a student researcher. I'd like to offer a tremendous thank you to my loving, supportive family: Joan Byer, Larry Simon, Casey Simon, and Kevin Katz. Honestly, this would have been impossible without y'all. Serving as a fount of encouragement, love, and cucumber seltzer, my partner Margot Raicek is worthy of my unending gratitude.

Finally, I must graciously thank my exemplary mentor and friend, Michela Fagiolini—I never thought it possible to feel so completely at home in a research laboratory.

Chapter 1

Introduction

Rett syndrome: from humans to mice

Rett syndrome (RTT), a debilitating neurodevelopmental disorder, is the second most common cause of severe intellectual disability. Predominately affecting young girls, RTT arises in approximately 1 in 10,000 live female births (Neul et al., 2010). The first comprehensive report of patients with this disorder characterized the distinct temporal stages of its progression: (1) normal neurological and mental development during the first 6 to 18 months of life; (2) stagnation of developmental acquisitions after this period; (3) rapid deterioration of behavioral and mental status; (4) a protracted period with a relatively stable status (Hagberg et al., 1983). The life expectancy of RTT patients is estimated to be 55 years, meaning that most patients will spend their lives in this final stage until they die, most often of cardiorespiratory failure (Coppus, 2013; Tarquinio et al., 2015).

When the development of these girls stagnates during infancy, they cease to meet major milestones related to word development, social interaction, and motor function (Hagberg, 2005). During the phase of rapid deterioration, patients lose the previously gained abilities of speaking words, walking, or pulling to a stand. Stereotypic motor patterns of hand wringing or teeth grinding begin to emerge, along with respiratory abnormalities such as apneas and hyperventilation, particularly while awake (Lombardi et al., 2015). As the patients move through childhood they develop compounding issues with muscle tone, scoliosis, sleep patterns, and often epilepsy

(Nomura and Segawa, 2005). They also begin to express many features of characteristic of autism spectrum disorders (Amir et al., 1999). Once in adulthood, symptoms stabilize, rendering RTT women in a state of profound physical and intellectual disability (Nomura and Segawa, 2005). Unable to move independently, feed themselves, or communicate effectively, adult patients are completely dependent on the support of their parents or other caregivers.

Through the post-mortem examination of RTT brains, doctors and researchers have identified numerous anatomical and cellular abnormalities attributable to the disorder. The undersized brains of patients exhibit reduced white-matter volume throughout and substantial decreases in cortical gray-matter volume, which corresponds with reduced cortical thickness and enlarged ventricles (Jellinger et al., 1988; Subramaniam et al., 1997). Cortical neurons themselves are reduced in size, and present with less dendritic branching and fewer dendritic spines (Armstrong, 2005; Bauman et al., 1995). Yet, RTT brains do not experience neuronal migration deficits nor do they show evidence of cell loss or atrophy (Neul and Zoghbi, 2004).

Notably, Rett syndrome patients are nearly 100% female, which prompted the early hypothesis that the disorder was engendered by a dominant X-linked mutation (Hagberg et al., 1983). By performing a systematic mutational analysis on genomic DNA from 29 RTT patients, Dr. Zoghbi and colleagues discovered that Rett syndrome was associated with the gene encoding methyl-CpG binding protein 2 (*MECP2*) (Amir

et al., 1999). In fact, 95% of diagnosed RTT patients have mutations in the *MECP2* gene (Neul et al., 2008). Although a handful of familial examples have been observed, 99% of RTT patients acquire *MECP2* mutations *de novo*, often from C to T transitions at CpG dinucleotides (Chahrour and Zoghbi, 2007; Wan et al., 1999).

While the 53 kDa MeCP2 protein is expressed ubiquitously, it is especially abundant in the brain where it was first understood to mediate transcriptional repression and chromatin remodeling (Lewis et al., 1992; Meehan et al., 1992). In neuronal nuclei, MeCP2 is nearly as abundant as the histone octamer, and through its DNA-binding domain (MBD), it binds globally to methylated DNA sites that contain 5-methylcytosine-adenine (mCA) and 5-methylcytosine-guanine (mCG) sequences (Kinde et al., 2015; Skene et al., 2010). DNA methylation is a modification strongly linked to gene silencing (Nan et al., 1997). Both mCA and mCG are widely distributed throughout the genome, but are absent at the CpG islands that flank the promoter region of most genes (Deaton and Bird, 2011). Correspondingly, MeCP2 binds uniformly to all regions of the brain genome, except for CpG islands (Chen et al., 2015), Further emphasizing MeCP2's relationship to gene repression, it interacts with SIN3A, a co-repressor complex that contains chromatin-compacting histone deacetylases (Jones et al., 1998; Nan et al., 1998).

The capability for MeCP2 to bind DNA is paramount to its function, as mutations in the MBD elicit the phenotypes of Rett syndrome (Fig. 1.1) (Ballestar et al., 2000).

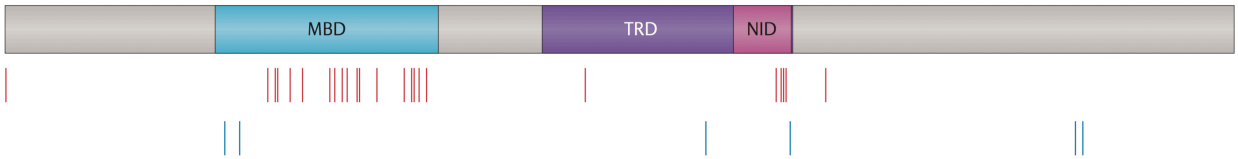

Figure 1.1 – MeCP2's functional domains and sites of mutation

MeCP2 has two key domains: the methyl-CpG-binding domain (MBD) and the transcriptional repression domain (TRD), which contains the NCOR–SMRT interaction domain (NID).

Plotted in red, missense mutations causing Rett syndrome highlight the importance of the MBD and the TRD for protein function.

Plotted in blue are MeCP2's phosphorylation sites, which respond to neuronal activity.

Adapted by permission from Macmillan Publishers Limited: Nature Vol. 16 (2015)

Similarly, mutations in another domain of MeCP2, the transcriptional repression domain (TRD), also lead to RTT. The TRD, which contains the NCOR-SMRT interaction domain (NID), binds two critical co-repressor complexes, NCOR (nuclear receptor co-repressor) and SMRT (silencing mediator of retinoic acid and thyroid hormone receptor) (Lyst et al., 2013). The import of the MBD and TRD for proper function is evident, since the vast majority of missense mutations that cause RTT occur in these regions (Lyst and Bird, 2015). One common human RTT missense mutation located in the TRD/NID, R306C, obstructs the phosphorylation of T308, which in turn disrupts the activity-dependent regulation of MeCP2 with the NCoR complex (Ebert et al., 2013). Truncation mutations of MeCP2 can result in a gradation of symptomatic severity depending on how early they appear in the gene. Truncating mutations located at R270X and before disrupt the TRD, and are thus associated with worse outcomes. Mutations at R294X or more C-terminal–truncating mutations largely spare the TRD and NID, resulting in milder RTT symptoms (Lombardi et al., 2015).

Although traditionally viewed as transcriptional repressor, recent studies have identified alternative biological functions for MeCP2. For example, MeCP2 can behave like a transcriptional activator by recruiting cyclic AMP-responsive element-binding protein 1 (CREB1) to gene promoters (Chahrour et al., 2008). Furthermore, MeCP2 has been implicated in alternative splicing through its interactions with the transcription factor YB1, and also with microRNA processing by preventing the formation of the

Drosha-DGCR8 complex (Cheng et al., 2014; Young et al., 2005). Thus, in the absence of MeCP2, RNA transcript levels are significantly disrupted; however, this occurs in a brain region-specific manner, while the global gene expression landscape remains unchanged (Zhao et al., 2013).

The diverse modes of MeCP2 function aren't solely limited to neuronal cells. *In vitro* co-culture experiments have illuminated the non-cell autonomous influence that MeCP2-deficient glia exert on dendritic morphology (Ballas et al., 2009). Moreover, astrocytic expression of MeCP2 in an otherwise *Mecp2*-null mouse can effectively rescue breathing abnormalities and increase life expectancy (Lioy et al., 2011). The employ of RTT mouse models such as these have allowed researchers to gain remarkable insights into the etiology of the disorder.

To be accepted as a legitimate reproduction of a disease, mouse models must fulfill certain conditions. The first of these is 'predictive validity,' which concerns whether one can make predictions on the human model based upon the mouse model's performance. The criterion, 'construct validity,' pertains to how similar the creation of the mouse model is compared to the origins of the human disorder. Lastly, 'face validity,' measures the likeness of the mouse model's behavior to the symptoms of the human condition.

The earliest and most essential Rett syndrome mouse model was created in 2001 in the lab of Adrian Bird. Their construct resulted in deletion of everything but the

first 8 amino acids of MeCP2, thus representing the most severe form of the disease: a truncation of both the MBD and TRD (Guy et al., 2001). The *Mecp2*-null mouse demonstrated excellent face validity; the mice experienced normal development, followed by an early post-natal regression. Furthermore, like human patients, *Mecp2*-null mice exhibited motor deficits, breathing abnormalities, limb clasping, shortened lifespans, lower brain weight, and reduced cortical thickness (Guy et al., 2001). In the years since this mouse became widely available, it's predictive validity has been substantiated by several reports from translational neuroscience labs.

Notably, the *Mecp2*-null mouse is male, whereas human RTT patients are female. Unlike their human counterparts, *Mecp2*-null mice survive for ~10 weeks, during which they undergo a repeatable, stereotyped development of Rett syndrome phenotypes. Although female mice heterozygous for *Mecp2* more closely approximate the genetics of the human disorder, these mice develop symptoms slowly and with significant variability over 3-6 months, thereby multiplying difficulties for experimental design (Guy et al., 2001). Nevertheless, to justify any type of experimental translation into human patients, consistent results must be confirmed in both *Mecp2*-null males and *Mecp2*-het females.

Rett syndrome researchers have progressed from merely replicating the human condition to creating scores of experimental mouse models with the intent to elucidate the circuits and cells responsible for the phenotypes of the MeCP2-deficient brain.

With Cre-mediated genetic tools, *Mecp2* can be conditionally expressed or deleted from certain regions of the brain or from particular classes of neuronal subtypes. Moreover, temporal control over *Mecp2* expression or deletion can be achieved by using a tamoxifen-based Cre system (Calfa et al., 2011; Guy et al., 2007).

Rett syndrome impairs cortical circuits and synapses

Rett syndrome symptoms are not outwardly apparent until the initial phase of normal development has passed; however, abnormalities in MeCP2-deficient neurons and circuits begin quite early in the postnatal stages of life. For instance, *Mecp2*-null cortices at embryonic day 15 (E15) display a transcriptional deregulation of numerous glutamatergic receptors and ionic channels. Furthermore, when primary cultures are established with *Mecp2*-null E15.5 neurons, morphological defects are apparent by 3 days *in vitro* (Bedogni et al., 2015).

Widespread disruptions of synaptic structure and function become readily apparent after RTT mice are weaned. An overarching mechanism for these issues may be explained by MeCP2's bias towards repressing long genes (Gabel et al., 2015; Sugino et al., 2014). Importantly, genes that encode molecules involved in neuronal connectivity are disproportionally longer than others. Accordingly, in *Mecp2*-null mice, RNA transcripts for cell adhesion and cell-cell signaling molecules are significantly overrepresented (Sugino et al., 2014). This synaptic dysregulation in part gives rise to

impairments in cellular long-term plasticity, widely considered to be a major mechanism underlying learning and memory (Asaka et al., 2006; Dani and Nelson, 2009; Lonetti et al., 2010).

These synaptic abnormalities give rise to inappropriate shifts in excitatory and inhibitory (E/I) balance across multiple brain regions, which in part explains the 70% rate of recurrent seizures in RTT patients (Cardoza et al., 2011; Dani and Nelson, 2009; Kron et al., 2012; Shepherd and Katz, 2011). Cortical circuits in somatosensory, visual, motor-frontal, and medial frontal regions all exhibit reduced excitation and/or increased inhibition (Katz et al., 2016). In contrast, brainstem structures such as the nucleus solitarius and rostral ventrolateral medulla are shifted towards hyperexcitability (Medrihan et al., 2008). *In vitro*, MeCP2-deficient mice form weaker glutamatergic synapses and exhibit depressed GABAergic synaptic transmission (Chao et al., 2007; Medrihan et al., 2008). Additionally, when MeCP2 is selectively knocked out from 90% of GABAergic neurons, mice recapitulate definitive Rett syndrome phenotypes, such as respiratory arrhythmias, motor deficits, and social interaction irregularities (Chao et al., 2010).

The visual system

In humans as in mice, proper development of the visual systems necessitates a precise balance between excitation and inhibition. To function normally, this sensory

system must balance activity arising from internal cues, as well as activity that originates from external visual stimulation. Between P0 and P8—a week before eye opening—retinal ganglion cells form connections to relay neurons in the lateral geniculate nucleus (LGN). Although the LGN receives both contralateral and ipsilateral innervation from the retina, these inputs are anatomically split into eye-specific layers (Muir-Robinson et al., 2002). The initial process of eye specific segregation, as well as the synaptic strengthening and remodeling of retinogeniculate inputs from P5-P20, is driven by spontaneous activity in the form of cholinergic retinal waves—not from vision (Chen and Regehr, 2000; Hooks and Chen, 2006; Penn et al., 1998).

Neurons from the retina project their axons on to neighboring neurons in the lateral geniculate nucleus (LGN), which then project to neighboring targets in primary visual cortex (V1) (Fig. 1.2). This connectivity prefigures a topographic map that ensures that the receptive fields of V1 neurons represent a specific locations in visual space (Espinosa and Stryker, 2012). Similarly experience-independent, this process of topographic map formation is controlled by cortical EphA-ephrin-A signaling plus spontaneous waves of neuronal activity (Feldheim and O'Leary, 2010).

The inputs that cortical neurons receive from the LGN provides them the means to exhibit receptive field properties, such as orientation selectivity. In cortical layer 4, neurons known as 'simple cells' receive direct inputs from the LGN. These simple cells

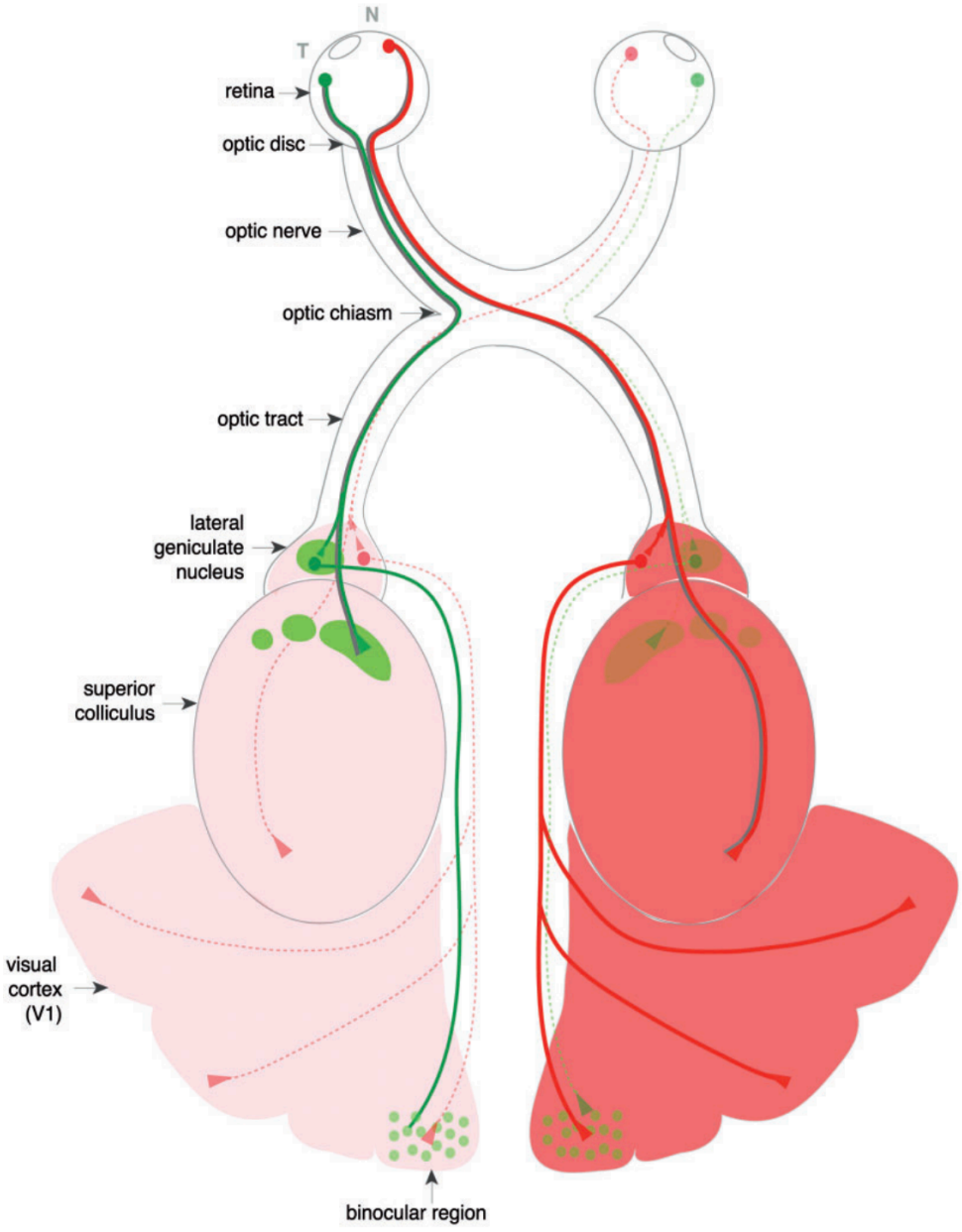

Figure 1.2 – Schematic representation of the mouse visual system

Adapted by permission from SAGE Publications: ASN Neuro Vol. 6 (2014)

respond strongly when visually stimulated with lines or bars of a particular orientation, but not to the orthogonal orientation. Hubel and Wiesel proposed a "feed-forward" model, which theorized that orientation selectivity in a V1 simple cell arose from a linear summation of inputs from ON-center and OFF-center cells in the LGN (Hubel and Wiesel, 1962). In recent years, however, studies have found populations of LGN neurons in mice that are themselves orientation selective (Piscopo et al., 2013; X. Zhao et al., 2013). These orientation selective relay neurons most often project to superficial cortical layers—rather than layer 4—suggesting that they play a modulatory role, but not a primary one (Cruz-Martín et al., 2014; Kondo and Ohki, 2015; Niell, 2015).

In the three weeks that follow eye-opening (~P12-P33), the visual system, which has heretofore been effectively wiring without external stimulation, becomes both sensitive to and reliant on visual activity from the outside world. Indeed, rearing mice in the dark interferes with the normal postnatal maturation of visual cortical functions (Fagiolini et al., 1994; Kang et al., 2013). In order for visual development to proceed without negative consequences, visual stimulation must be present during this sensitive time known as a 'critical period.' In humans for example, binocular vision compromised by a cataract or strabismus will result in permanent loss of the affected eye's acuity if treatment is not provided during early childhood (Mitchell and Mackinnon, 2002).

Disturbances that occur during critical periods can result in negative outcomes for both cortical and sub-cortical visual systems. In the LGN, visual deprivation during

the critical period evokes a disruption in retinogeniculate synaptic connectivity (Hooks and Chen, 2008). Furthermore, mice who've been chronically dark reared are unable to maintain retinocollicular projections (Carrasco et al., 2005). In cortex, depriving visual experience from one eye (monocular deprivation) during the critical period permanently blocks the binocular matching of orientation preference when the mice are adults (Wang et al., 2010). Furthermore, in ferrets, dark rearing impairs the development of direction selectivity, which cannot be re-established with re-exposure to vision after the critical period (Li et al., 2008). These examples illustrate how visual system disruptions during the critical period can result in A) insufficient maintenance of previously wired circuits and B) irreversible impairments of cortical receptive field properties.

Importantly, sensory critical periods like those of the visual system are followed in a hierarchical manner by critical periods for language and social skills (Hensch, 2004). Thus, early perturbations during the visual critical period could portend far-ranging issues with more advanced sensory and social features, such as those observed in Rett syndrome.

In animal models of RTT, numerous deficits in sensory processing, including vision, have been described in the literature. Emphasizing MeCP2's important contribution to sensory function in vertebrates, knocking out the gene from a zebrafish stunts the growth of sensory neuron axons and reduces their response rate to tactile

stimulation (Leong et al., 2015). In mice, conditional deletion of *Mecp2* from peripheral somatosensory neurons evokes not just an aberrant sensitivity to touch, but also social interaction deficits and anxiety-like behaviors (Orefice et al., 2016). In the auditory system, *Mecp2*-het mice implanted with EEGs express latency abnormalities with auditory event-related potentials (ERPs) (Liao et al., 2012). The auditory ERP of the *Mecp2*$^{T158A/y}$ mouse model also displays impaired phase locking, which is considered to reflect the reliability and sensitivity of communications between neural circuits (Goffin et al., 2011; Winterer et al., 2000). For these reasons, many researchers have proposed the ERP waveform as a biomarker for Rett syndrome onset, as well as a target for assessing the efficacy of clinical therapeutics (Pozzo-Miller et al., 2015). Indeed in both mice and humans, the degree to which the visually evoked potential (VEP) waveform is disrupted correlates with the severity of disease as a whole (LeBlanc et al., 2015).

In RTT mouse models, cortical sensory systems exemplify the E/I imbalance characteristic of the disorder. To begin, *Mecp2*-null mice exhibit dramatically reduced visual acuity, hypoactive V1 activity, and decreased neuronal response reliability in visual cortex (Durand et al., 2012; Patrizi et al., 2015). Anatomically in V1, *Mecp2*-null mice experience a precocious maturation and hyper-function of inhibitory parvalbumin+ (PV) GABAergic interneurons (Durand et al., 2012; Krishnan et al., 2015). At P15, PV cells are hyper-connected, displaying an increased number of PV-positive boutons on pyramidal cells (Durand et al., 2012). By P30, PV mRNA and protein

expression is up-regulated (Cheng et al., 2014; Krishnan et al., 2015). *In vitro* voltage-sensitive dye imaging detects the functional consequences of this PV hyper-function: enhanced inhibitory gating in layer 4, which reduces spatial propagation of activity to layer 2/3 (Durand et al., 2012; Griffen et al., 2012).

Sub-cortically, in *Mecp2*-null males, retinal inputs from each eye segregate into eye-specific layers in early development, but as the health of the mouse deteriorates, the inputs erroneously de-segregate (Fig. 1.3a) (Noutel et al., 2011). Optomotor visual acuity, which is mediated by the LGN and superior colliculus, regresses as well (Fig. 1.3b) (Durand et al., 2012).

The assorted cortical and sub-cortical regions where these visual phenotypes localize demonstrate variable degrees of plasticity depending on their intrinsic properties and stage of development. Understanding the potential for their re-wiring and repair is paramount for generating effective therapeutic strategies for Rett syndrome.

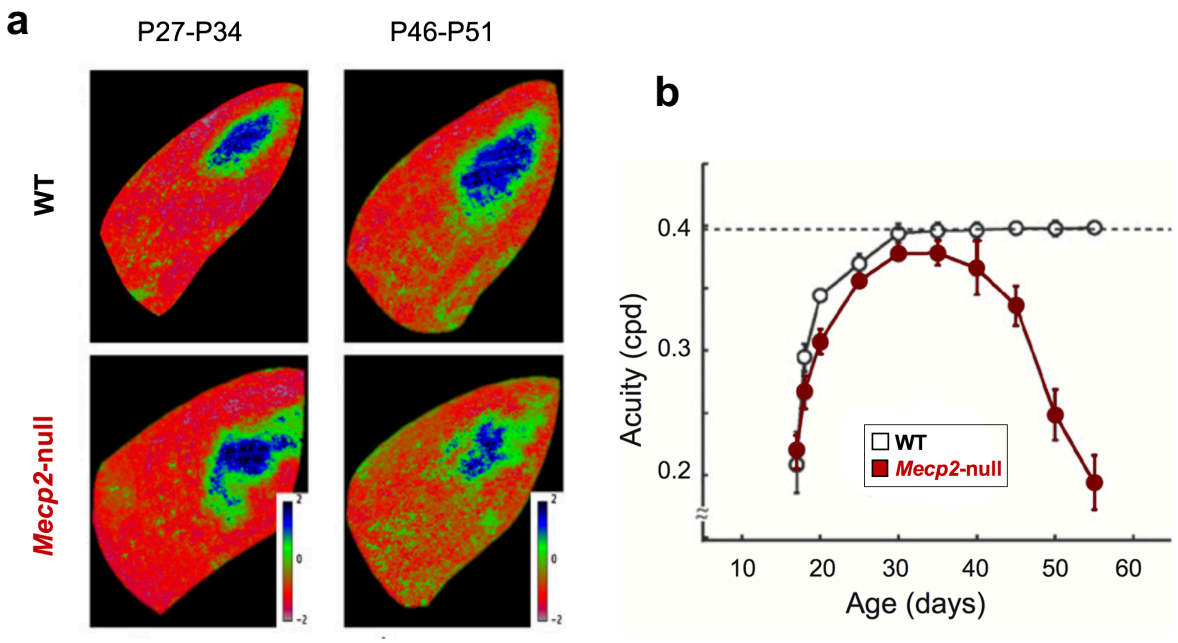

Figure 1.3 – Sub-cortical deficits in the *Mecp2*-null visual system

a. Abnormalities in eye-specific segregation are detectable after P34. Eye-specific segregation is shown in WT and *Mecp2*-null mice at P27–P34 (left) and P46–P51 (right). Images show pseudocolored R values where contradominant and ipsidominant pixels are red and blue, respectively (see pseudocolor scale). The significantly increased overlap of contralateral and ipsilateral inputs in the bottom right image reports that eye-specific layers de-segregate in P50 *Mecp2*-null mice.

b. As measured by a behavioral optomotor task, visual acuity emerges normally but then drastically regresses after 40 days of age in *Mecp2*-null mice.

Adapted by permission from Elsevier: Neuron Vol. 70 (2011) and Elsevier: Neuron Vol. 76 (2012).

Chapter 2

Methods

Mice

All procedures were approved by the Boston Children's Hospital Institutional Animal Care and Use Committee. Animals were housed on a 12-hour light/dark cycle with food and water available *ad libitum*. Both *Mecp2*-null and *Mecp2*$^{lox/y}$ mice were generated by A. Bird and colleagues (Guy et al., 2001). *Mecp2*$^{stop/y}$ mice were generated by R. Jaenisch and colleagues (Guy et al., 2007). The Cre-ER mouse, whose Cre is activated by tamoxifen was developed by S. Hayashi and A.P. McMahon (Hayashi and McMahon, 2002). 2mg of 20mg/mL tamoxifen in corn oil solution was delivered per injection, i.p. as performed previously (Guy et al., 2007). To conditionally express MeCP2 in parvalbumin positive neurons, we used either an IRES-PV-Cre mouse (Hippenmeyer et al., 2005) or a 2A-PV-Cre mouse (Madisen et al., 2010). All mouse lines were on a c57bl/6 background. Experimenters were blind to genotype and the animal's previously recorded behavioral analyses. Only male animals were used and control animals were age-matched littermates of mutant mice.

Genotyping

All mice were genotyped prior to weaning using *Mecp2*$^{stop/y}$ and *Mecp2*$^{lox/y}$ primers as well as primers specific for each Cre line. After use in experiments, tail clippings were taken from each mouse and stored at -20°C. In Cre lines, undesired germline recombination is known to occur. In a conditional deletion or re-expression strategy,

recombination in the testis must be avoided since it could result in the complete global knockout or re-expression of the gene (Kobayashi and Hensch, 2013). Thus, we semi-annually checked our Cre lines to ensure that our conditional manipulations remained constant. By probing for the MeCP2 protein with immunohistochemistry, these mice were anatomically analyzed to confirm their genotype.

Western blot

Protein lysates were prepared in RIPA buffer and equal amounts of total protein—as measured by NanoDrop—were loaded onto 10% SDS-polyacrylamide gels. After electrophoresis, gels were electro-transferred onto nitrocellulose membranes and incubated overnight at 4°C with primary antibodies. Blots were incubated for 1 hour with secondary antibodies conjugated with horseradish peroxidase (HRP) to develop chemiluminescent bands. Fluorescent signal was detected by photographic film and analyzed by densitometry with Fiji. For primary antibodies, we used a rabbit polyclonal antibody directed to the C-terminal of MeCP2 (EMD Millipore 07-013, 1:500), a mouse antibody to GAPDH (Abcam ab8245, 1:20000), a rabbit antibody to NR2A (Frontier Scientific GluRe1C-Rb-Af542, 1:1000), a rabbit antibody to NR2B (Abcam ab65783 1:1000), and rabbit antibodies to NR2B-pS1303, NR2B-pY1472, and NR2B-pS1480 (Abcam ab81271, Abcam ab3856, PhosphoSolutions p1516-1480; all 1:1000). For

secondary antibodies, we used goat anti-mouse IgG (HRP) and goat anti-rabbit IgG (HRP) (Abcam).

Immunofluorescence

Mice were transcardially perfused with saline, followed by 45 mL of phosphate-buffered 4% paraformaldehyde solution. Brains were extracted, post-fixed for two hours in the same fixative, cryoprotected in ascending sucrose solution (20% and 30%), and sectioned with a cryostat. Cryosections were first incubated for 30 minutes at room temperature in blocking solution (10% normal goat serum, 0.5% Triton X-100 (Sigma) in PBS), then transferred into primary antibody solution for overnight RT incubation (3% normal goat serum, 0.5% Triton X-100, rabbit anti-MeCP2 (M. Greenberg Lab, 1:2000 dilution), guinea pig anti-parvalbumin (Frontier Institute, 1:1000 dilution). After rinsing in washing buffer (0.1% Triton X-100 in PBS), the sections were incubated for one hour at room temperature in secondary antibody solution (3% normal goat serum, 0.5% Triton-X, goat anti-rabbit Alexa 647 (Invitrogen, 1:800 dilution) and goat anti-guinea pig Alexa 594 (Invitrogen, 1:500 dilution) in PBS). Sections were again washed in three 15-minute rounds of washing buffer, and mounted on glass slides with DAPI Fluoromount-G mounting medium (Southern Biotech).

Confocal microscopy

Brain sections were analyzed with a laser scanning confocal microscope (Olympus FluoView, FV1000), using the multi-channel acquisition mode to avoid fluorescence cross-talk. Quantitative analyses were performed on a minimum of three to five mice per genotype. The binocular zone of visual cortex across all layers and the lateral geniculate nucleus were analyzed in 3 coronal sections at corresponding anterior-posterior, medial-lateral coordinates. In addition, *in vivo* electrophysiological recordings confirmed the histological identification of binocular region of primary visual cortex. For parvalbumin and MeCP2 intensity analysis, 1024x1024 fields of primary visual cortex were imaged using a 20X objective (0.75 numerical aperture). The mean pixel intensity of the parvalbumin or MeCP2 signal in the cell bodies was measured. For MeCP2 intensity measurements, 100 cell bodies were analyzed at random per slice.

Presynaptic parvalbumin innervation on pyramidal neurons

The PV presynaptic structures were analyzed on images acquired with an 100X oil-immersion objective (1.4 numerical aperture) and the pinhole set at 1 Airy unit. The number of perisomatic synapses was determined on images by triple staining for parvalbumin, GAD65 and DAPI. Presynaptic innervation on pyramidal neurons was analyzed using Fiji. Pyramidal neurons were identified and traced on DAPI channel by their typical morphology (triangular shaped cell body).

Single-cell electrophysiology *in vivo*

Electrophysiological recordings were performed under Nembutal (50mg/kg, i.p.) anesthesia and chlorprothixene (0.2 mg, i.m.) using standard techniques (Durand et al., 2012). If necessary, anesthesia was maintained with ≤ 0.5% isoflurane. To ensure consistent anesthesia between animals, heart rate and oxygen saturation were actively monitored during recordings using a pulse oximeter (MouseOx, Starr Life Sciences Corp.). Heart rates measured immediately before recording did not differ between P30 WT (n=6) and P30 *Mecp2*$^{stop/y}$ (n=7) mice (344 ± 18 bpm vs. 356 ± 46 bpm). Single-unit responses were recorded using multichannel probes (a1x16-3mm50-177, Neuronexus Technologies). The signal was amplified, thresholded and discriminated (SortClient, Plexon Technologies).

For each V1 recording: 5-8 single units were recorded in each of 3 to 5 penetrations spaced evenly (> 200μm intervals) across the medio-lateral extent of binocular primary visual cortex. Spontaneous and evoked activities were recorded in response to full-screen, high contrast low spatial frequency sine wave gratings (100% contrast, 0.03 cpd, 2 Hz) presented on a CRT computer monitor (mean luminance = 32 cd/m^2). Twelve different orientations varying between 0° - 360° (12 steps - 30° spacing) were presented in random order (3 seconds each). A uniform gray screen of intermediate luminance was interleaved to monitor spontaneous activity (3 seconds each).

For each LGN recording: 4–8 single units were recorded in 4 penetrations spaced evenly (> 200μm intervals) across the anterior-posterior extent of the LGN. Activities were recorded in response to high contrast low spatial frequency sine wave gratings (100% contrast, 0.03 cpd, 3.2 Hz) presented on a CRT computer monitor (mean luminance = 32 cd/m^2). Eight different orientations varying between 0° - 360° (8 steps - 45° spacing) were presented in random order (3 seconds each). A uniform gray screen of intermediate luminance was interleaved to monitor spontaneous activity (3 seconds each).

Analysis of *in vivo* recordings

Response firing rate to each orientation was averaged over 10 trials. Spontaneous activity was averaged over 10 random repeats of the gray screen and the maximum evoked response was taken as the preferred visual stimulus. Neurons were not selected for analysis if <100 spike waveforms were measured during a stimulation trial. To ensure single-unit isolation, the waveforms of recorded units were further examined offline (Offline Sorter, Plexon Technologies) and discriminated on the basis of their individual characteristics. Single-units were classified as narrow (putative inhibitory cells) and broad-spiking (putative excitatory cells) based on shape properties of their average waveforms. Two parameters were used for discrimination: the ratio of the height of the positive peak to the initial negative trough and the time from the initial

trough minimum to the following peak maximum (Niell and Stryker, 2008). These two parameters were sufficient to distinguish the two groups of waveforms. Spike clusters were separated from noise using K-means clustering and principal component analysis with the Offline Sorter.

Excitatory spikes were analyzed in MATLAB using sigTOOL (Lidierth, 2009). A neuron was considered to be visually driven if a Mann-Whitney U Test determined that cell's visually evoked activity was significantly above the level of spontaneous activity. Firing properties of neurons of WT mice ± tamoxifen, and Cre-ER mice ± tamoxifen were not statistically different and combined into a WT group. Coefficient of variation (the neuronal response variability to the preferred orientation) was calculated according to a previous study (Ko et al., 2013). The preferred orientation was determined as the one giving the maximum response (R_{max}). The orientation selectivity index (OSI) was calculated as $(R_{max} - R_{orth}) / (R_{max} + R_{orth})$, where R_{orth} was the mean response of the two orientations orthogonal to the preferred orientation. OSI was calculated without subtracting spontaneous activity.

Visually evoked potentials

Visually evoked potentials (VEPs) were recorded from anesthetized mice with Nembutal (50mg/kg i.p.) and chlorprothixene (0.2mg i.m.) using standard techniques described

previously (Durand et al., 2012). The contralateral eye of the mouse was presented with horizontal black and white sinusoidal bars that alternated contrast (100%) at 2Hz. A tungsten electrode was inserted into the binocular visual cortex at 2.8mm from the midline where the visual receptive field was approximately 2.8mm from the vertical meridian. VEPs were recorded by filtering the signal from 0.1 to 100Hz and amplifying 10,000x. VEPs were measured at the cortical depth where the largest amplitude signal was obtained in response to a 0.05 cycles per degree (cpd) stimulus (400–600μm). For each different spatial frequency (SF), 3 to 4 repetitions of 20 trials each were averaged in synchrony with the abrupt contrast reversal. The signal was baseline corrected to the mean voltage of the first 50 milliseconds after stimulus onset. VEP amplitude was calculated by finding the minimum voltage (negative peak) within a 50-150 millisecond time window after stimulus onset. For acuity measurements, VEP amplitude was plotted against the log of the SF, and the threshold of visual acuity was determined by linear extrapolation to 0 μV.

Eye specific segregation

Mice anesthetized with 2% isofluorane were injected with 2–3 μl of a 2% solution of cholera toxin b subunit conjugated with Alexa 488 (Green) or 594 (Red) (Invitrogen) by using a glass pipette and a picospritzer (Picospritzer III, Parker Hannifin Corp.). After 2–4 days, mice were deeply anesthethized with Nembutal (50 mg/kg i.p.) and

transcardially perfused with PBS followed by 4% paraformaldehyde. After post-fixation, 60–70 mm thick coronal sections of the brains were mounted and allowed to absorb the mounting medium before fluorescence imaging. Slices showing the largest projections were used. Generally, 1–3 slices were analyzed per animal. Images were analyzed by using previously described threshold-independent quantitative measures of eye-specific layer segregation (Torborg and Feller, 2004).

LGN slice preparation

Mice were anesthetized with isoflurane, decapitated, and the brain was immediately removed and immersed into an ice-cold cutting solution (in mM: 78.3 NaCl, 23 $NaHCO_3$, 23 glucose, 33.8 choline chloride, 2.3 KCl, 1.1 NaH_2PO_3, 6.4 $MgCl_2$, and 0.45 $CaCl_2$). 250 µm brain slices through the LGN were cut using a sapphire blade (Delaware Diamond Knives). Before electrophysiological recordings, slices were incubated at 31°C for 20 minutes in cutting solution followed by 20 minutes in isotonic saline solution (in mM: 125 NaCl, 25 $NaHCO_3$, 2.5 KCl, 1.25 NaH_2PO_4, 25 glucose, 1 $MgCl_2$, and 2 $CaCl_2$). Oxygenation (95% O_2 / 5% CO_2) was supplied continuously.

LGN electrophysiology

Whole-cell voltage-clamp recordings of LGN neurons were performed at 25°C using patch electrodes of 1.2-2.0 MΩ filled with internal solution (in mM: 35 CsF, 100 CsCl,

10 EGTA, and 10 HEPES, pH adjusted to 7.3 with CsOH) supplemented with D600 0.1mM methoxyverapamil hydrochloride (Sigma-Aldrich) to block voltage-gated calcium channels. A pair of electrodes filled with saline solution were placed in the optic tract in a location that optimized the maximal evoked current. Slices were continuously perfused with oxygenated saline solution to which the $GABA_A$ receptor antagonist, 20 μM bicuculline (Tocris) was added. Evoked quantal events were monitored in the presence of an oxygenated extracellular saline solution containing (in mM): 125 NaCl, 2.5 KCl, 2.6 $NaHCO_3$, 1.25 NaH_2PO_4, 25 glucose, 3 $SrCl_2$, 2 $MgCl_2$ and 20 μM bicuculline, 20 μM CPP).

Quantifying synaptic remodeling measurements of single fiber strength

For minimal stimulation, we stimulated the optic tract using pairs of stimuli separated by a 50 ms inter-stimulus interval and an inter-trial interval of 20 seconds. For each stimulus intensity trial, we examined the synaptic response at a holding potential at -70 mV and at +40 mV. If we obtained a response at one holding potential, but not at another, we repeated the trial again at the same stimulus intensity. If there was failure at both holding potentials, we increased the intensity by 0.25 μA and stimulated again. This continued until we found a stimulus intensity where the smallest possible response for both AMPAR and NMDAR could be reliably evoked.

Fiber fraction ratio

The relative innervation of a given relay neuron by RGCs was estimated using the fiber fraction (FF) method (Hooks and Chen, 2008). FF was calculated as [Σ (SF_i / maximal $response_i$)] / N, where N is the total number of single/maximal response pairs obtained from all recorded cells. When inverted, FF gives a rough estimate of the number of retinal inputs to a LGN neuron.

Phenotypic scoring

Blinded to both genotype and treatment, phenotypic scoring was performed to test for the absence or presence of RTT-like symptoms, including mobility, gait, hindlimb clasping, tremor, breathing, and general condition (Guy et al., 2007).

Accelerating rotarod

Mice were placed on an accelerating rotarod apparatus for 5 trials. During each trial, the rod accelerated linearly from 4 rpm at 0.1 rpm/sec. The amount of time for each mouse to fall from the rod was recorded for each trial and averaged.

Optomotor acuity task

Behavioral threshold acuity was evaluated using the optomotor task (Prusky et al., 2004). In brief, vertical sine wave gratings were projected as a virtual cylinder in three-

dimensional coordinate space on four computer monitors arranged in a quadrangle around a testing arena (OptoMotry, CerebralMechanics). Unrestrained animals were placed on an elevated platform at the epicenter of the arena. The experimenter followed the mouse's head with a crosshair superimposed on the video image to center the rotation of the cylinder at the mouse's viewing position, thereby clamping the spatial frequency of the grating. If the mouse's head tracked the cylinder rotation, it was judged that the animal could see the grating. A process of incrementally changing the spatial frequency of the test grating was repeated until the highest spatial frequency tracked was identified as the threshold. A threshold for each direction of rotation was assessed and the highest spatial frequency tracked in either direction was recorded as the visual acuity. Each session lasted generally 15-20 minutes per mouse. All animals were habituated before the onset of testing by gentle handling and by placing them on the arena platform for a few minutes at a time.

Immunoprecipitation and MS sample preparation

For the immunoprecipitation of NR2A and NR2B, four visual cortices from either WT or *Mecp2*-null male mice were dissected and homogenized via sonication into a RIPA lysis buffer containing 1% protease inhibitor, 1% phosphatase inhibitor 2, and 1% phosphatase inhibitor 3 (all Sigma Aldrich). Following quantification of concentration by

Nanodrop 1000 (ThermoFisher), 3 mg of protein (750 µg from each of the 4 animals) was incubated with Affi-Prep Protein A Support Beads (Biorad) appended to either an NR2A (Frontier Scientific) or NR2B (Abcam) antibody. The bead-antibody-protein complex was loaded and resolved on an SDS-PAGE gel, whereupon the lane was partitioned and excised. The gel pieces were washed, digested overnight with trypsin at 37°C, and eluted into sample buffer (50% acetonitrile / 5% formic acid in water). 4µL of each sample was loaded, in replicate, into a Q Exactive benchtop LC-MS/MS (ThermoFisher).

Spectral counting

Following fragmentation in the mass spectrometer, the mass spectra of peptide fragments were compared against a library. Total spectrum counts were normalized by the top three common contaminants (isoforms of human keratin). Then, the average value from three normalizations was used to represent the protein level. The peptide signal intensity method is based upon a previously published method (Steen et al., 2005). In brief, outlier peptides were removed based on the median relative deviation of all the non-modified peptide signal intensities. The mean intensity of the remaining peptides was used to represent the total protein level.

With spectrum counting, the abundance of NR2A or NR2B peptides was calculated by normalizing the individual peptide signal intensity with the mean intensity. In this way, it was possible to extrapolate the differentially modified peptides of the NR2A and NR2B subunits.

Selected reaction-monitoring (SRM) assay development

A SRM assay was developed to measure the abundance of unmodified peptides using heavy-labeled, purified synthetic versions of each peptide. A spectral library generated in-house through a LC-MS/MS analysis of NR2B IP protein digest and AQUA peptide mixtures previously analyzed on a Q Exactive mass spectrometer guided development and validation of SRM assays for NR2B peptides. For each targeted peptide, the 10 most intense transitions were experimentally tested in SRM mode to select the most suitable transitions for quantification experiments. Samples were analyzed on a hybrid triple quadrupole mass spectrometer (5500 QTrap, AB Sciex) hyphenated to a micro-autosampler AS2 and a nanoflow HPCL pump (both Eksigent), using the trap-elute chip system (cHiPLC nanoflex, Eksigent). Measurements were performed in scheduled SRM mode, using a 30 minute gradient, retention time window of 10 minute and a cycle time of <3.0 seconds, which ensured a dwell time over 10 msec. Data were analyzed with Skyline and for the final SRM assay, the top 5-8 transitions per peptide were retained. For normalization purposes, the four highest abundant unmodified peptides

were monitored (top 4-5 transitions). The final transition list consisted of 236 transitions for NR2B.

SRM measurements and data analysis

Following tryptic in-gel digest, peptides were re-suspended in sample buffer containing heavy isotope labeled peptides (final concentration: 5-50 fmol on column). Measurements were performed on a 5500 QTrap, using a retention time window of 10 minutes and a cycle time of 1 second, ensuring a dwell time of 20 msec. Data were analyzed with Skyline and the top three or four transitions per peptide were used for quantification. Raw data (ratio light-to-heavy) were exported from Skyline and further analyzed using Excel. Values were normalized on the basis of unmodified peptides in order to remove technical variation.

Statistics

Bar graphs are presented as mean ± standard error. Box and whisker plots have whiskers at 10-90 percent. The following parametric tests were used: one-way ANOVA with Holm-Sidek's multiple comparison test for comparison of multiple groups. The following nonparametric tests were used: Mann-Whitney rank-sum test for comparing between two groups and Kruskal-Wallis with Dunn's post hoc test for comparison of multiple groups. Behavioral data were resampled 1000 times in MATLAB to find new

bootstrapped means. Ranges shown in figures are the 95% confidence intervals of means. Similar groups (i.e. WT ± tamoxifen) were only combined after being calculated to be non-significantly different by Mann-Whitney test.

Chapter 3

Re-expression and deletion of MeCP2 in early adulthood

Introduction

Resulting from *de novo* mutations in *Mecp2,* Rett syndrome (RTT) is a neurodevelopmental disorder characterized by both physical and cognitive regression. The critical need for MeCP2 in development initially aroused the question of whether MeCP2 was required for proper function of the adult brain. To answer this question, an inducible knockout mouse was created that had both a floxed *Mecp2* allele and a Cre-Estrogen Receptor (Cre-ER) allele (Hayashi and McMahon, 2002). When delivered intraperitoneally at an age of the researcher's choosing, tamoxifen promotes the Cre-ER complex's translocation to the nucleus whereupon Cre recombinase excises the *Mecp2* gene.

When MeCP2 is deleted at P60, these mice recapitulate the phenotypes observed in *Mecp2*-null mice. These include impairments in motor performance, issues with learning and memory, disruptions in expression of NMDAR subunits, reduction of dendritic complexity, and shortened lifespan (Du et al., 2012; McGraw et al., 2011). In fact, MeCP2 function at older ages appears to be more critical for health than at younger ages. Mice who have MeCP2 deleted at 20 weeks of age develop RTT symptoms far more rapidly than mice who have MeCP2 deleted at 3 weeks of age (Cheval et al., 2012).

On the other hand, this tamoxifen-inducible Cre-ER system can be employed to reactivate endogenous *Mecp2*, which has allowed researchers to investigate the

possibilities for recovery of RTT phenotypes in adult mice. Inspiring hope for human patients, MeCP2 reactivation in adult mice results in significantly increased life expectancy and dramatic reversal of the phenotypic manifestations of the disorder (Guy et al., 2007). Furthermore, restoring MeCP2 to symptomatic adult mice via tamoxifen significantly improves respiratory function, grip strength, and rotarod performance (Robinson et al., 2012).

Gene therapy approaches utilizing recombinant adeno associated virus (AAV) vectors to deliver *Mecp2* to the central nervous system of adult *Mecp2*-null mice also show promise. Intravenous injection of an AAV9/*MECP2* vector into one-month old *Mecp2*-null males has a paltry 3% neuronal transduction efficiency, but nevertheless improves median lifespan from 10.6 to 15.4 weeks (Gadalla et al., 2013). When this AAV9/*MECP2* vector is systemically delivered to 10-month-old *Mecp2*-het female mice, their lifespans are similarly increased. When observed 5 months after AAV/*MECP2* delivery, these mice exhibit significantly improved rotarod performance, nesting ability, and muscular strength and coordination as assessed by an inverted screen test (Garg et al., 2013).

Presently, no information exists regarding the temporal importance of MeCP2 for sensory processing in Rett syndrome. Sensory circuits are fundamentally distinct from those responsible for motor or respiratory function. Uniquely, sensory processing and related cognitive capabilities such as language are acquired in an experience-

dependent manner during well-defined critical periods early in life (Hensch, 2005a; Hooks and Chen, 2007; Knudsen, 2004). In the course of these periods, underlying sensory circuits are adjusted and refined before settling into mature configurations in adulthood. In typically developing brains, the possibility for re-wiring is limited after this especially plastic time (Hensch, 2005b; Knudsen, 2004; Popescu and Polley, 2010).

Consequently, using the visual system as a model, we intended to answer the following questions: 1) subsequent to the correct writing of sensory circuits in early life, can sensory systems be disrupted by deletion of MeCP2 in adulthood? and 2) can degraded sensory modalities be recovered by MeCP2 re-expression in adulthood?

The table below outlines the visual phenotypes we will be assessing in our study.

Brain Region	Phenotype	Reference
Visual Cortex	Disrupted visually evoked potentials	LeBlanc et al., 2015
	Increased expression of inhibitory markers and inhibitory hyperconnectivity	Durand et al., 2015 Krishnan et al., 2015
	Reduced spontaneous and evoked activity	Durand et al., 2012; Patrizi et al., 2015
	Decreased neuronal response reliability	Patrizi et al., 2015
Lateral Geniculate Nucleus	De-segregation of eye-specific layers	Noutel et al., 2011
	Abnormal synaptic strength and connectivity of retinogeniculate synapse	Noutel et al., 2011
Superior Colliculus / LGN	Decreased optomotor visual acuity	Durand et al., 2012 Patrizi et al., 2015

Results

First we addressed whether the visual system was susceptible to disruption upon MeCP2 deletion. We began tamoxifen treatment at early adulthood (P35), after the peak of plasticity in the visual system had subsided (Fig. 3.1a) (Gordon and Stryker, 1996; Hooks and Chen, 2007; Kang et al., 2013) Consistent with prior reports, tamoxifen injections resulted in a significant reduction of MeCP2 protein in the visual cortex (Cheval et al., 2012; McGraw et al., 2011). Using immunohistochemistry, we found that MeCP2 protein in the soma of visual cortical neurons from Late Deletion mice was significantly reduced compared to tamoxifen treated *Mecp2*$^{lox/y}$ mice that lacked the Cre-ER allele (Lox/y Control) (Fig. 3.1b). No changes were observed in gross anatomy, as measured by cortical thickness (Fig. 3.2a). Behaviorally, the reduction of MeCP2 protein elicited RTT motor phenotypes, as reflected by impaired performance on the accelerating rotarod task (Fig. 3.2b) (Cheval et al., 2012; McGraw et al., 2011).

In *Mecp2*-null mice, excitatory/inhibitory balance is shifted in favor of inhibition (Kron et al., 2012). As previously reported, there was a significant increase in the intensity of the inhibitory marker, parvalbumin (PV), in visual cortex (Fig. 3.3a) (Durand et al., 2012; Krishnan et al., 2015). However, the density of perisomatic PV-boutons upon pyramidal cell somata was not altered in Late Deletion mice (Fig. 3.3b), consistent with previous studies which post-natally deleted MeCP2 specifically from PV neurons (Durand et al., 2012).

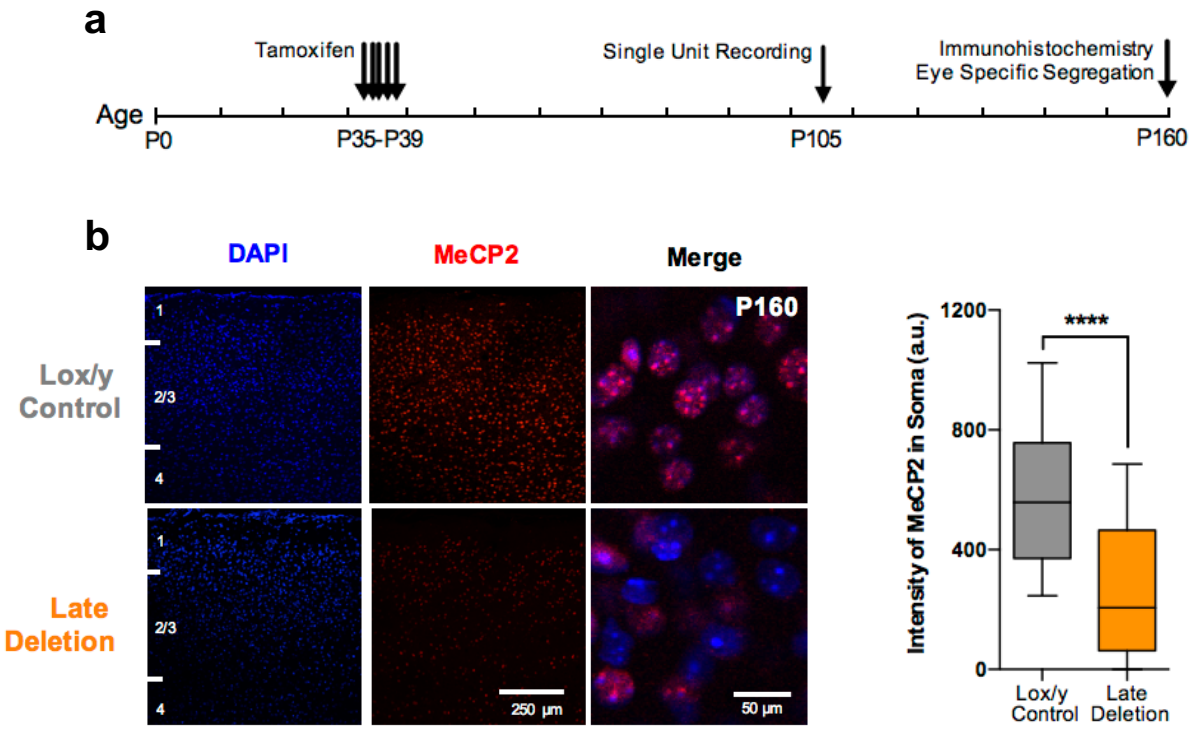

Figure 3.1 – Late Deletion mice express less MeCP2 than Lox/y Control mice

a. Late Deletion mice and Lox/y Controls were injected with tamoxifen from P35-P39. Terminal single unit recordings were performed at P105. At P160, mice were either prepared for eye specific segregation experiments or perfused for immunohistochemistry.

b. Immunohistochemical quantification of V1 neurons at P160 determined that MeCP2 intensity in Late Deletion mice was significantly reduced compared to Lox/y Controls. Late Deletion: n=800 cells, 8 slices, 3 mice. Lox/y Control: n=800 cells, 8 slices, 3 mice. Mann-Whitney (**** $P \leq 0.0001$).

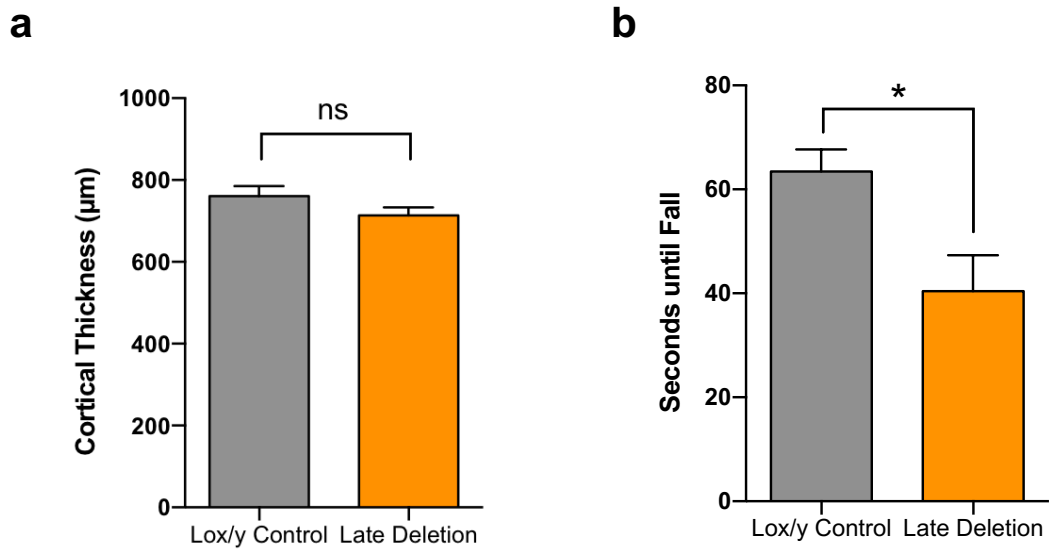

Figure 3.2 – Gross anatomy and motor behavior in Late Deletion mice at P160

a. No changes were observed in cortical thickness at P160 between Lox/y Control and Late Deletion groups. Lox/y Control: n=3 mice, 9 slices each. Late Deletion: n=4 mice, 9 slices each.

b. Late Deletion mice were unable to remain on an accelerating rotarod for as much time as Lox/y Controls at P160. Lox/y Control: n=6. Late Deletion: n=13. Mann-Whitney (* $P \leq .05$).

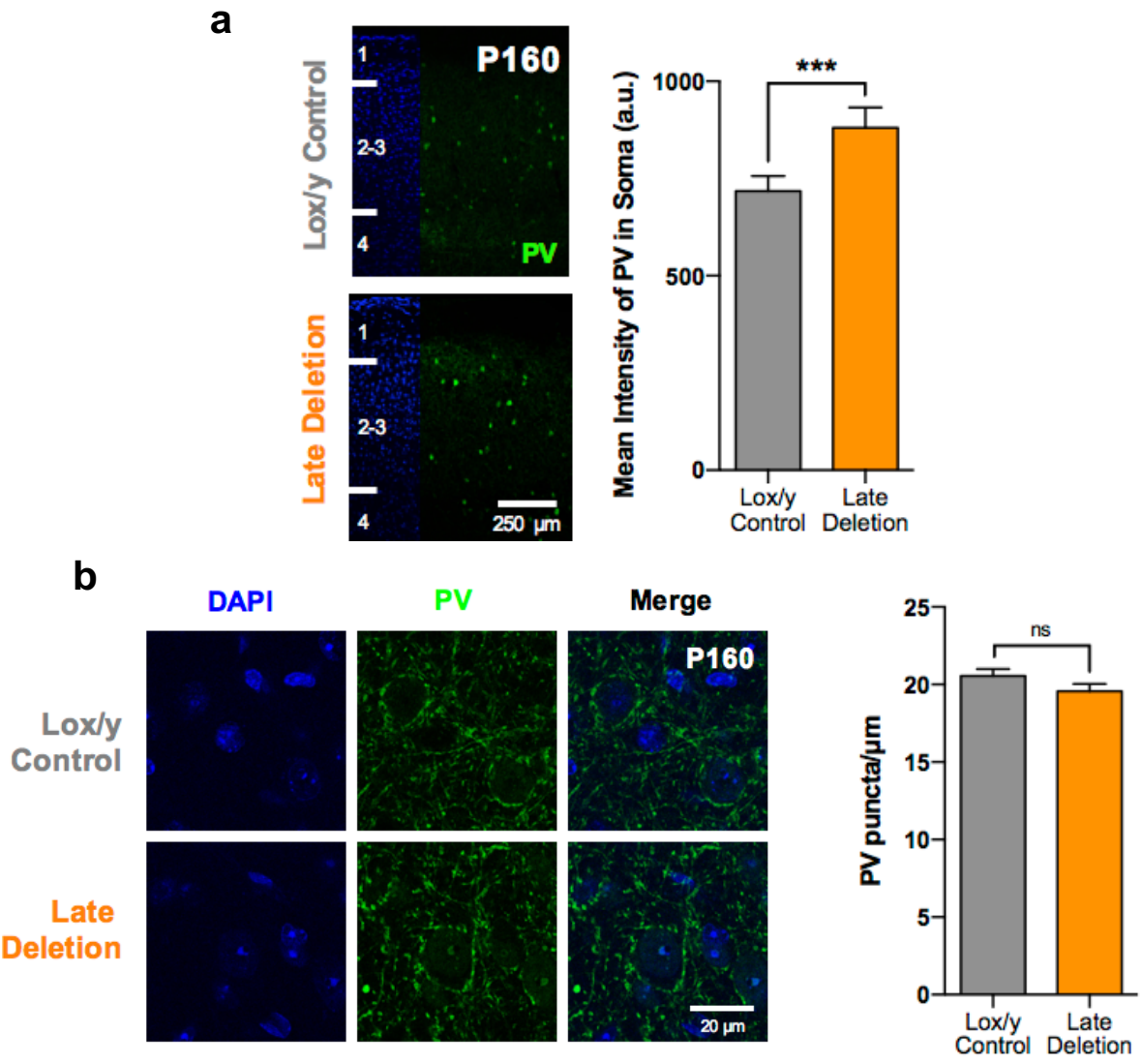

Figure 3.3 – Late Deletion mice exhibit normal anatomical connectivity of PV cells onto pyramidal somata

a. At P160 in V1, the intensity of parvalbumin in PV+ basket cells was elevated in Late Deletion mice as compared to Lox/y Control mice. Representative images from V1 show increased PV expression in neuronal soma in Late Deletion mice at P160. Blue overlay shows cell population with DAPI. Lox/y Control: n= 5 mice, 196 cells. Late Deletion: n= 3 mice, 54 cells. Mann-Whitney (*** $P \leq 0.001$).

b. The extent of PV innervation onto excitatory cells at P160 was evaluated by analyzing the density of somatic PV+ inhibitory synapses in visual cortex. No differences in PV connectivity were present between Lox/y Control and Late Deletion groups. Lox/y Control: n=3 mice, 55 cells. Late Deletion: n=3 mice, 44 cells.

To evaluate the impact of MeCP2 loss on the function of the visual system at single cell resolution, we performed *in vivo* extracellular recordings of excitatory neurons across all V1 cortical layers using multi-channel probes (Fig. 3.4). At P105, ten weeks after completion of tamoxifen treatment, both the evoked and spontaneous activities of single cells in V1 of Late Deletion mice were significantly reduced compared to Lox/y Control mice (Fig. 3.5a). We also calculated neuronal response reliability, which is decreased in neurological disorders with autistic features such as RTT (Dinstein et al., 2012; Patrizi et al., 2015). Response reliability was decreased in Late Deletion mice as measured by an increase in the coefficient of variation at the preferred orientation (Fig. 3.5b). Orientation selectivity, however, was not disrupted in these Late Deletion mice (Fig. 3.5c).

We then moved to the LGN where we analyzed the mapping of retinal inputs in Late Deletion mice. Typically, retinal axons organize into eye-specific regions in the LGN in a process that is largely complete by P10 (Huberman et al., 2008). In *Mecp2*-null mice, segregation of retinal input occurs normally, but then desegregates by P50 (Noutel et al., 2011). In Late Deletion mice, however, we found that desegregation did not occur, even upon waiting until P160, a full 4 months after MeCP2 deletion initially began (Fig. 3.6a). Visual optomotor acuity, which is mediated through lateral geniculate and superior colliculal circuits, was also unaffected in Late Deletion mice (Fig. 3.6b) (Huberman et al., 2009). Thus cortical circuits rely on the expression of

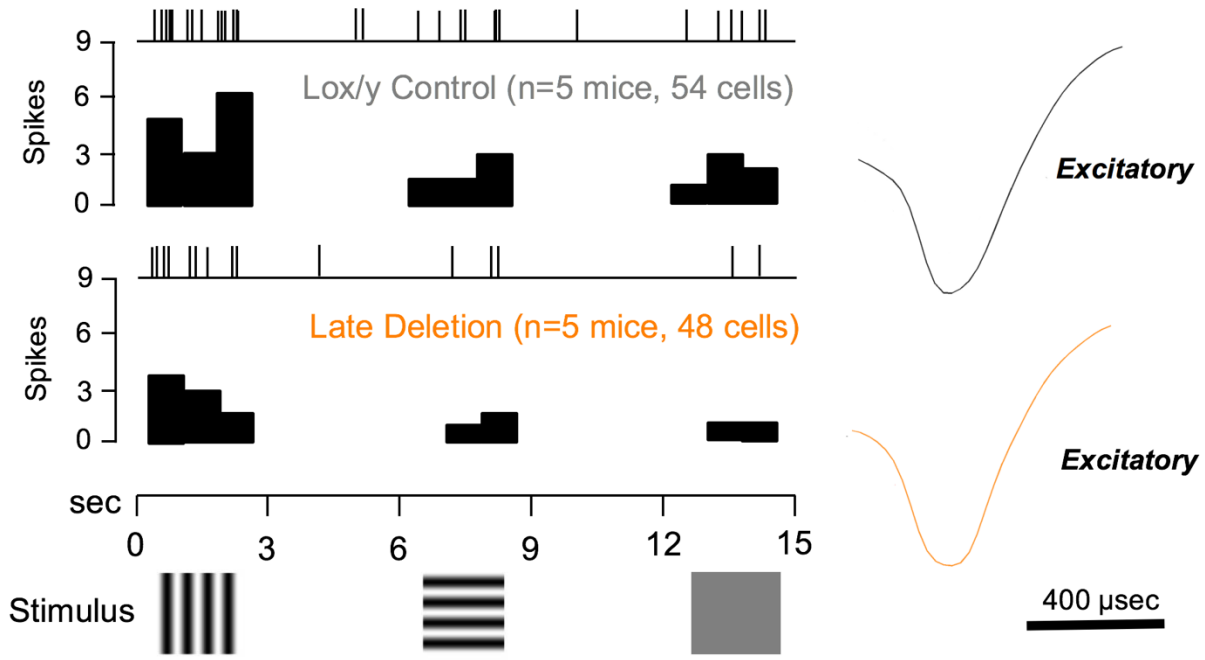

Figure 3.4 – Extracellular electrodes record single-unit activity in V1

Left: Representative Lox/y Control and Late Deletion spike trains and corresponding peristimulus time histogram in response to two oriented gratings or a uniform gray stimulus. *Right*: For each genotype, excitatory cells were differentiated from inhibitory cells by analysis of waveform properties. Only excitatory cells were included in our analyses.

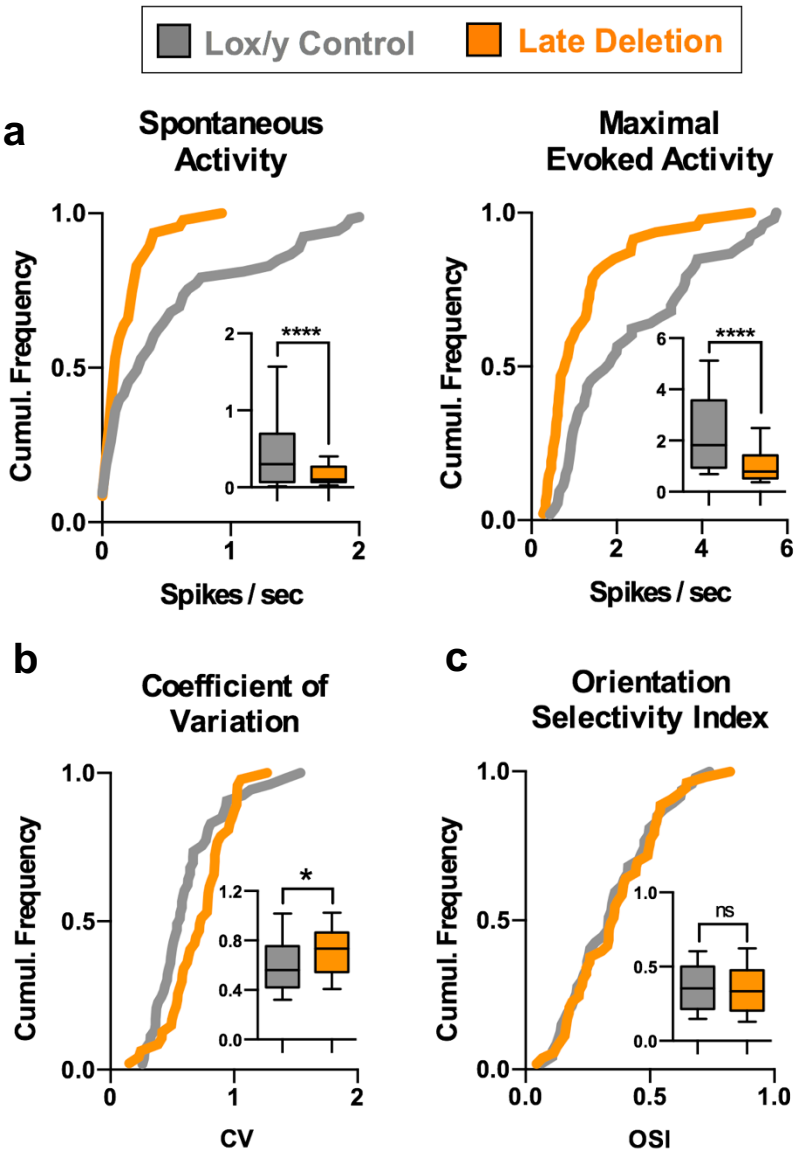

Figure 3.5 – Late MeCP2 deletion disrupts visual cortical function

a. In Late Deletion mice, both the evoked and spontaneous activities of single units in V1 were significantly reduced compared to Lox/y Control mice.

b. Deficits were observed in neuronal response reliability as measured by an increase in the coefficient of variation at preferred orientation.

c. Orientation selectivity in Late Deletion mice at P105 was not significantly different from Lox/y Control mice.

Lox/y Control: n=5 mice, 54 cells. Late Deletion: n=5 mice, 48 cells. Mann-Whitney (* $P \leq 0.05$, **** $P \leq 0.001$)

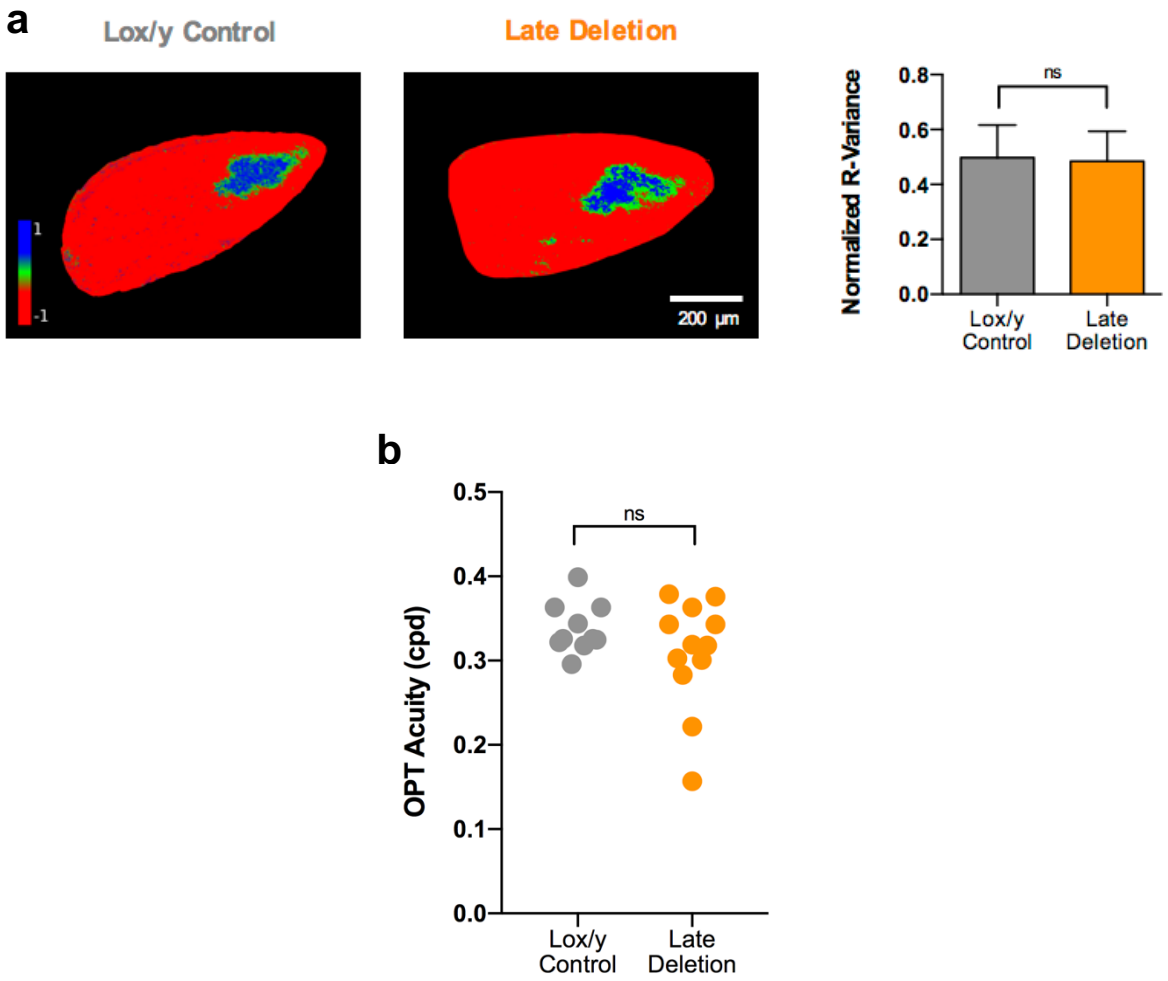

Figure 3.6 – MeCP2 deletion fails to disturb retinogeniculate anatomy or optomotor acuity

a. In Late Deletion mice, desegregation of retinal input to the LGN was not apparent to when measured at P160. Lox/y Control: n=40 sections, 4 mice. Late Deletion: n=24 sections, 5 mice.

b. When measured at P130, optomotor visual acuity was not significantly between Lox/y Control and Late Deletion mice. Lox/y Control: n=10, Late Deletion: n=12.

proper visual function even in adulthood, while subcortical circuits such as the LGN are comparatively less vulnerable once their development has completed.

In sum, anatomical LGN segregation, cortical PV connectivity, and V1 orientation selectivity were unaffected by MeCP2 deletion after the visual system had properly developed. We consequently hypothesized that abnormal sensory circuits could therefore prove difficult to repair once plasticity had subsided in early adulthood. With this in mind, we examined the possibility for proper sensory system re-wiring following an abnormal development in the absence of MeCP2. To this end, we utilized the *Mecp2*$^{stop/y}$ mouse, a conditional model that only expresses MeCP2 in the presence of Cre. Appropriately, these *Mecp2*$^{stop/y}$ mice faithfully replicate numerous features of the *Mecp2*-null mouse model (Fig. 3.7) (Guy et al., 2001).

To establish the baseline conditions of the visual system in mice lacking MeCP2, we initiated experiments with *Mecp2*$^{stop/y}$ mice during early adulthood; our endpoint for assessment would occur seven weeks later at P105 (Fig. 3.8). We found that the *Mecp2*$^{stop/y}$ mouse's visual cortex was already electrophysiologically impaired at P30, well before the outward onset of behavioral RTT phenotypes. In V1, we measured decreased spontaneous and evoked activity of single units, as well as decreased neuronal response reliability compared to WT (Fig. 3.9). However, orientation selectivity appeared normal in P30 *Mecp2*$^{stop/y}$ mice (Fig. 3.9). Like the Late Deletion mice with diminished MeCP2, and consistent with prior anatomical reports, we also

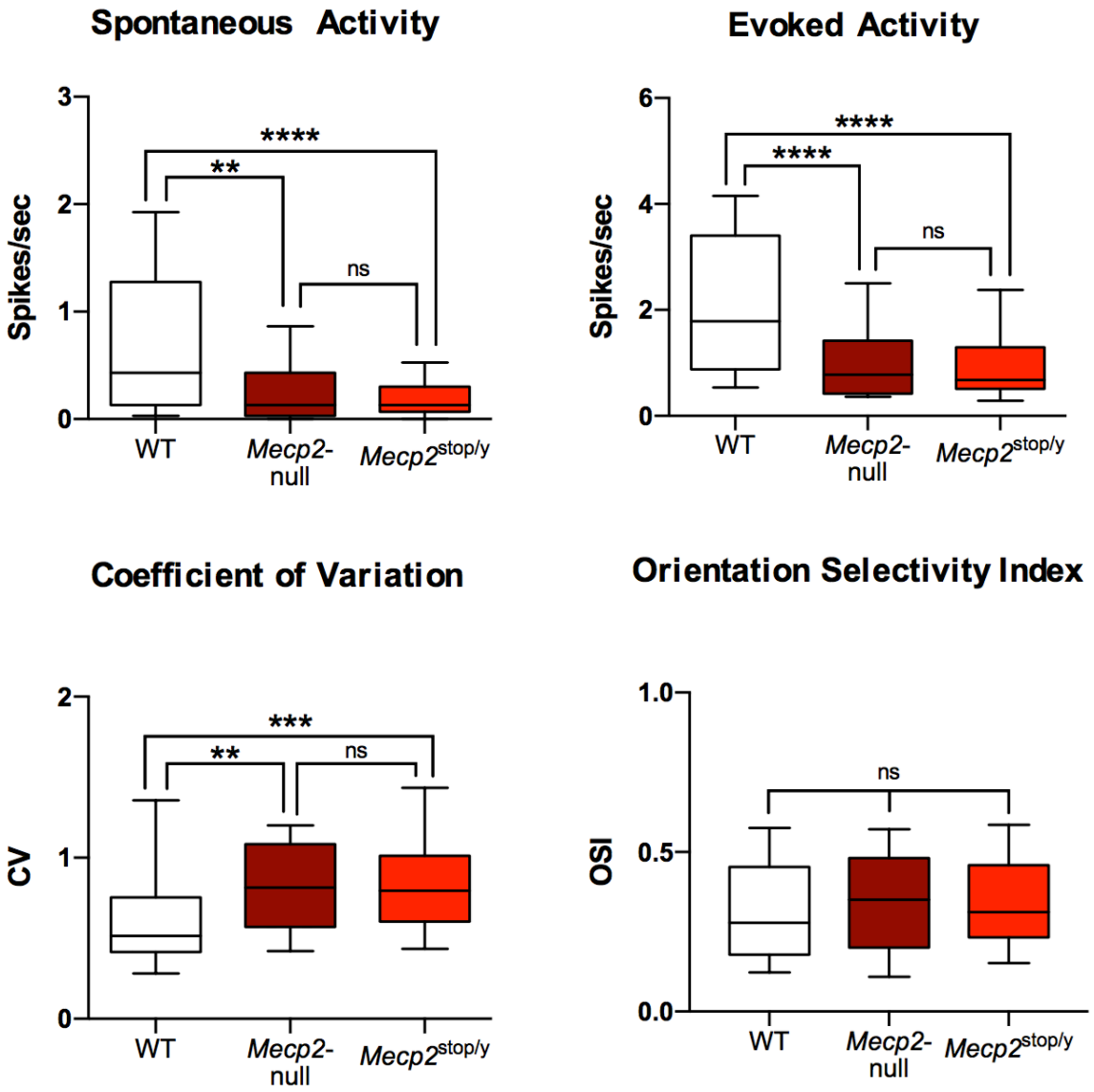

Figure 3.7 – Single-unit activity in the visual cortex of *Mecp2*$^{stop/y}$ mice and *Mecp2*-null mice is comparable at P30

Single unit activity at P30 was statistically similar between *Mecp2*$^{stop/y}$ mice and *Mecp2*-null mice when measuring spontaneous activity, maximal evoked activity at the preferred orientation, the coefficient of variation at the preferred orientation, and the orientation selectivity index. WT: 6 mice, 73 cells. *Mecp2*$^{stop/y}$: n=9 mice, 69 cells. *Mecp2*-null: n=4 mice, 45 cells. Kruskal-Wallis with Dunn's Test (** $P \leq .01$, *** $P \leq .001$, **** $P \leq .0001$).

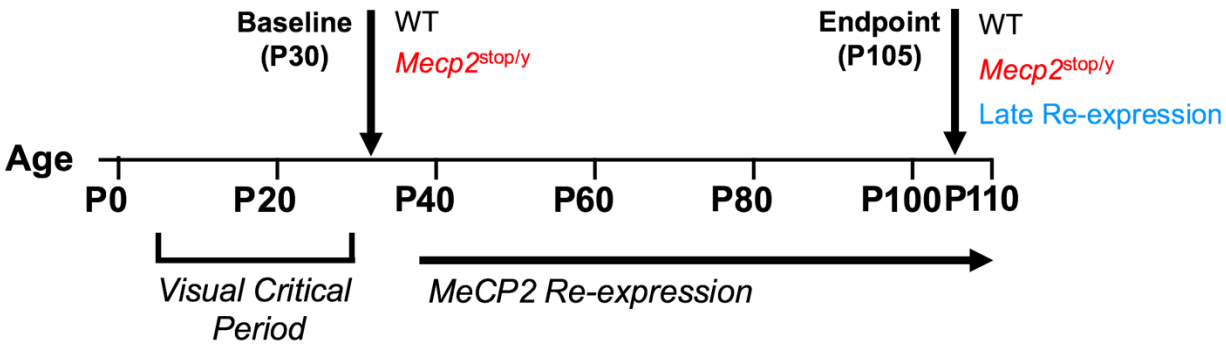

Figure 3.8 – Experimental paradigm to assess visual system recovery in RTT mouse model

First, we established the P30 baseline status of the visual system at the end of the visual critical period. During the subsequent weeks, tamoxifen was utilized to restore MeCP2 to *Mecp2*$^{stop/y}$ mice who initially lacked MeCP2. These 'Late Re-expression' mice were assessed at P105 along with WT and *Mecp2*$^{stop/y}$ littermates. This experimental design allowed us to distinguish if, by reactivating *Mecp2*, we were rescuing sensory defects or preventing regression at P105.

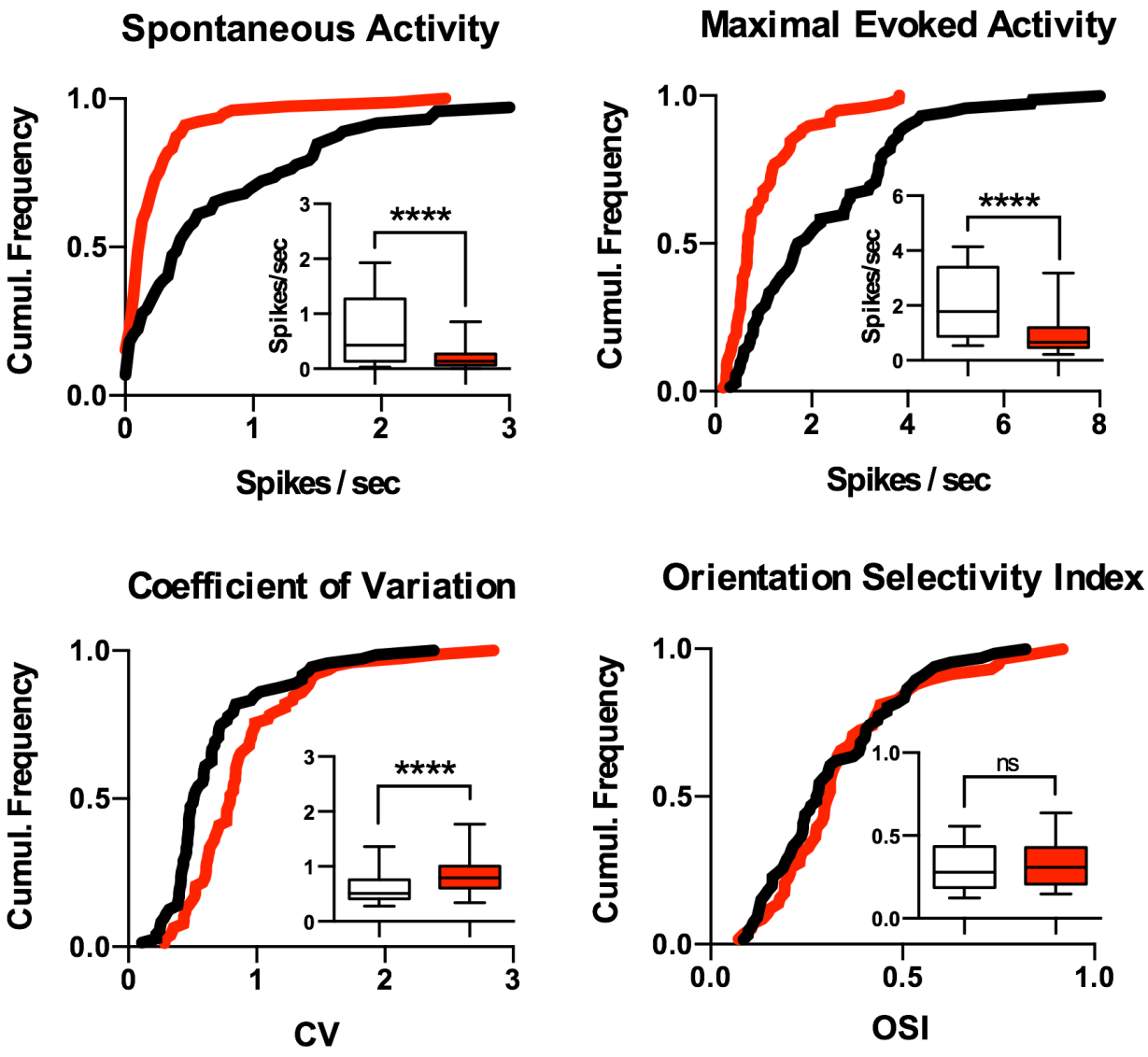

Figure 3.9 – Cortical function is impaired during early adulthood in Mecp2$^{stop/y}$ mice

In P30 *Mecp2*$^{stop/y}$ mice, electrophysiological deficits in spontaneous and evoked activity as well as the coefficient of variation were observed when recording from excitatory single units in the binocular zone of primary visual cortex. However, orientation selectivity of *Mecp2*$^{stop/y}$ neurons were not significantly different than WT controls. WT: n=6 mice, 72 cells. *Mecp2*$^{stop/y}$ n=9 mice, 78 cells. Mann Whitney (**** P ≤ 0.0001).

observed both an increase in PV soma intensity and also PV hyperconnectivity onto pyramidal cells in V1 of P30 *Mecp2*$^{stop/y}$ mice (Fig. 3.10a,b) (Durand et al., 2012; Tomassy GS, Morello N, Calcagno E, 2014). Cortical thickness was diminished at P30 as well (Fig. 3.10c).

Although sensory system disruptions were present in V1 at P30 in *Mecp2*$^{stop/y}$ mice, it was unknown if LGN was also abnormal at this age. Using a similar visual stimulation paradigm as in V1, we then recorded neuronal activity in the dorsal and ventral LGN (Fig. 3.11a). We found no significant difference in the spontaneous activity of *Mecp2*$^{stop/y}$ excitatory neurons at P30 (Fig. 3.11b). The subset of *Mecp2*$^{stop/y}$ relay cells responsive to the high contrast gratings also exhibited comparable spontaneous and maximal evoked activities as WT (Fig. 3.11c).

To probe for LGN abnormalities of sensory input onto visual thalamus, we examined synaptic strength and connectivity at the retinogeniculate synapse at P30 in *Mecp2*$^{stop/y}$ mice. In typically developing mice, retinal ganglion cells innervate the LGN by P0 (Godement et al., 1984). At P30, we recorded excitatory postsynaptic currents (EPSCs) from relay neurons of WT and *Mecp2*$^{stop/y}$ mice while incrementally increasing the intensity of optic tract stimulation intensity (Fig. 3.12a). Synaptic strength, quantified by the peak single-fiber (SF) AMPAR and NMDAR EPSC amplitudes, was not significantly different between *Mecp2*$^{stop/y}$ mice and their WT littermates (Fig. 3.12b,c). AMPAR and NMDAR maximal EPSC currents were also intact (Fig. 3.12c). The

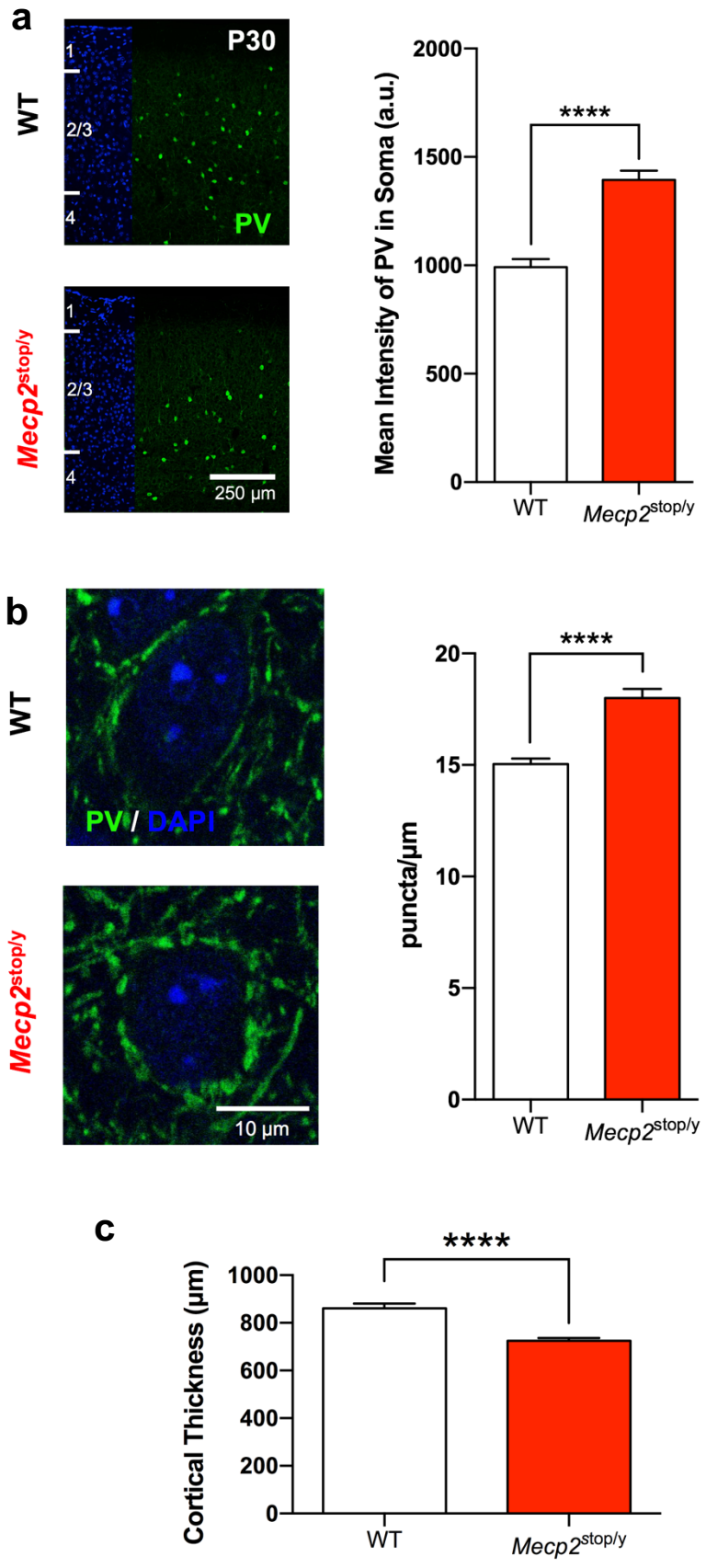

Figure 3.10 – PV intensity and hyperconnectivity is present in V1 at P30 in *Mecp2*$^{stop/y}$ mice

a. The intensity of parvalbumin in PV+ basket cells in V1 was elevated at P30 in *Mecp2*$^{stop/y}$ mice. Total cell population shown in blue was stained with DAPI. WT: n=390 cells, *Mecp2*$^{stop/y}$: n=409 cells. 3 slices per animal, 3 animals per group. Mann-Whitney (**** $P \leq 0.0001$).

b. The number of somatic PV+ inhibitory synapses was increased at P30 in *Mecp2*$^{stop/y}$ mice. WT: n=3 mice, 64 cells. *Mecp2*$^{stop/y}$: n=3 mice, 49 cells. Mann-Whitney (**** $P \leq 0.0001$).

c. Cortical thickness was reduced at P30 in *Mecp2*$^{stop/y}$ mice. WT: n=3 mice, 9 slices each. *Mecp2*$^{stop/y}$: n=3 mice, 9 slices each. Mann-Whitney (**** $P \leq 0.0001$).

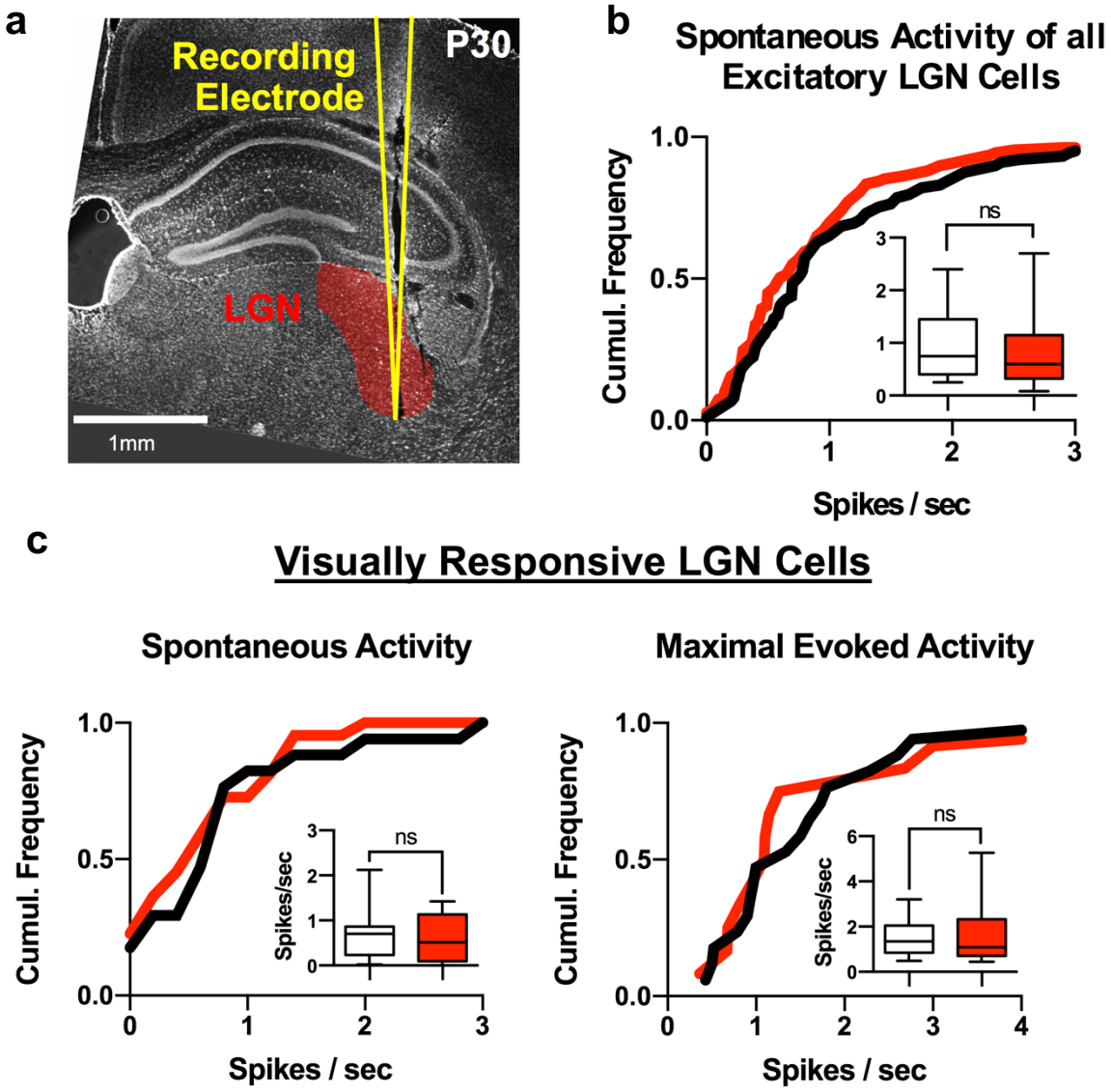

Figure 3.11 – Levels of single-unit activity in the *Mecp2*$^{stop/y}$ LGN are not significantly different from WT at P30

a. Single unit recordings were performed in the lateral geniculate nucleus. DAPI stained slice shows the electrode's path into both the dorsal and ventral LGN.

b. In P30 *Mecp2*$^{stop/y}$ mice, the population average of the spontaneous activity of all excitatory units in LGN was not significantly different from WT. WT: n=5 mice, 89 cells. *Mecp2*$^{stop/y}$: n=8 mice, 109 cells.

c. The subset of LGN neurons in *Mecp2*$^{stop/y}$ mice that were responsive to visual stimulation had spontaneous and maximal evoked activities that did not differ from WT.

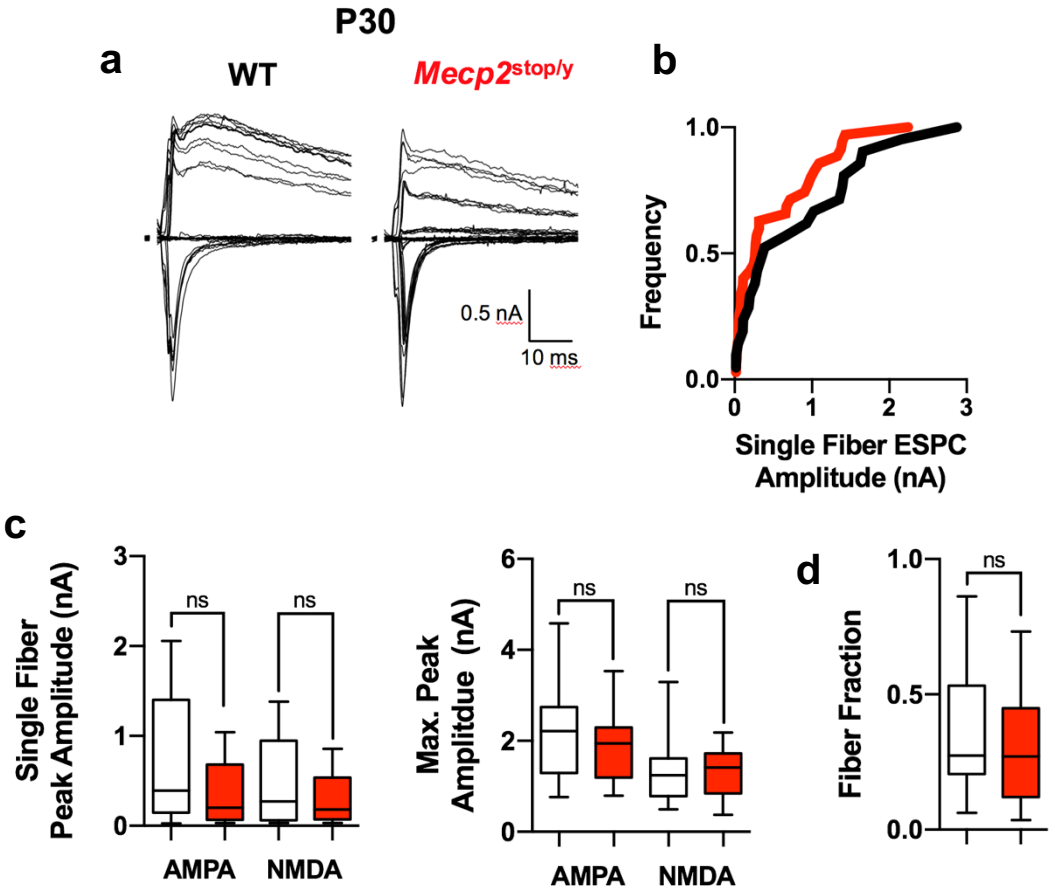

Figure 3.12 – Synaptic strength and connectivity at the retinogeniculate synapse is normal at P30 in *Mecp2*$^{stop/y}$ mice

a. Representative WT and *Mecp2*$^{stop/y}$ AMPAR and NMDAR current traces from single LGN neurons. Traces were evoked from a holding potential of -70 mV (AMPAR) and +40 mV (NMDAR, slow component) while increasing the intensity of optic nerve stimulation. Stimulation artifact was blanked for clarity.

b. Cumulative probability plot of single-fiber AMPAR currents, measured at a holding potential of −70 mV.

c. Average single-fiber and maximal current amplitude for AMPAR and NMDAR current assessed in WT and *Mecp2*$^{stop/y}$ mice were statistically similar. Single Fibers: WT: n=21. *Mecp2*$^{stop/y}$: n=35. Maximal Peak Amplitude: WT: n=18. *Mecp2*$^{stop/y}$: n=26.

d. No difference in the fiber fraction ratio was observed between WT at *Mecp2*$^{stop/y}$ groups at P30.

strengthening of the retinogeniculate synapse is accompanied by a process of synaptic pruning (Hooks and Chen, 2006). To address whether synapse elimination was affected in P30 *Mecp2*$^{stop/y}$ mice, we compared fiber fraction ratios, which estimates the number of functionally connected RGC afferents (Hooks and Chen, 2006). We found that synaptic pruning was not disrupted in *Mecp2*$^{stop/y}$ mice at P30 (Fig. 3.12d). Thus, as we began our re-expression paradigm, we primarily sought to reverse the numerous anatomical and functional deficits observed in V1, since we did not observe overt phenotypes in LGN.

To assess if we could rescue an initially abnormal visual cortex, we crossed a *Mecp2*$^{stop/y}$ mouse with a Cre-ER mouse and administered tamoxifen to trigger global expression of the MeCP2 protein (hereafter referred to as 'Late Re-expression') (Guy et al., 2007). During early adulthood, we began a sequence of staggered tamoxifen injections that dramatically increased the life expectancy of Late Re-expression mice (Fig. 3.13a). As previously reported, Late Re-expression mice did not experience a progression of RTT symptoms and failed to develop motor phenotypes or respiratory apneas (Fig. 3.13b-d) (Guy et al., 2007). At P75, MeCP2 reached 69% of WT protein levels in the Late Re-expression visual cortex and statistically similar levels sub-cortically (Fig. 3.14a,b). Concordantly, immunohistochemistry analysis showed detectable MeCP2 expression occurring in 63% of all neurons by P105 (Fig. 3.15). Although the level of somatic expression of PV was restored to WT levels in Late Re-expression mice,

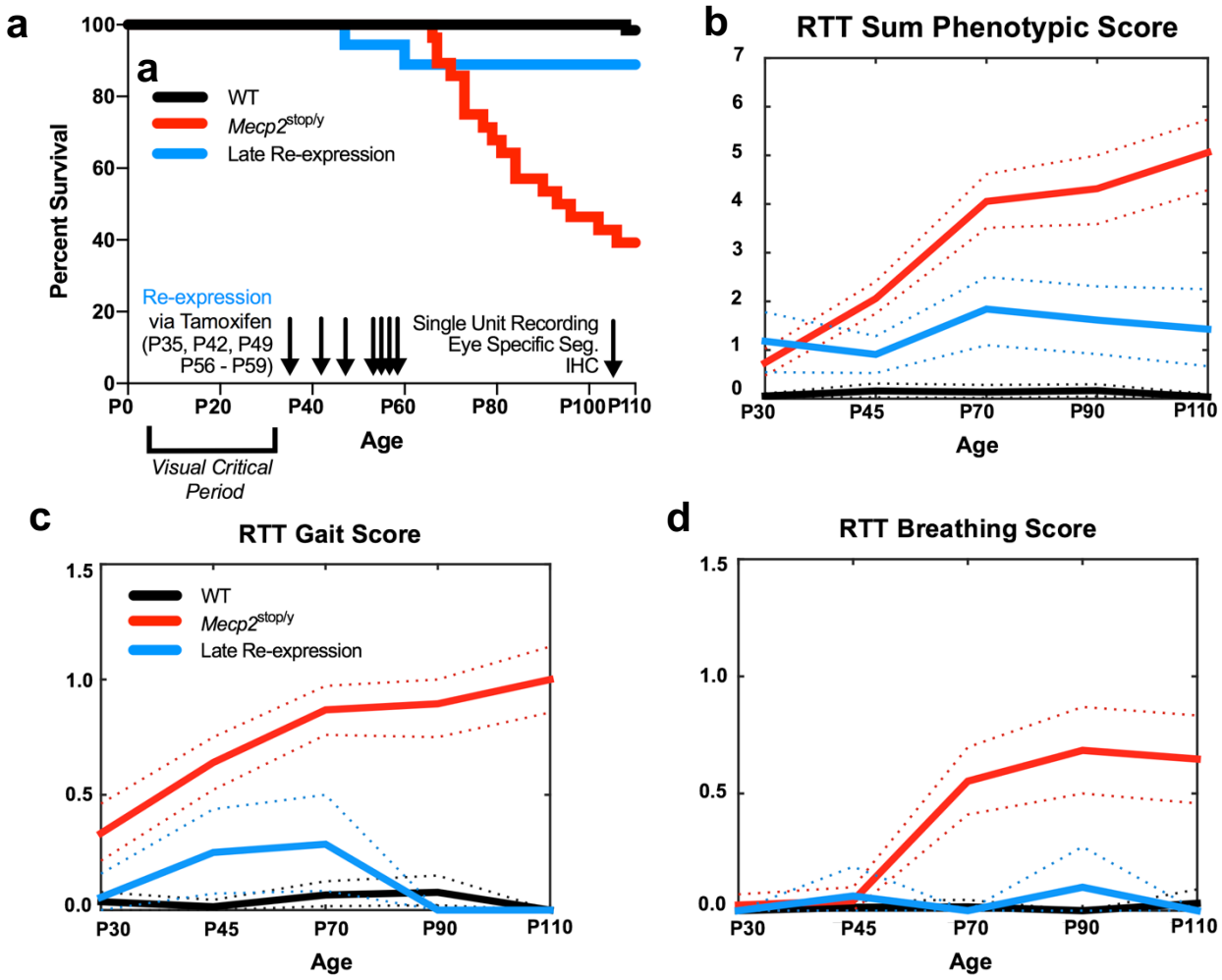

Figure 3.13 – Re-activation of *Mecp2* improves RTT phenotypes and increases life expectancy

a. Late Re-expression mice and littermates were injected with tamoxifen at P35, P42, P49, and P56-59. At the P105 endpoint, mice were used for single unit recordings, immunohistochemistry and eye-specific segregation experiments. The lifespan of Late Re-expression mice was prolonged compared to *Mecp2*$^{stop/y}$ mice (Mdn: 95 days). WT: n=66 mice. *Mecp2*$^{stop/y}$: n=28 mice. Late Re-expression: n=18 mice.

b. The phenotypic progression of Rett syndrome symptoms was prevented in Late Re-expression mice. WT: n=28-68 mice. *Mecp2*$^{stop/y}$: n=15-48 mice. Late Re-expression: n=5-18 mice. Dotted lines indicate 95% confidence intervals.

c. Gait component of the sum RTT phenotypic score in (b).

d. Breathing component of the sum RTT phenotypic score in (b).

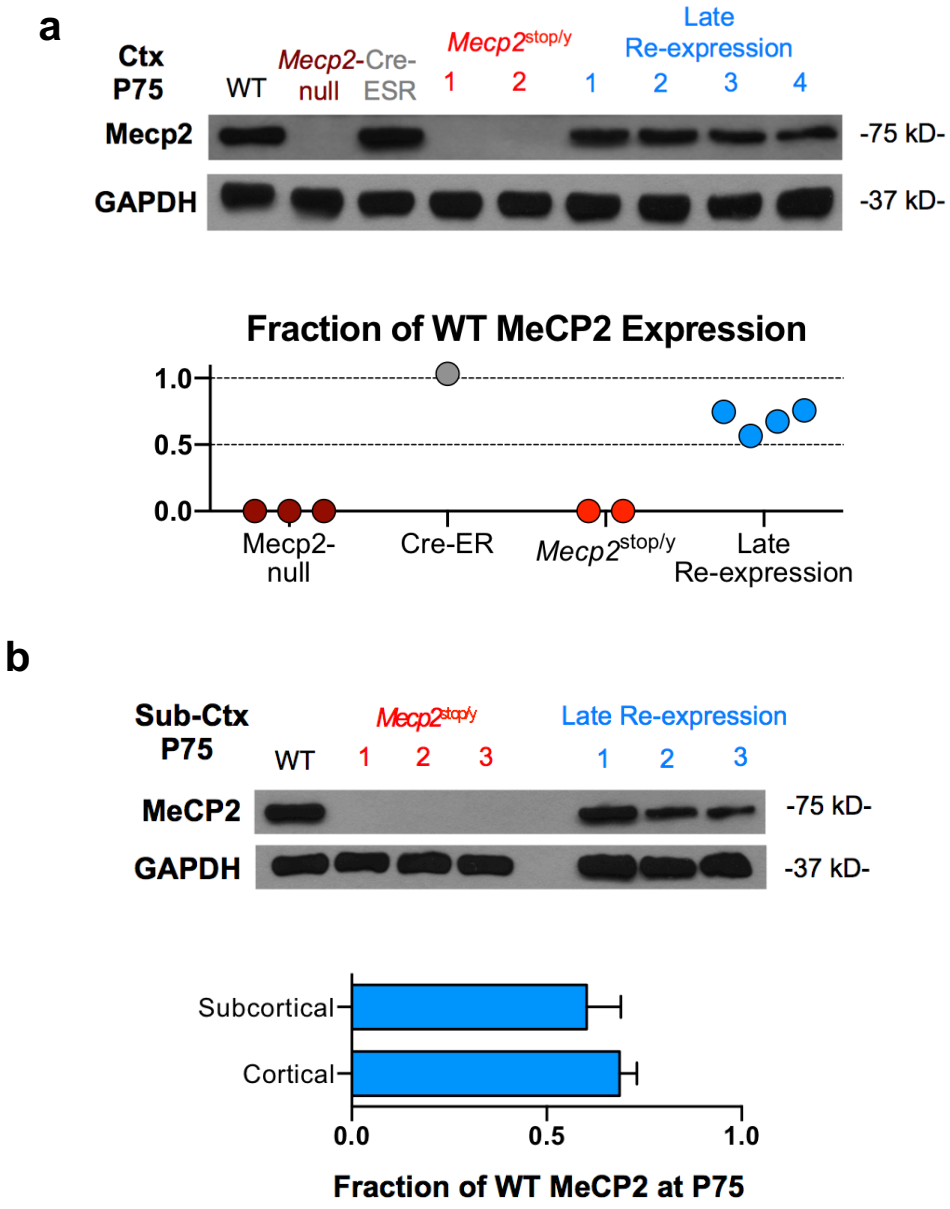

Figure 3.14 – Tamoxifen treatment results in robust MeCP2 expression in cortical and sub-cortical regions

a. *Mecp2*$^{stop/y}$ mice expressed an undetectable amount MeCP2 protein at P75, whereas Late Re-expression mice reached 69% of WT MeCP2 expression by P75.

b. At P75, re-expression of MeCP2 occurred at similar levels in the cortex and sub-cortex of Late Re-expression mice as measured by Western blot from brain lysates.

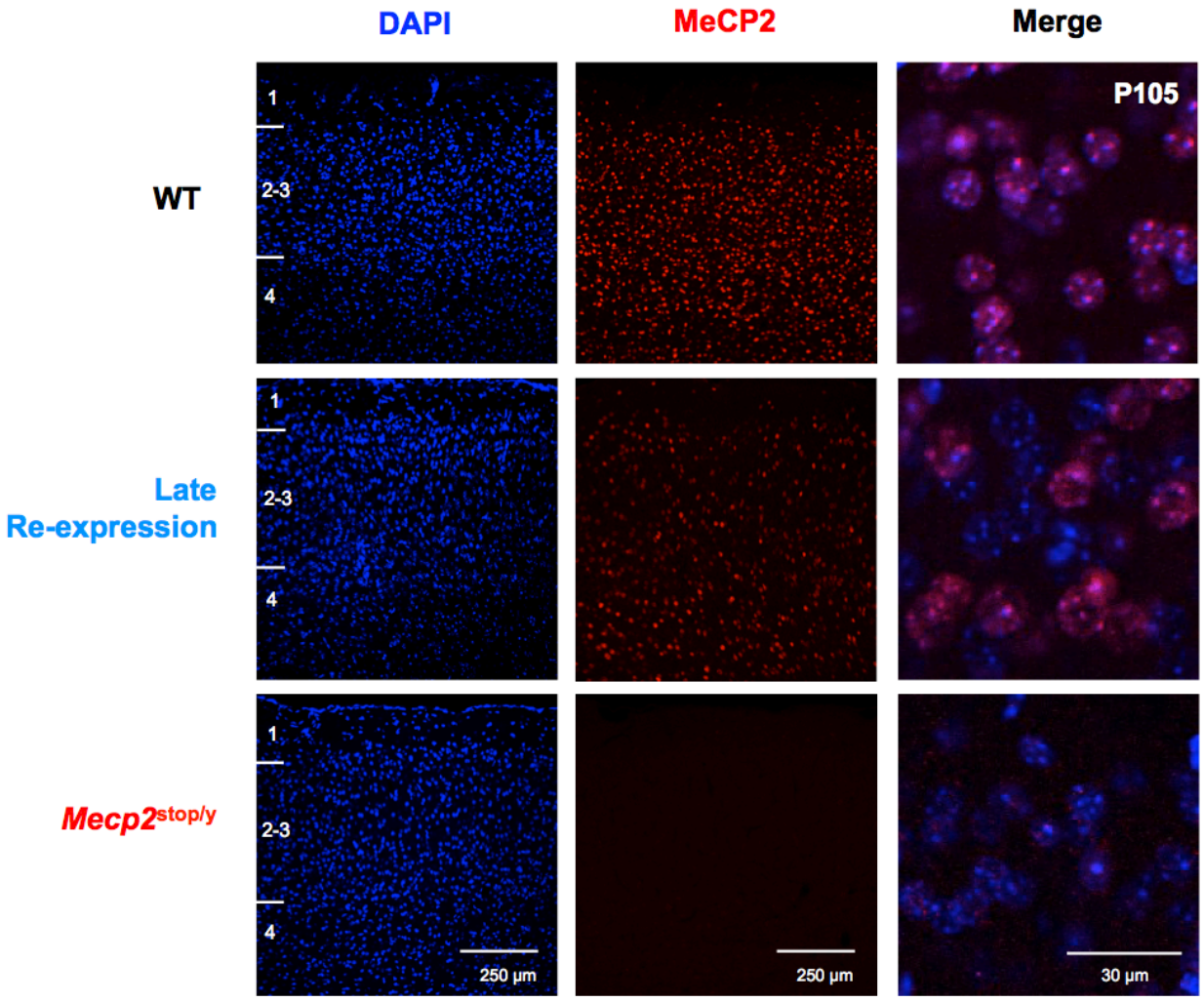

Figure 3.15 – MeCP2 expression levels in V1 of Late Re-expression mice align with Western blot data

Representative V1 images of P105 samples. In V1 of Late Re-expression mice, 63% of neurons expressed detectable levels of MeCP2, as compared to 6% of *Mecp2*$^{stop/y}$ neurons. WT: n=700 cells, 7 slices, 3 mice. *Mecp2*$^{stop/y}$: n=700 cells, 7 slices, 3 mice. Late Re-expression: n=600 cells, 6 slices, 3 mice.

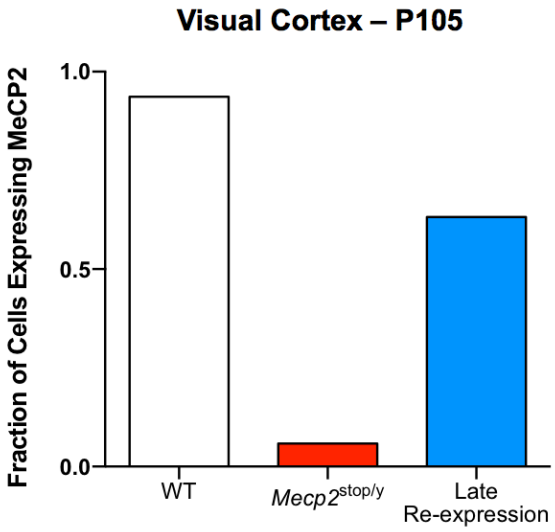

the density of perisomatic PV-boutons upon pyramidal cell somata was still significantly increased as compared to WT (Fig. 3.16a,b). This PV hyperconnectivity arises as early as P15 in *Mecp2*-null mice, and persists throughout adulthood (Durand et al., 2012). Ergo, while re-expression of MeCP2 dynamically regulated the protein levels of PV, it could not reverse the established mature—and abnormal—anatomical connectivity in V1. In a similar vein, Late Re-expression mice failed to experience any rescue in the thickness of their cortices (Fig. 3.17) (Robinson et al., 2012).

To evaluate cortical function, we again performed single unit recordings and discovered that many features had been normalized from their aberrant state at P30. By P105, we found both the spontaneous activity and the maximal evoked activity of Late Re-expression visual cortical neurons were similar to WT (Fig. 3.18). Furthermore, the decreased response reliability of neurons observed at P30 and P105 in *Mecp2*$^{stop/y}$ mice was also recovered (Fig. 3.18). Orientation selectivity, however, was a component that remained significantly different from WT (Fig. 3.18).

In Rett syndrome patients, the visually evoked potential (VEP) has been proposed as a quantitative biomarker of cortical function, as it tracks disease severity (LeBlanc et al., 2015). We therefore measured VEP in P105 *Mecp2*$^{stop/y}$ mice and found dramatically reduced VEP amplitudes in response to low-spatial frequency gratings (Fig. 3.19), as well as diminished spatial acuity (Fig. 3.20a). Importantly, Late Re-expression mice exhibited VEP amplitudes and spatial acuity significantly higher than

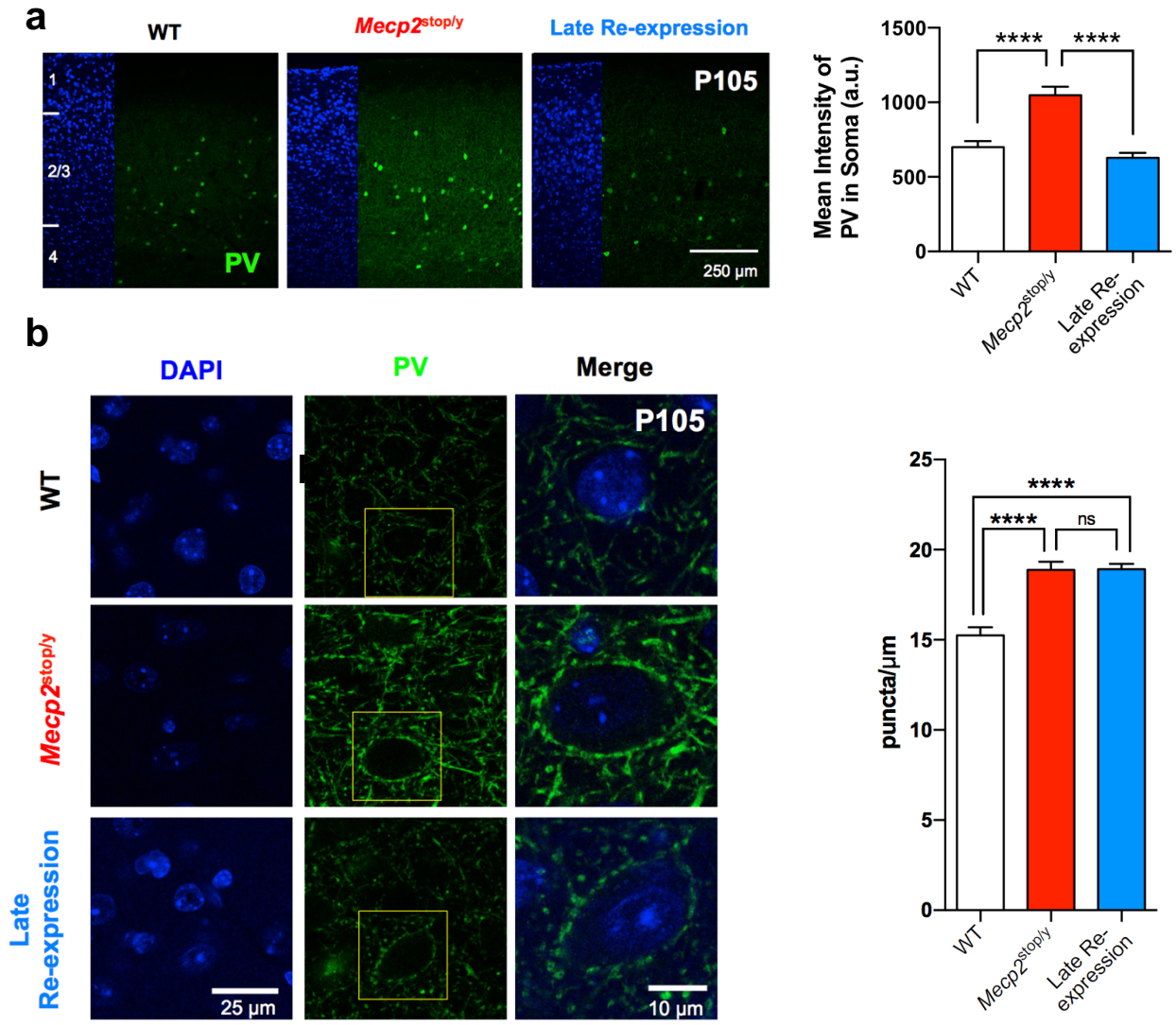

Figure 3.16 – PV intensity, but not hyperconnectivity is rescued in Late Re-expression mice at P105

a. The intensity of parvalbumin in PV+ basket cells in V1 was not elevated in P105 Late Re-expression mice. Total cell population shown in blue was stained with DAPI. WT: n=104 cells. *Mecp2*$^{stop/y}$: n=94 cells. Late Re-expression: n=200 cells. Kruskal-Wallis with Dunn's Test (**** $P \leq 0.0001$).

b. PV connectivity onto excitatory neurons in V1 was assessed by analyzing the density of somatic PV+ inhibitory synapses. Yellow boxes indicate the location of the zoomed and merged image. Elevation of somatic PV puncta density seen in *Mecp2*$^{stop/y}$ mice was not reversed in Late Re-expression mice. WT: n= 38 cells. *Mecp2*$^{stop/y}$: n=46 cells. Late Re-expression n=70 cells. 3 slices per animal, 3 animals per group Kruskal-Wallis with Dunn's Test (**** $P \leq 0.0001$).

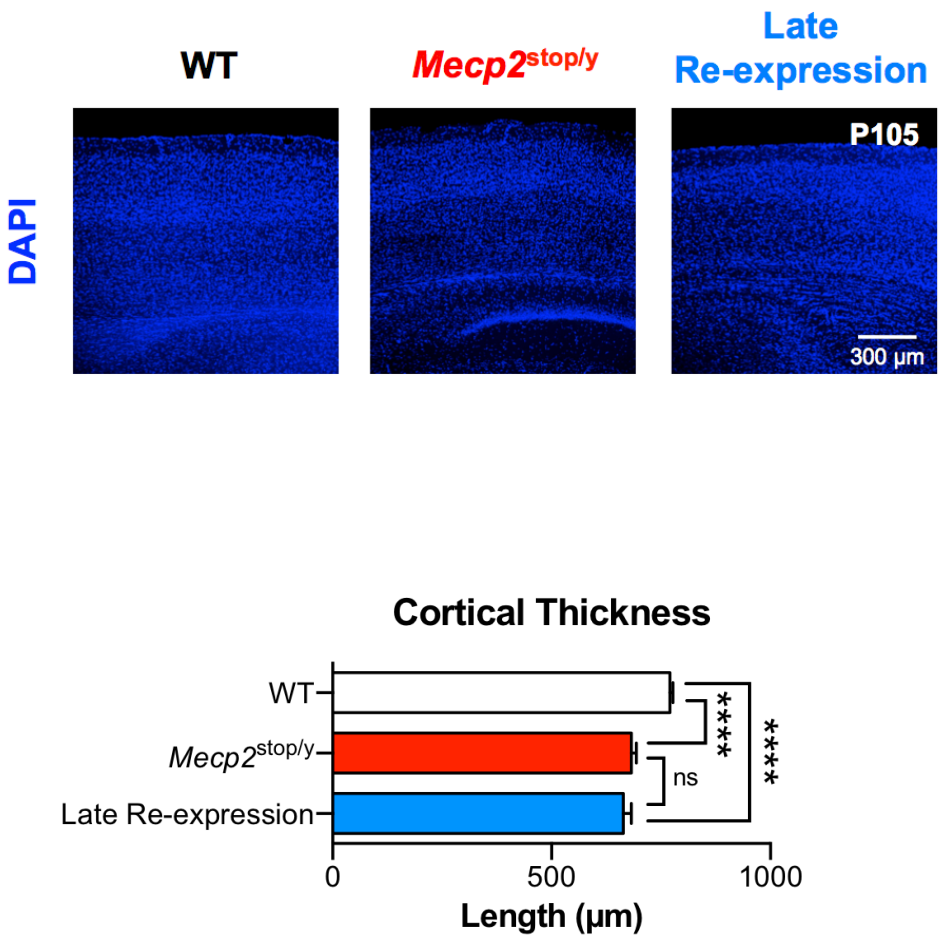

Figure 3.17 – Cortical thickness is not rescued at P105 in Late Re-expression mice

At P105, Late re-expression mice exhibited cortical thicknesses that were not significantly different from *Mecp2*$^{stop/y}$ mice. 9 slices per animal, 3 animals per group. Kruskal-Wallis with Dunn's Test (**** $P \leq 0.0001$).

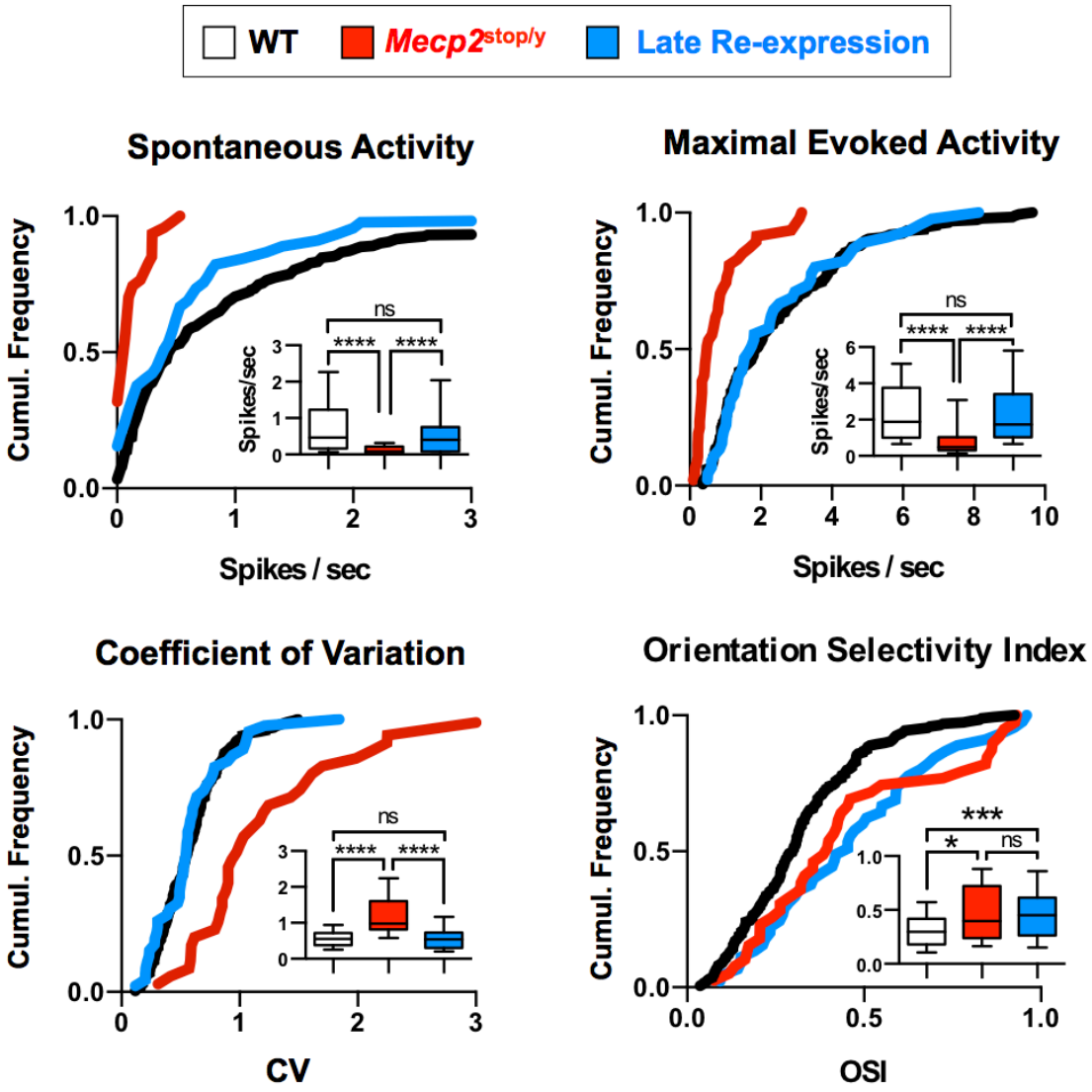

Figure 3.18 – Late Re-expression mice recovered proper cortical function by P105

Spontaneous activity, evoked activity, and coefficient of variation of V1 excitatory single units in Late Re-expression mice were statistically similar to P105 WT and significantly different from P105 *Mecp2*$^{stop/y}$ mice.

However, orientation selectivity was significantly increased at P105 in Late Re-expression and *Mecp2*$^{stop/y}$ mice as compared to WT.

WT: n=16 mice, 199 cells. *Mecp2*$^{stop/y}$: n=9 mice, 69 cells. Late Re-expression: n=45 cells, 5 mice. Kruskal-Wallis with Dunn's Test (* $P \leq 0.05$, *** $P \leq 0.001$ **** $P \leq 0.0001$).

Mecp2$^{stop/y}$ mice and not different from WT mice (Fig. 3.19, Fig 3.20a). Performance on the behavioral optomotor task was also improved compared to *Mecp2*$^{stop/y}$ mice (Fig. 3.20b). Therefore, de-silencing MeCP2 after the visual critical period staved off the progressive loss of vision observed in both *Mecp2*$^{stop/y}$ and *Mecp2*-null mice (Durand et al., 2012).

In the thalamus, desegregation of *Mecp2*$^{stop/y}$ retinal inputs to the LGN only became significantly different from WT mice around P105. Nevertheless, re-expression of MeCP2 beginning at P35 proved sufficient to prevent such desegregation seen in *Mecp2*$^{stop/y}$ mice (Fig. 3.21).

Discussion

These experiments indicate that key features of cortical circuit function can be recovered if at least 70% of WT MeCP2 protein levels can be re-expressed. Other features, such as PV hyperconnectivity and the heightened orientation selectivity of V1 neurons, failed to be corrected at P105 in Late Re-expression mice. Although thalamocortical excitatory input usually establishes the orientation preference of V1 excitatory neurons, their orientation selectivity is sharpened by local, cortical inhibition (Liu et al., 2011). Specifically, augmented inhibitory PV input has been demonstrated to sharpen the orientation tuning of V1 pyramidal neurons in awake mice (Lee et al., 2012). The enduring hyperconnectivity of inhibitory PV cells at P105 in both *Mecp2*$^{stop/y}$

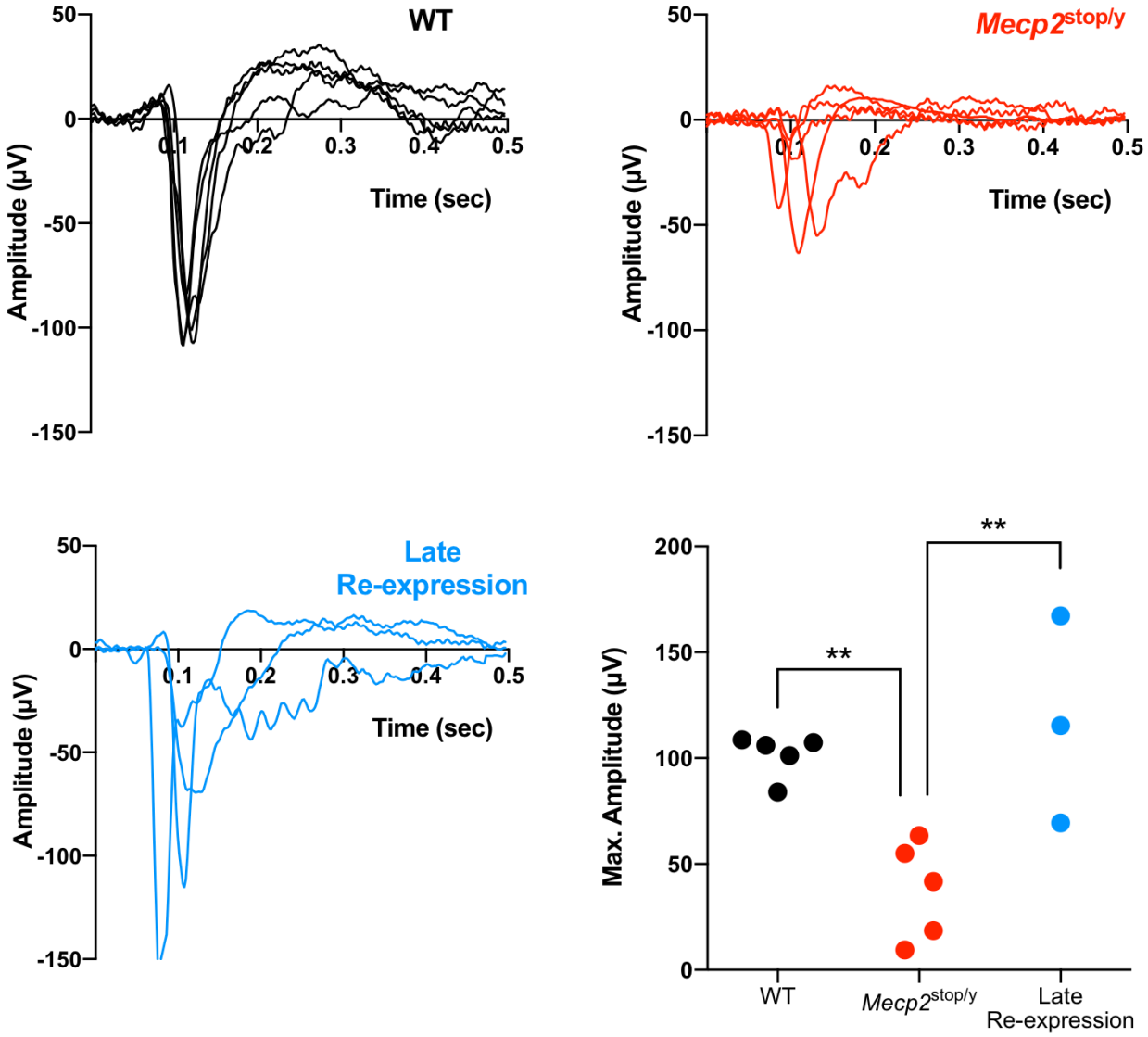

Figure 3.19 – VEP waveform is significantly improved in Late Re-expression mice at P105

VEP responses to 0.05 cycles per degree (cpd) gratings measured at P105. One averaged waveform for each animal is graphed for each genotype. WT: n=5 mice, *Mecp2*$^{stop/y}$: n=5 mice, Late Re-expression: n=3 mice

The amplitude of the main negative component of the VEP is quantified in the scatter plot on the bottom-right. Both WT and Late Re-expression maximal amplitudes were significantly higher than those of *Mecp2*$^{stop/y}$ mice. ANOVA with Holm-Sidak's Test (** $P \leq 0.01$).

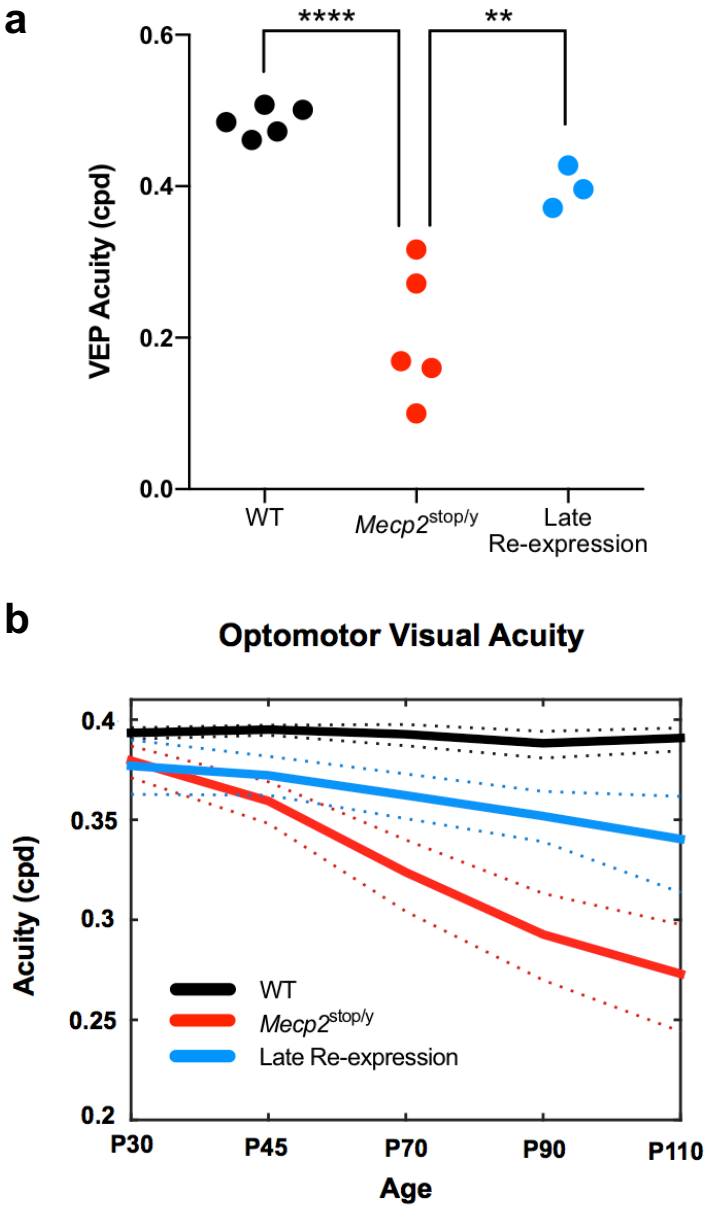

Figure 3.20 – Visual acuity is improved in Late Re-expression mice at P105

a. Acuity threshold was significantly higher in WT and Late Re-expression mice, as compared to the *Mecp2*$^{stop/y}$. ANOVA with Holm-Sidak's Test (** $P \leq 0.01$, **** $P \leq 0.0001$).

b. Late Re-expression mice exhibit higher acuity compared to *Mecp2*$^{stop/y}$ mice, but do not recover visual acuity to the same level as WT mice. WT: n=28-68 mice. *Mecp2*$^{stop/y}$: n=15-48 mice. Late Re-expression: n=5-18 mice. Dotted lines indicate 95% confidence interval.

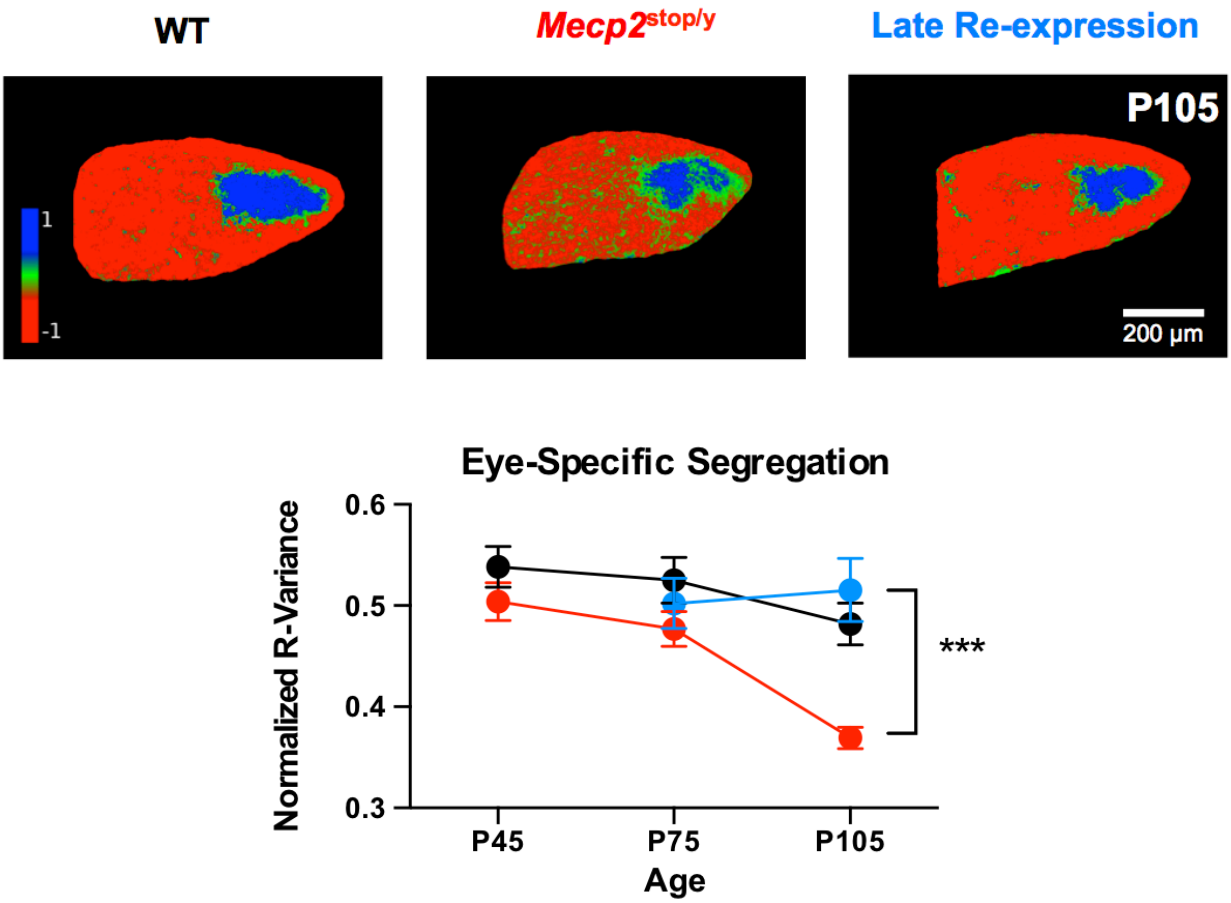

Figure 3.21 – De-segregation of eye-specific layers is counteracted in Late Re-expression mice

Eye-specific segregation in WT, Loxstop/y KO, and Late Re-expression mice. Fluorescently labeled contralateral and ipsilateral retinal projections in coronal sections of LGN show eye specific segregation of input from the retina. Images display these measurements in pseudo-colored R-values. In *Mecp2*$^{stop/y}$ mice, eye specific layers are desegregated by P105. Late re-expression of MeCP2 prevents this desegregation of retinal input at P105.

WT: n=27-39 sections. *Mecp2*$^{stop/y}$: n=24-45 sections. Late Re-expression: n=14-15 sections. Ages P27 – P36. Kruskal-Wallis with Dunn's Test (*** $P \leq 0.001$).

and Late Re-expression mice could potentially explain the abnormally increased orientation selectivity as compared to WT mice. In support of this hypothesis, when PV hyperconnectivity is rescued in *Mecp2*-null mice in response to chronic low-dose ketamine treatment (Patrizi et al., 2015), orientation selectivity is renormalized as well (data not shown). On the other hand, PV connectivity is augmented at P30 in *Mecp2*$^{stop/y}$ mice, yet they exhibit normal orientation selectivity at this age (Fig. 3.9, Fig. 3.10).

Despite retaining certain deficits, Late Re-expression cortices produced VEP waveforms that appeared much more akin to WT mice than *Mecp2*$^{stop/y}$ mice (Fig. 3.19). Although we only had three mice in our experimental group, we believe this robust effect could be explained by the pivotal role MeCP2 plays in synaptic scaling (Blackman et al., 2012; Qiu et al., 2012; Zhong et al., 2012). Once MeCP2 returns to the brain, it could effectively rebalance the excitatory/inhibitory inputs rather than directly modifying the connections themselves. Lastly, our results hint that cortical sensory circuits may be more sensitive to the absence/deletion of MeCP2 than subcortical structures. With regards to future Rett syndrome therapeutics, we are optimistic about the possibility for sensory system recovery after patients have undergone regression, but advocate remaining mindful of distinctions in regional sensitivity.

Contributions

This work was accomplished through the collaboration of the Fagiolini and Chen labs. Enchi Chang performed and analyzed the cortical thickness experiments (Figs. 3.2, 3.10, and 3.17), as well as the PV connectivity experiments (Figs. 3.3, 3.10, and 3.16). Matthew Taylor performed the eye-specific segregation experiments (Figs. 3.6, and 3.21). Chinfei Chen executed the *in vitro* analysis of the retinogeniculate synapse (Fig. 3.12). Georgia Gunner of the Neurodevelopmental Behavioral Core at Boston Children's Hospital assessed experimental mice with the rotarod test (Fig. 3.2) and the behavioral optomotor task (Figs. 3.6 and 3.20). Eleonora Centofante performed and the VEP experiments (Fig. 3.19 and Fig. 3.20). All other experiments were designed by Alex Simon, Michela Fagiolini and Chinfei Chen, and performed and analyzed by Alex Simon.

Chapter 4

Conditional re-expression of MeCP2 in an inhibitory circuit

Introduction

Accounting for roughly 20% of all cortical neurons, inhibitory interneurons exhibit a wide variety of morphological, physiological, and synaptic characteristics (Markram et al., 2004). Within this group exist GABAergic neurons that express parvalbumin (PV), a calcium-binding protein. These PV neurons comprise about half of all interneurons in the mouse cortex.

What function does this protein marker, parvalbumin, play in so-called PV cells? PV belongs to the EF-hand family of calcium binding proteins; it expresses two mixed Ca^{++}/Mg^{++} binding sites (Schwaller et al., 2002). In the brain, PV acts a slow buffer of cytosolic calcium, that modulation of which can exert an influence on neuronal firing (Bischop et al., 2012).

Along with somatostatin-positive interneurons, PV neurons tangentially migrate from the medial ganglionic eminence during early development and enter the developing cortex by E13 (Kepecs and Fishell, 2014; Wang et al., 2010). PV-positive neurons can be morphologically defined into two categories: chandelier cells and basket cells. While chandelier cells synapse onto the axon initial segment, PV-positive basket cells typically make $GABA_A$ receptor mediated perisomatic synapses on excitatory pyramidal neurons (DeFelipe et al., 1989; Fish et al., 2013; Katagiri et al., 2007). Cortical PV cells directly receive input from the thalamus and connect with other PV cells throughout the cortex via chemical synapses and gap junctions (Cruikshank et

al., 2007; Galarreta and Hestrin, 2002). Thus, PV neurons have the capability to detect sensory input, control pyramidal cell excitability, and synchronize the activity of entire neural networks (Huang, 2009; Somogyi et al., 1998).

Distinctively, these inhibitory parvalbumin-positive basket cells play a critical role regulating the timing of plasticity in visual cortex. The opening of the visual critical period is triggered by the maturation of cortical inhibitory circuitry. Mice in which inhibition remains immature (such as GAD65 KOs) fail to enter the critical period, while WT mice treated with diazepam enter the critical period precociously (Fagiolini and Hensch, 2000). Likewise, abnormally heightened PV activity in early development acts to prematurely trigger the visual critical period (Hensch and Fagiolini, 2005). Beginning at P15, *Mecp2*-null mice exhibit an accelerated functional maturation of parvalbumin interneurons, as indicated by elevated GABA synthetic enzymes, vesicular GABA transporter, perineuronal nets, and GABAergic transmission. Correlatively, timing of the critical period window for ocular dominance plasticity shifts ten days earlier in *Mecp2*-null mice (Krishnan et al., 2015).

In RTT mice, PV-related cellular and circuit abnormalities present themselves early in post-natal life, during the visual critical period. Arising by eye-opening, these issues become apparent before the vast majority of other RTT behavioral phenotypes. This initial disruption of PV interneurons could likely precipitate aberrations in other sensory circuits during this plastic time, resulting in enduring abnormal connectivity. In

the following studies, we selectively expressed *Mecp2* in PV cells in two separate *Mecp2*$^{stop/y}$ x PV-Cre mouse lines both controlled by the parvalbumin promotor. Perhaps by renormalizing the E/I milieu during the critical period, we could prevent the regression of visual and sensory function.

Results

The first PV-Cre line we examined was 2A-PV-Cre, where the *2A-Cre* sequence was inserted into the *PV* 3' untranslated region (Madisen et al., 2010). We crossed 2A-PV-Cre males with *Mecp2*$^{stop/x}$ females to create male mice that would express MeCP2 only in PV cells. Although the PV-2A-Cre line has previously been used to specifically manipulate MeCP2 expression in PV cells, we found that MeCP2 reactivation was not limited only to PV neurons (Goffin et al., 2014; Ito-Ishida et al., 2015). In fact, in *Mecp2*$^{stop/y}$ x 2A-PV-Cre mice, 31% of all neurons in visual cortex expressed measurable levels of MeCP2 at P30; only 5% of these neurons were PV+ (Fig. 4.1a). The extent of non-specific MeCP2 expression increased when analyzed again at P105 (Fig. 4.1a). Nevertheless, the vast majority of PV neurons did express MeCP2 in the *Mecp2*$^{stop/y}$ x 2A-PV-Cre mouse line, 76% of them by P30 (Fig. 4.1b).

Re-expression of MeCP2 in the 2A-PV-Cre mouse increased life span and prevented the progression of RTT phenotypic symptoms (Fig. 4.2a). *Mecp2*$^{stop/y}$ x 2A-PV-Cre mice demonstrated significant improvements on the accelerating rotarod task

compared to *Mecp2*$^{stop/y}$ mice, but only at the P110 time point (Fig. 4.2b). Optomotor visual acuity declined compared to WT, but was significantly better than *Mecp2*$^{stop/y}$ mice at multiple ages (Fig. 4.2c). Thus, when assessed behaviorally, *Mecp2*$^{stop/y}$ x 2A-PV-Cre mice represented an intermediate phenotype between WT and *Mecp2*$^{stop/y}$ mice. We then performed single-unit recordings in the visual cortex of these mice at

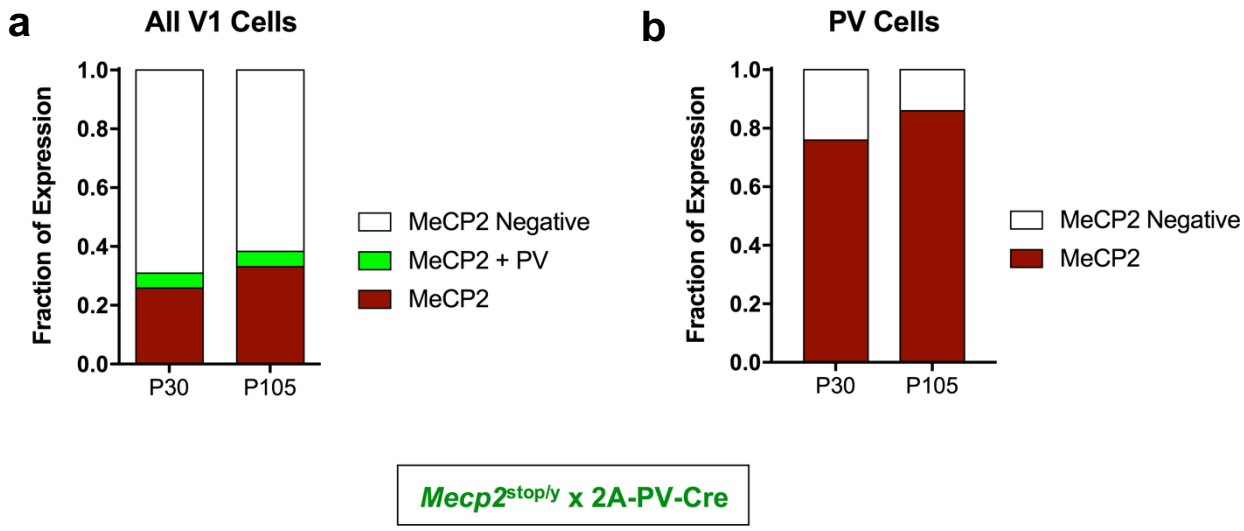

Figure 4.1 – In *Mecp2*$^{stop/y}$ x 2A-PV-Cre mice, 80% of PV cells express MeCP2, but many non-PV cells also express MeCP2

a. The fraction of all V1 neurons that express MeCP2, MeCP2 and PV, or do not express MeCP2 at all. 3 mice per age, 3 slices per mouse.

b. The fraction of PV cells in V1 that are MeCP2 positive or MeCP2 negative. 3 mice per age, 3 slices per mouse.

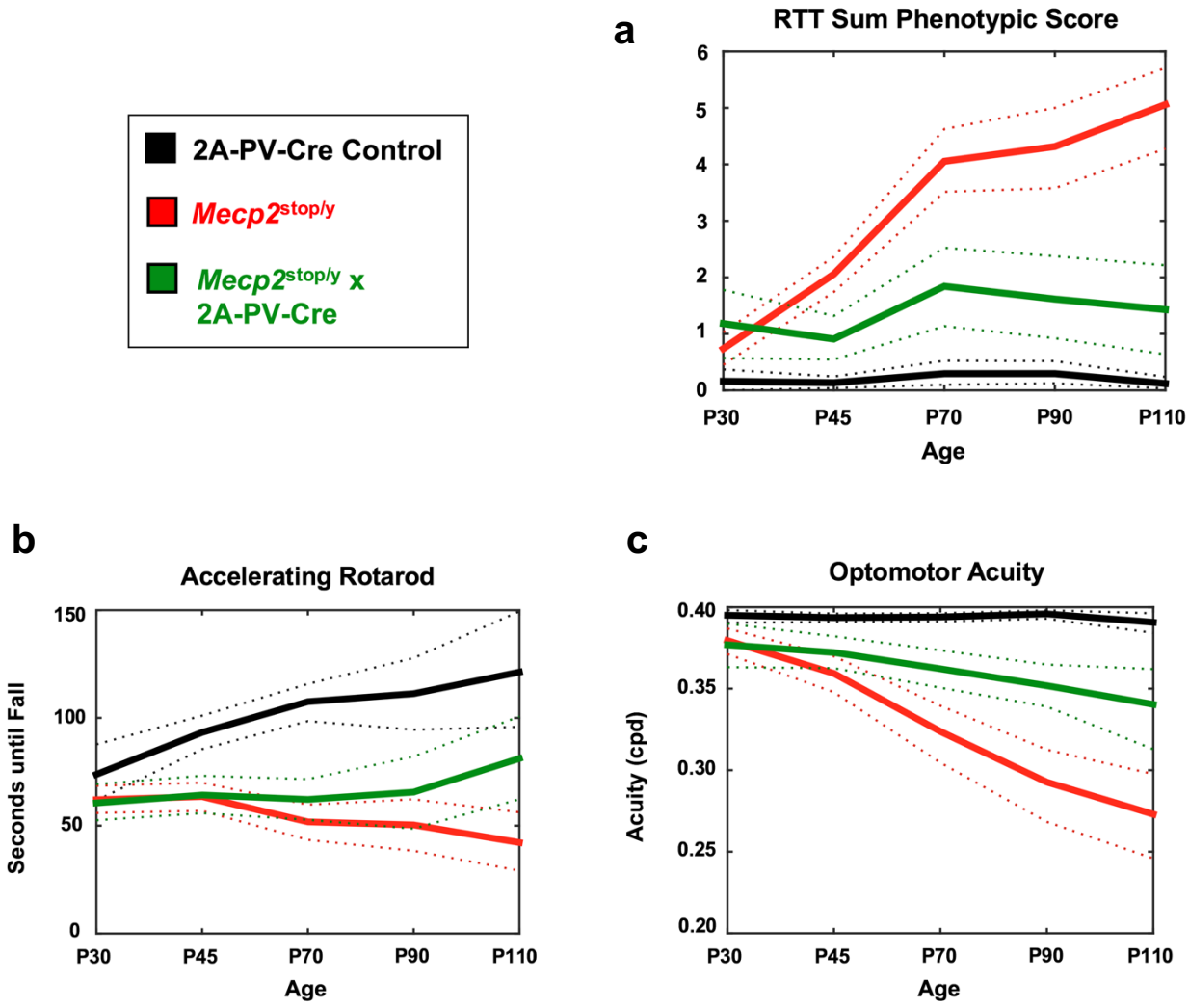

Figure 4.2 – RTT phenotypes are ameliorated in *Mecp2*$^{stop/y}$ x 2A-PV-Cre mice

a. The phenotypic progression of Rett syndrome symptoms was hampered in *Mecp2*$^{stop/y}$ x 2A-PV-Cre mice.

b. Performance on the accelerating rotarod task.

c. Performance on the optomotor acuity task.

2A-PV-Cre Control: n=9-26 mice. *Mecp2*$^{stop/y}$: n=11-24 mice. *Mecp2*$^{stop/y}$ x 2A-PV-Cre: n=9-26 mice. Dotted lines indicate 95% confidence intervals.

P105 to discern how individual neurons responded to semi-conditional PV expression of MeCP2. Similar to results from our Late Re-expression mice, which expressed MeCP2 everywhere in the brain, *Mecp2*$^{stop/y}$ x 2A-PV-Cre mice exhibited normal levels of spontaneous activity, evoked activity, and neuronal response reliability as measured by the coefficient of variation (Fig. 4.3). However, no differences in orientation selectivity between groups was observed. (Fig. 4.3). While we observed striking improvements in the function of *Mecp2*$^{stop/y}$ x 2A-PV-Cre animals, the non-specific expression of MeCP2 does not allow us to ascribe these benefits to PV neurons alone.

Our second attempt at conditional expression of MeCP2 in PV cells used the IRES-PV-Cre mouse, which we crossed like before with a *Mecp2*$^{stop/x}$ female (Hippenmeyer et al., 2005). Unlike the 2A-PV-Cre mouse, no MeCP2 was expressed outside of PV cells at P30 or P110 in *Mecp2*$^{stop/y}$ x IRES-PV-Cre mice (Fig. 4.4a). However, the fraction of PV cells that expressed MeCP2 at P30 was only 69%, meaning that some PV cells in visual cortex still lacked MeCP2 protein during the critical period (Fig. 4.4b).

Surprisingly, the behavioral phenotypes we observed in *Mecp2*$^{stop/y}$ x IRES-PV-Cre mice were dramatically different from their 2A-PV-Cre counterparts. These mice developed RTT phenotypes more quickly than *Mecp2*$^{stop/y}$ animals that express no MeCP2 whatsoever (Fig. 4.5a). Their rotarod ability was identical to *Mecp2*$^{stop/y}$ mice,

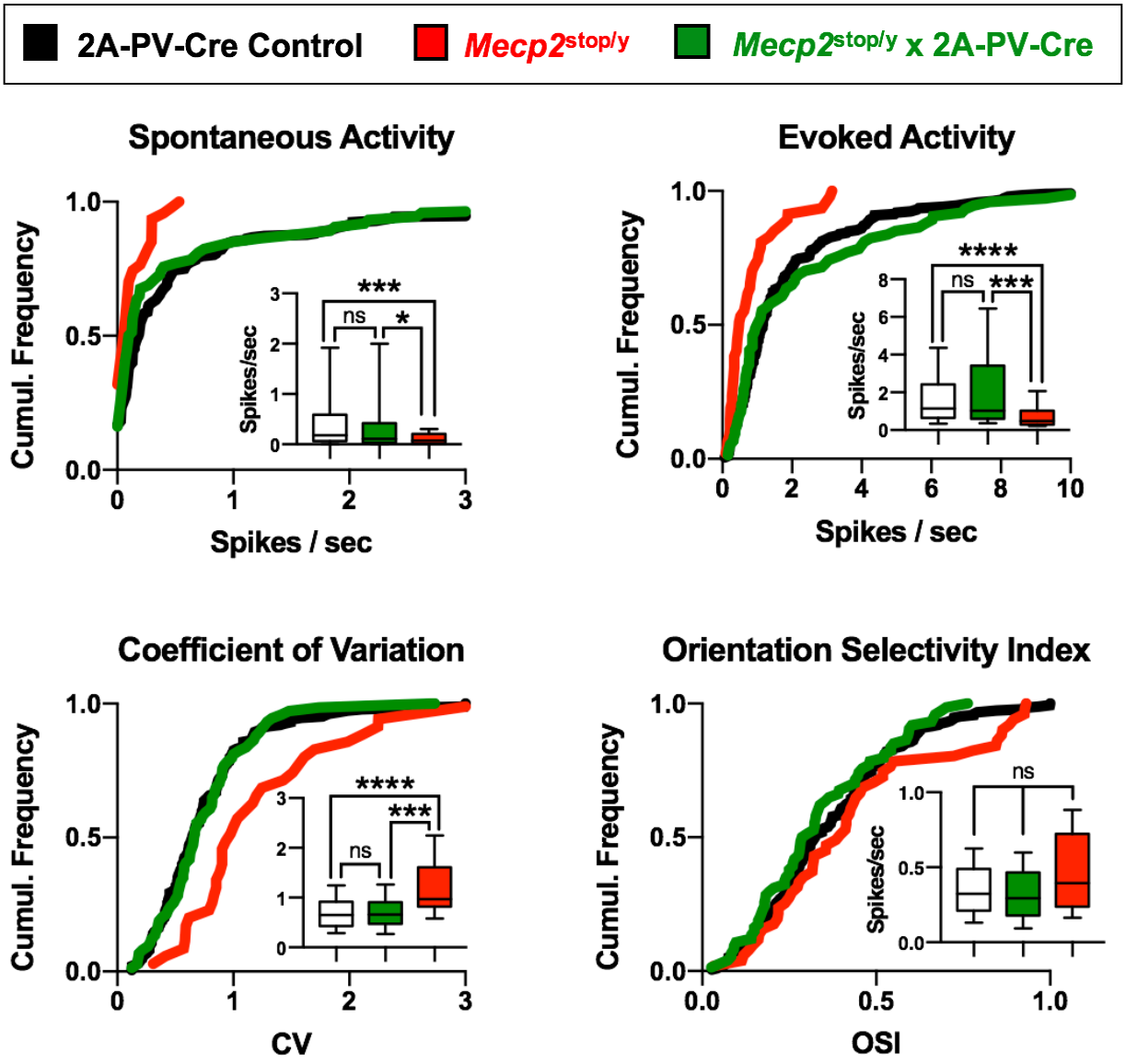

Figure 4.3 – Cortical function in *Mecp2*$^{stop/y}$ x 2A-PV-Cre mice is not significantly different from 2A-PV-Cre Control at P105

Spontaneous activity, evoked activity, and coefficient of variation of V1 excitatory single units in *Mecp2*$^{stop/y}$ x 2A-PV-Cre mice were statistically similar to 2A-PV-Cre Control mice and significantly different from *Mecp2*$^{stop/y}$ mice.

Orientation selectivity was not significantly different between groups.

2A-PV-Cre Control: n=6 mice, 106 cells. *Mecp2*$^{stop/y}$: n=9 mice, 69 cells. *Mecp2*$^{stop/y}$ x 2A-PV-Cre: n=74 cells, 4 mice. Kruskal-Wallis with Dunn's Test (* $P \leq 0.05$, *** $P \leq 0.001$ **** $P \leq 0.0001$).

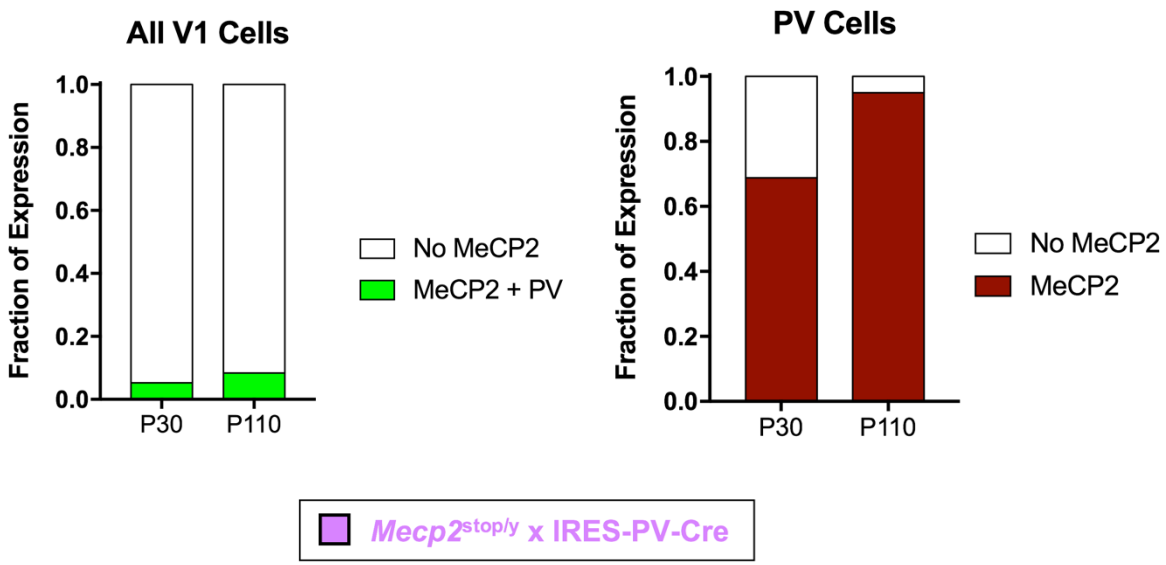

Figure 4.4 – In *Mecp2*$^{stop/y}$ x IRES-PV-Cre mice, MeCP2 expression in PV cells is specific

a. The fraction of all V1 neurons that express MeCP2 and PV, or do not express MeCP2 at all. 3 mice per age, 3 slices per mouse.

b. The fraction of PV cells in V1 that are MeCP2 positive or MeCP2 negative. 3 mice per age, 3 slices per mouse.

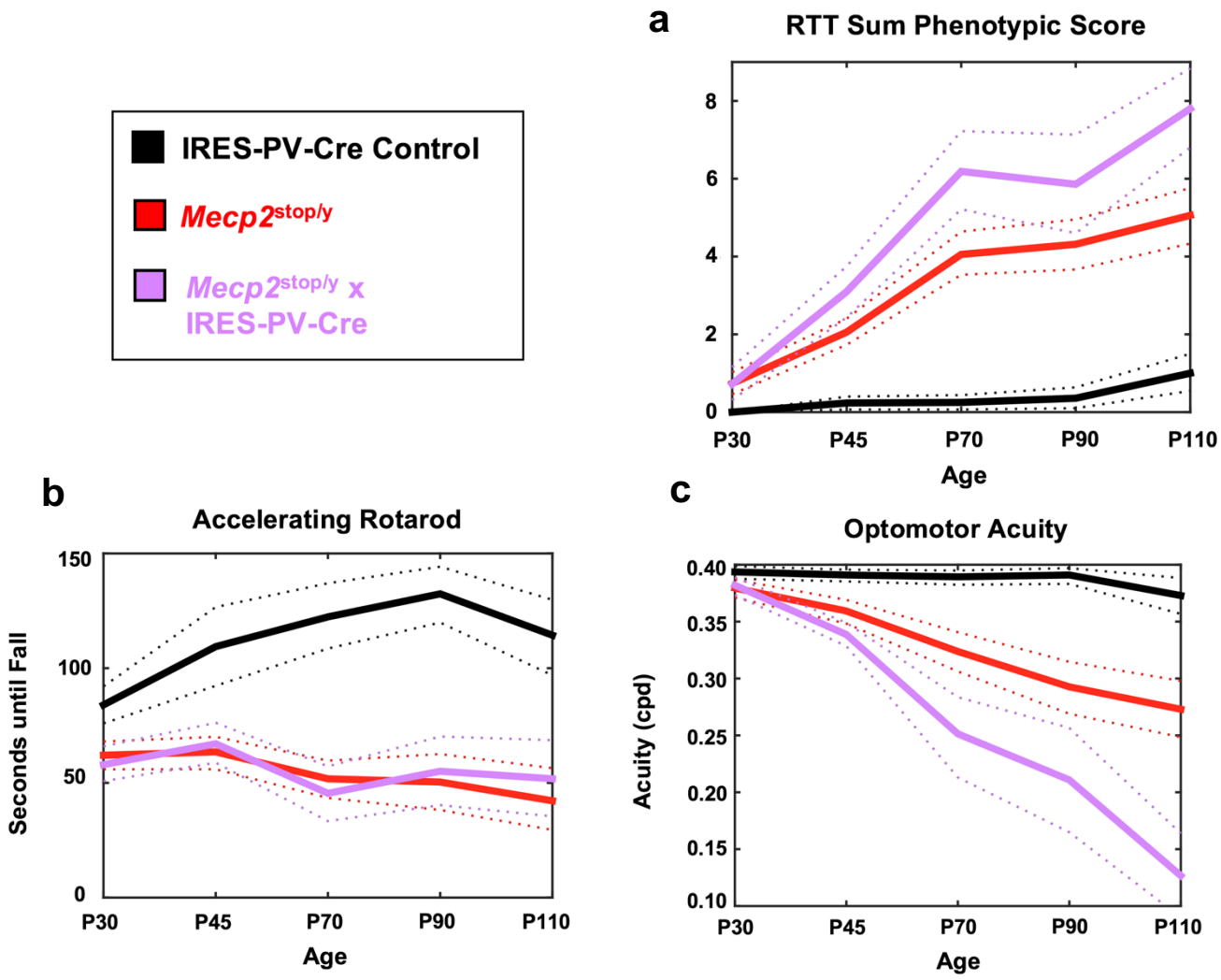

Figure 4.5 – RTT phenotypes are exacerbated in *Mecp2*$^{stop/y}$ x IRES-PV-Cre mice

a. The phenotypic progression of Rett syndrome symptoms was accelerated in *Mecp2*$^{stop/y}$ x IRES-PV-Cre mice.

b. Performance on the accelerating rotarod task.

c. Performance on the optomotor acuity task.

IRES-PV-Cre Control: n=13-17 mice. *Mecp2*$^{stop/y}$: n=11-24 mice. *Mecp2*$^{stop/y}$ x IRES-PV-Cre: n=10-20 mice. Dotted lines indicate 95% confidence intervals.

but their optomotor acuity regressed even faster than *Mecp2*$^{stop/y}$ mice (Fig. 4.5b,c).

Upon assessment of visual cortical function, we found that deficits on a cellular level did not necessarily correspond to the degree of physical regression. Although *Mecp2*$^{stop/y}$ x IRES-PV-Cre animals were outwardly unhealthier than *Mecp2*$^{stop/y}$ mice, their cortical function was significantly improved by comparison. With regards to spontaneous activity, evoked activity, and response reliability, *Mecp2*$^{stop/y}$ x IRES-PV-Cre mice represented a statistically significant intermediate phenotype (Fig. 4.6). Interestingly, PV cell-specific MeCP2 expression prevented the abnormal increase in orientation selectivity observed in *Mecp2*$^{stop/y}$ mice at P105 (Fig. 4.6). Notably, this receptive field property was not rescued when we globally re-activated MeCP2 after the critical period in Late Re-expression mice (Fig. 3.18). These results suggest that properly functioning PV cells are necessary early in life to ensure that appropriate orientation selectivity continues into adulthood.

Discussion

Both PV-Cre models we tested have their associated caveats. Although the 2A-PV-Cre mouse may begin expressing MeCP2 earlier than the IRES-PV-Cre mouse, the MeCP2 protein is not restricted to PV cells. Conversely, the IRES-PV-Cre mouse is specific for PV neurons, but MeCP2 expression does not reach maximal levels until

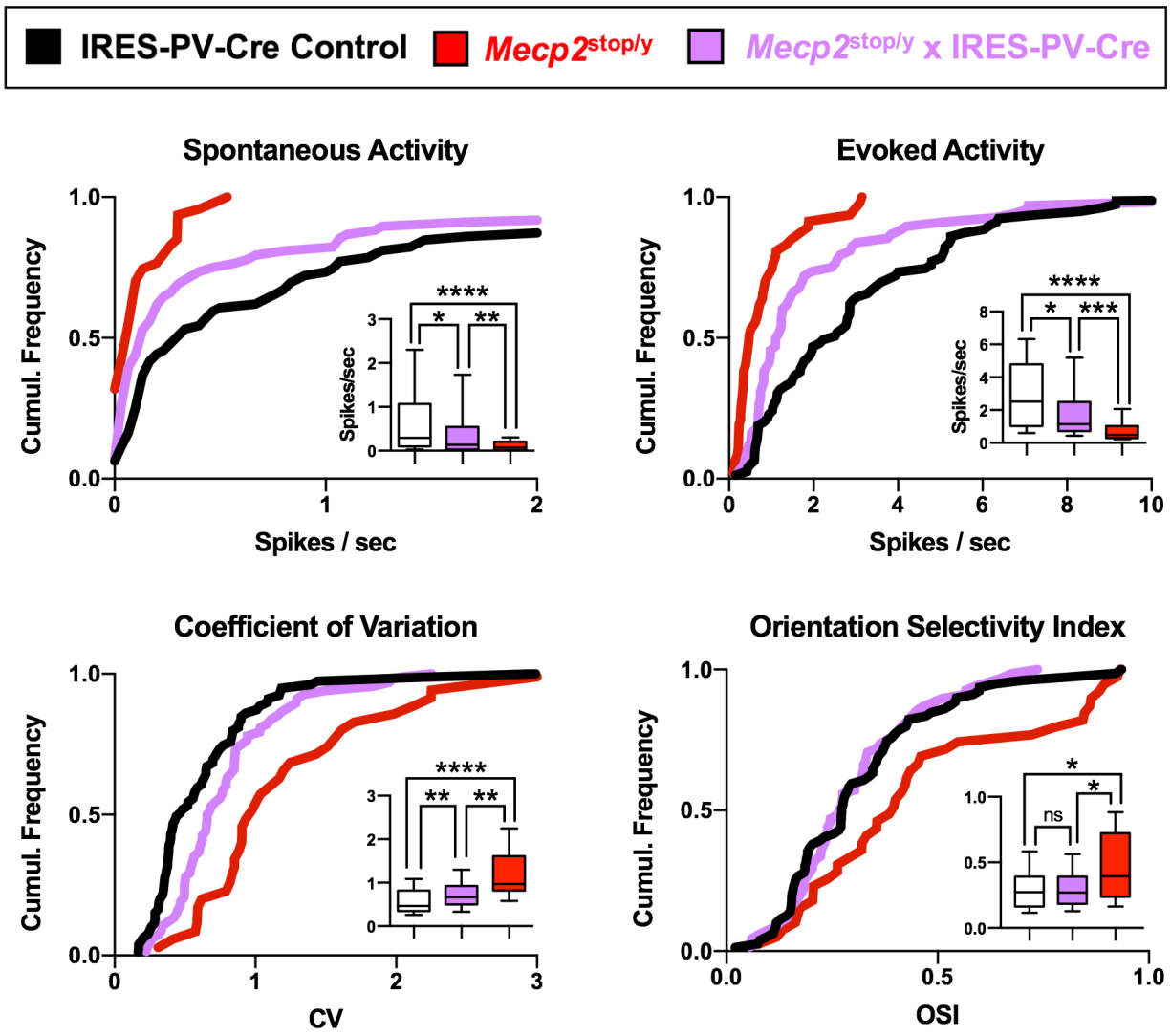

Figure 4.6 – *Mecp2*$^{stop/y}$ x IRES-PV-Cre mice express an intermediate cortical function phenotype in V1

Spontaneous activity, evoked activity, and coefficient of variation of V1 excitatory single units in *Mecp2*$^{stop/y}$ x IRES-PV-Cre mice were statistically different from both to IRES-PV-Cre Control mice and *Mecp2*$^{stop/y}$ mice.

Orientation selectivity of *Mecp2*$^{stop/y}$ x IRES-PV-Cre neurons were statistically similar to IRES-PV-Cre Controls.

IRES-PV-Cre Control: n=5 mice, 79 cells. *Mecp2*$^{stop/y}$: n=9 mice, 69 cells. *Mecp2*$^{stop/y}$ x IRES-PV-Cre: n=6 mice, 68 cells mice. Kruskal-Wallis with Dunn's Test (* $P \leq 0.05$, ** $P \leq 0.01$, *** $P \leq 0.001$ **** $P \leq 0.0001$).

P60-P90. Consequently, its unfeasible to use these mouse lines to investigate the potential for renormalizing the timing window of the ocular dominance critical period. One alternative for circumnavigating these concerns would be using a Dlx5/6-Cre line. This Cre line expresses only in developing and mature cortical interneurons, and does so from birth; thus, PV neurons are guaranteed to express MeCP2 before the critical period begins.

The central dogma for conditional Rett syndrome mouse models states that any type of additional MeCP2 conferred onto a *Mecp2*-deficient mouse should prove beneficial to their health provided it doesn't exceed WT levels (Chao and Zoghbi, 2012). However, the behavior observed in *Mecp2*$^{stop/y}$ x IRES-PV-Cre mice marks the first instance—to our knowledge—of cell-specific MeCP2 expression exacerbating RTT symptoms.

Contributions

In this chapter, Nathalie Picard recorded and analyzed the *Mecp2*$^{stop/y}$ x 2A-PV-Cre mice, Enchi Chang analyzed the immunohistochemistry, and the behavioral analyses were performed by Georgia Gunner of the Neurodevelopmental Behavioral Core at Boston Children's Hospital. All other experiments were designed by Alex Simon and Michela Fagiolini, and performed by Alex Simon.

Chapter 5

A mass spectrometry based analysis of NMDA receptor dysregulation in Rett syndrome

Introduction

The NMDAR (*N*-methyl-D-aspartate receptor) confers neurons with the capability for neurotransmission and synaptic plasticity. Functional NMDARs consist of two NR1 subunits and two NR2 or NR3 subunits, which form into a dimer of dimers *in vivo* (Paoletti, 2011). In particular, the NR2A and NR2B subunits have proven crucial for learning, memory, and regulation of synaptic plasticity. These two subunits exhibit distinct biophysical properties and couple to unique intracellular signaling cascades (Kim et al., 2005; Vanhoutte and Bading, 2003; Vicini et al., 1998).

During early post-natal development in mammals, NMDARs at excitatory synapses transition from NR2B-containing to NR2A-containing, which sharpens currents and restricts calcium influx. This process gradually tilts the synaptic balance from plasticity to stability (Dumas, 2005). Interfering with this 2A-to-2B transition will, by consequence, compromise the normal induction of plasticity during the visual critical period (Cho et al., 2009; Fagiolini et al., 2003).

Aberrant cortical NMDAR development has been previously reported in post-mortem studies from Rett syndrome patients (Blue et al., 1999). However, improper regulation of the NR2A and NR2B subunits has been best described in *Mecp2*-null mice. Multiple studies report that mRNA transcripts of the NMDAR subunits, NR2A and NR2B, are globally dysregulated in the *Mecp2*-deficient brain (Chahrour et al., 2008; McGraw et al., 2011), as well as specifically in the visual system (Durand et al.,

2012; Lee et al., 2008). In the primary visual cortex, NMDAR dysregulation manifests as an augmentation of the NR2A/NR2B ratio as measured by mRNA levels (Durand et al., 2012). Also in V1, *in vitro* electrophysiological data reveals cell-type specific disruptions in the 2A-to-2B transition. In pyramidal cells, this process occurs prematurely, while in PV cells, the transition is delayed (Mierau et al., 2014). These NMDAR irregularities may very well explain why *Mecp2*-null mice exhibit abnormal critical period timing and impaired visual processing (Durand et al., 2012; Krishnan et al., 2015).

Fortunately, certain techniques exist for re-normalizing NMDAR subunits. One *in vivo* method known to decrease the synaptic NR2A/NR2B ratio involves dark rearing, since visual experience modulates NMDAR subunit composition in an activity-dependent manner (Quinlan et al., 1999). When *Mecp2*-null mice are dark reared, the ratio of NR2A/NR2B mRNA transcripts in visual cortex is corrected that of a WT mouse (Durand et al., 2012). Strikingly, this dark-rearing manipulation completely prevents the regression of visual acuity that *Mecp2*-null experience. These visual deficits can similarly be corrected by creation of an *Mecp2*-null / *NR2A*-heterozgous mouse (Durand et al., 2012).

This recovery of a complex circuit function such as vision by manipulation of NMDAR subunits warrants further study since no drug treatment is currently available that prevents the loss or allows the recovery of brain function in RTT. Moreover, the NMDAR receptor represents an accessible membrane target for drug intervention

strategies in opposition to cumbersome *MECP2* gene therapy treatments (Gadalla et al., 2013; Garg et al., 2013). In fact, recent studies in mice have successfully used sub-anesthetic doses of the NMDAR antagonist ketamine to ameliorate RTT syndrome phenotypes, extend life span, and improve cortical processing and sensorimotor gating (Kron et al., 2012; Patrizi et al., 2015).

Identifying innovative strategies for pharmaceutical therapies requires a complete dissection of NMDAR subunit composition across the levels of transcription, translation, and post-translational modification (PTM). Thus far, aberrations of NMDAR subunit expression in RTT have only been quantified on the mRNA level in visual cortex. A precise analysis of protein quantity is crucial as mRNA levels are not necessarily consonant with protein levels (de Sousa Abreu et al., 2009). Furthermore, despite their extensive modification, the C-terminal domains of the NR2A and NR2B subunits have yet to be examined in RTT. Occurring predominately in the form of phosphorylation (Chen and Roche, 2007), PTMs on these intracellular residues are significant as they A) determine the composition of the intracellular NMDAR associated protein complex and B) modify the trafficking of NMDARs, thus controlling the types of NMDARs present at the synapse (Petralia et al., 2009). Numerous small molecules are presently available that target the kinases and phosphatases that regulate these potentially abnormally modified residues in *Mecp2*-null animals. Ergo, once identified,

these drugs could immediately be deployed in studies to rescue and reverse RTT phenotypes.

To elucidate NMDAR dysfunction in RTT, we employed a combination of traditional Western blot and mass spectrometry-based methods such as isotope-free spectral counting (Steen et al., 2005). We decided to focus our studies at P30, when the health of *Mecp2*-null mice begins to regress.

Results

From single-channel properties to signaling pathways, NMDAR subunit composition exerts significant effects on neuronal function and also the circuits in which these neurons are connected. Thus, understanding NMDAR subunit protein expression remains critical for understanding the etiology of visual processing deficits in *Mecp2*-null mice.

To this end, we probed visual cortical lysates from P30 WT and *Mecp2*-null mice for NR2A, NR2B, and NR1 (the obligate NMDAR subunit). We found no significant changes in NR1 or NR2B levels, but did measure a 20% increase in NR2A protein (Fig. 5.1). To analyze NR2A and NR2B with mass spectrometry (MS), we isolated the proteins from the same lysates using immunoprecipitation (IP). Following an in gel-digest, these samples were run on a mass spectrometer and subunit abundances were quantified by means of spectral counting and signal intensity (Fig. 5.2) (Steen et al., 2005). In

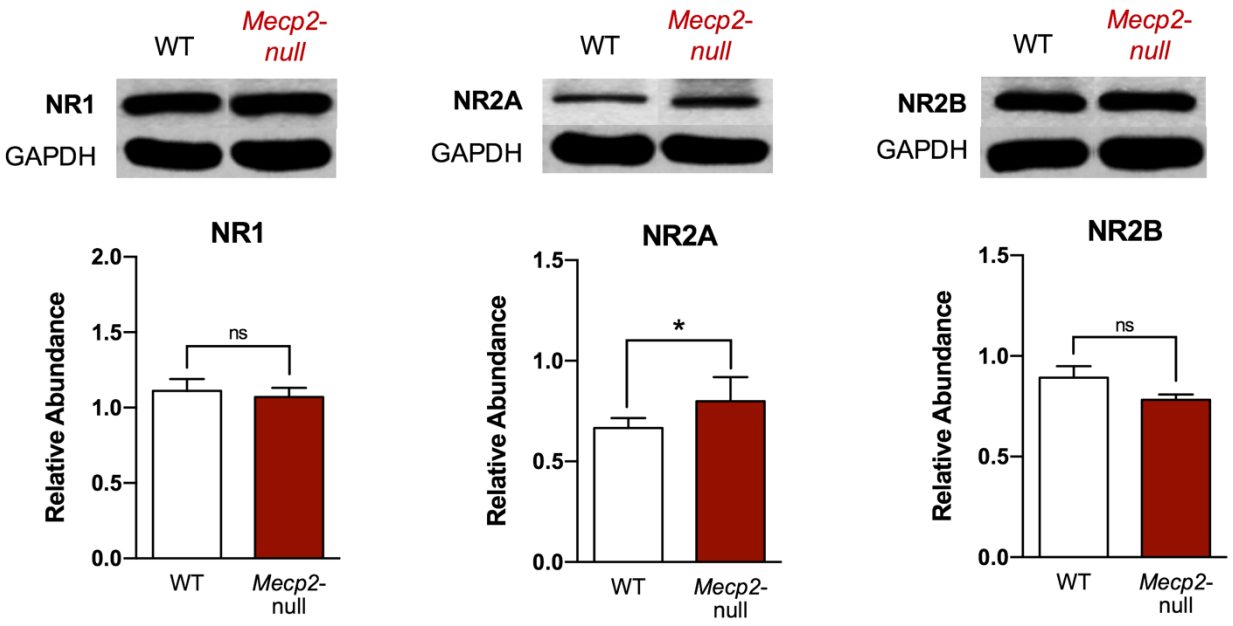

Figure 5.1 – Altered NMDA receptor subunit regulation in P30 *Mecp2*-null mice

Western blot data from visual cortex lysates demonstrates significantly higher NR2A levels in *Mecp2*-null mice, while NR1 and NR2B levels in visual cortex lysates are similar between genotypes. 6 animals per group, Mann-Whitney (* = $P \leq 0.05$).

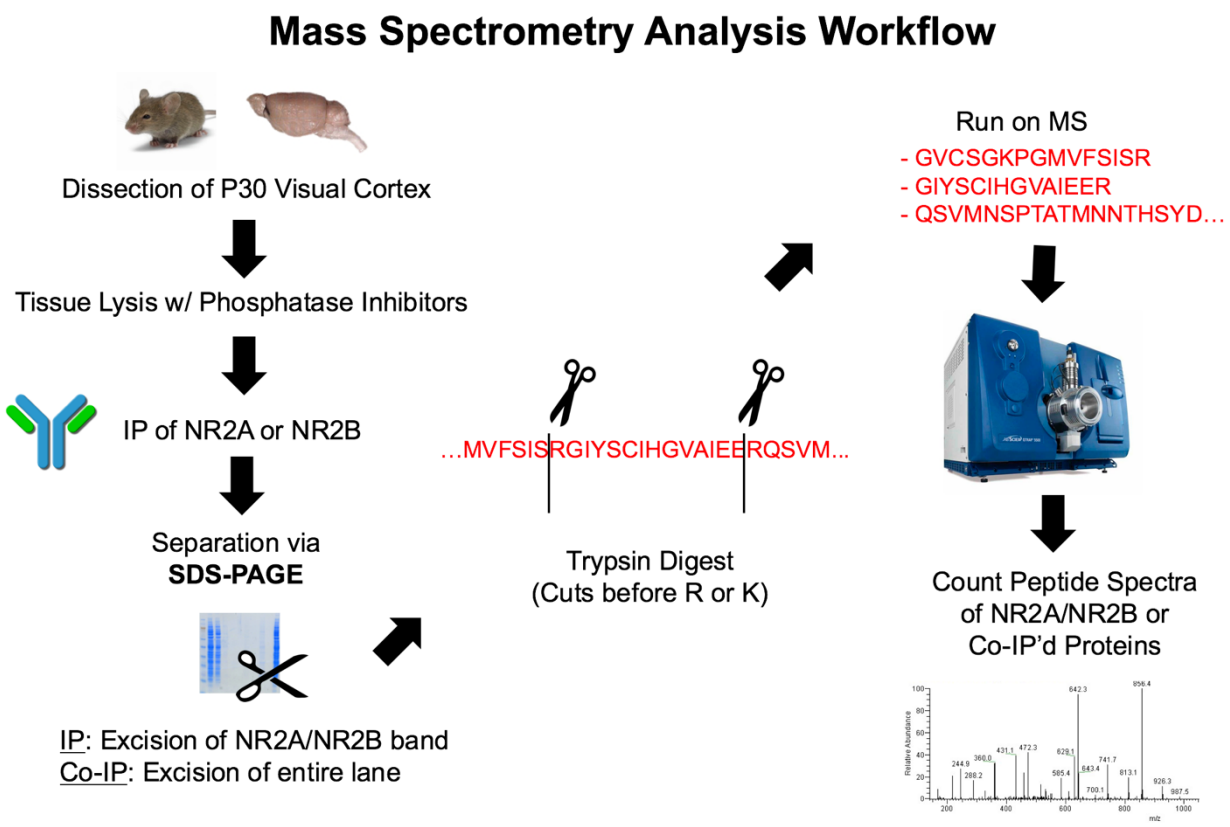

Figure 5.2 – Illustrative workflow of sample preparation for mass spectrometry

In this workflow we can digest and analyze just the NR2A or NR2B protein by excising that particular gel band after separation with SDS-PAGE. Alternatively, by excising the entire lane, we can measure the assortment of synaptic proteins that co-immunoprecipitate with either NR2A or NR2B.

accordance with our Western blot data, NR2A protein abundance was increased 20% in the *Mecp2*-null mouse's visual cortex, while NR2B protein levels remained constant (Fig. 5.3a). Additionally, we measured how much NR1 protein was co-immunoprecipitated (Co-IP) with either NR2A or NR2B, and confirmed again that NR1 levels were not altered in P30 *Mecp2*-null mice (Fig. 5.3b).

Beyond just NMDAR subunits, with mass spectrometry we can analyze the entire complement of proteins that Co-IP with either NR2A or NR2B to gain insight into the NMDAR-associated synaptic complex. Appropriately, we found that a wide range of synaptically localized proteins Co-IP with NR2A and NR2B (Fig. 5.4a). Of the 40 most abundant Co-IP'd proteins, six of them were expressed at aberrant levels (Fig. 5.4b). Interestingly, two of these down-regulated proteins, Shank 2 and Shank 3 are associated with autistic spectrum disorders (Chen et al., 2014). Additionally, cyclin dependent kinase-like 5 (CDKL5) was significantly decreased in the NR2A Co-IP and increased in the NR2B Co-IP from *Mecp2*-null mice. Patients with mutations in the *CDKL5* gene express a symptomology that's exceptionally similar to girls with RTT syndrome (Kilstrup-Nielsen et al., 2012). These synaptic disruptions suggest an interrelated molecular origin of the 'autistic' sensory system.

To date, no studies have investigated differences in NMDAR post-translational regulation in RTT. As these sites represent potential pharmacological targets, reporting this type of regulation is critical for designing new treatments. With an unbiased MS-

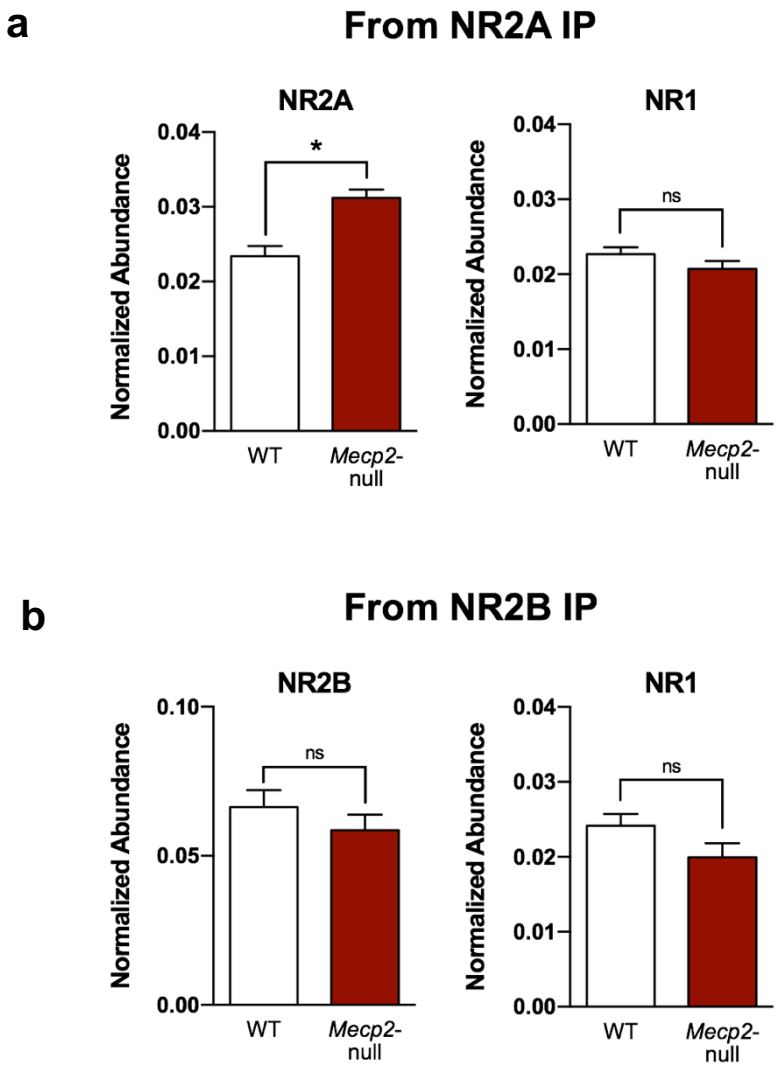

Figure 5.3 – Spectral counting data shows dysregulation of NR2A in P30 *Mecp2*-null mice

a. The number of normalized mass spectra of NR2A peptides observed are greater in *Mecp2*-null mice than WT. The number of mass spectra observed for NR1 peptides in a NR2A co-immunoprecipitation are not different between WT and Mecp2 KO. 6 Biological Repetitions, 2 Technical Repetitions, Mann-Whitney (* = $P \leq 0.05$).

b. The number of normalized mass spectra of NR2B and NR1 peptides observed in an immunoprecipitation for NR2B are not different between WT and Mecp2 KO. 6 Biological Repetitions, 2 Technical Repetitions, Mann-Whitney (* = $P \leq 0.05$).

a

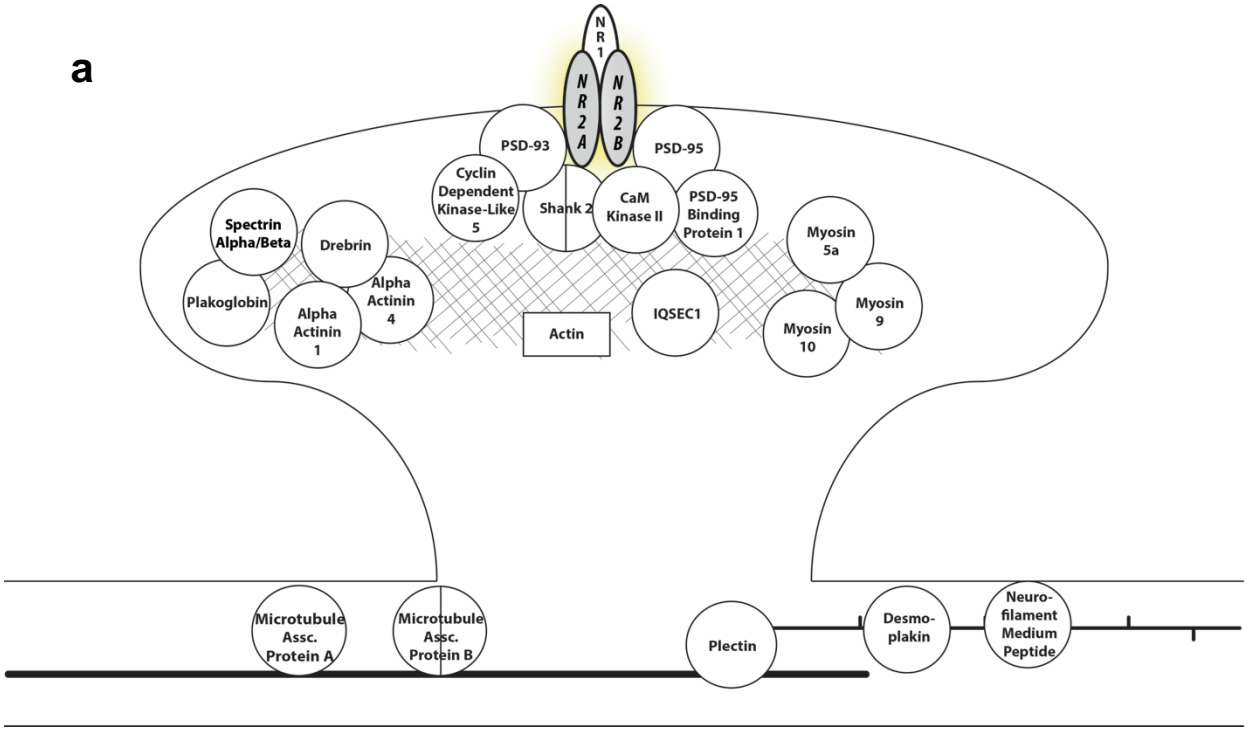

b

NR2A Co-IP	↑/↓	*Mecp2*-null / WT Ratio	SD
Cyclin Dependent Kinase-Like 5	↓	0.77	.10
Neurofilament Medium Polypeptide	↓	0.71	.12
Shank 2	↓	0.64	.17

NR2B Co-IP	↑/↓	*Mecp2*-null / WT Ratio	SD
Cyclin Dependent Kinase-Like 5	↑	1.6	.24
Spectrin Beta Chain	↓	0.36	.12
Shank 3	↓	0.65	.12
Myosin-10	↓	0.64	.13

Figure 5.4 – NR2 subunit co-immunoprecipitation uncovers abnormalities in the NMDAR-associated complex in *Mecp2*-null mice at P30

a. A range of synaptically co-localized proteins Co-IP with either NR2A or NR2B antibodies and are detected by mass spectrometry.

b. In *Mecp2*-null mice, 6/40 of the most abundant Co-IP'd proteins are dysregulated in either the NR2A or NR2B Co-IP. 6 Biological Repetitions, 2 Technical Repetitions, Mann-Whitney (* = $P \leq 0.05$).

based approach, we quantitatively measured individual, unmodified NR2A and NR2B peptides. Many of the peptides we analyzed were located on the C-terminal tail of NR2 subunits, where the vast majority of PTM occurs (Fig. 5.5). By normalizing for the total amount of NR2 protein, we compared the relative abundances of all the unmodified NR2 peptides for WT and *Mecp2*-null mice (Fig. 5.6). Importantly, we detect the unmodified version of the peptides with this MS analysis; consequently, a reduction in the levels of unmodified peptide is accounted for by an increase in the levels of modified (phosphorylated) peptide.

We detected 22 total peptides from the NR2A protein and 38 total peptides from the NR2B protein in both WT and *Mecp2*-null samples. Of these 60 total unmodified peptides, 5 *Mecp2*-null peptides differed in abundance from WT, and all were located on the intracellular C-terminal tail. Thus, while we can't state exactly which residue is phosphorylated on these peptides, we can confirm that one or more residues are undergoing modification to a significantly greater or lesser extent in the *Mecp2*-null mouse.

Across all 5 peptides, there were two phosphorylation sites that have been reported to have biological significance for NMDAR function: NR2B-S1303 and NR2B-Y1336 (Raveendran et al., 2009; Wu et al., 2007). We opted to interrogate the NR2B peptide containing S1303 (#34: QHSYDTFVDLQK), since phosphorylation at this site

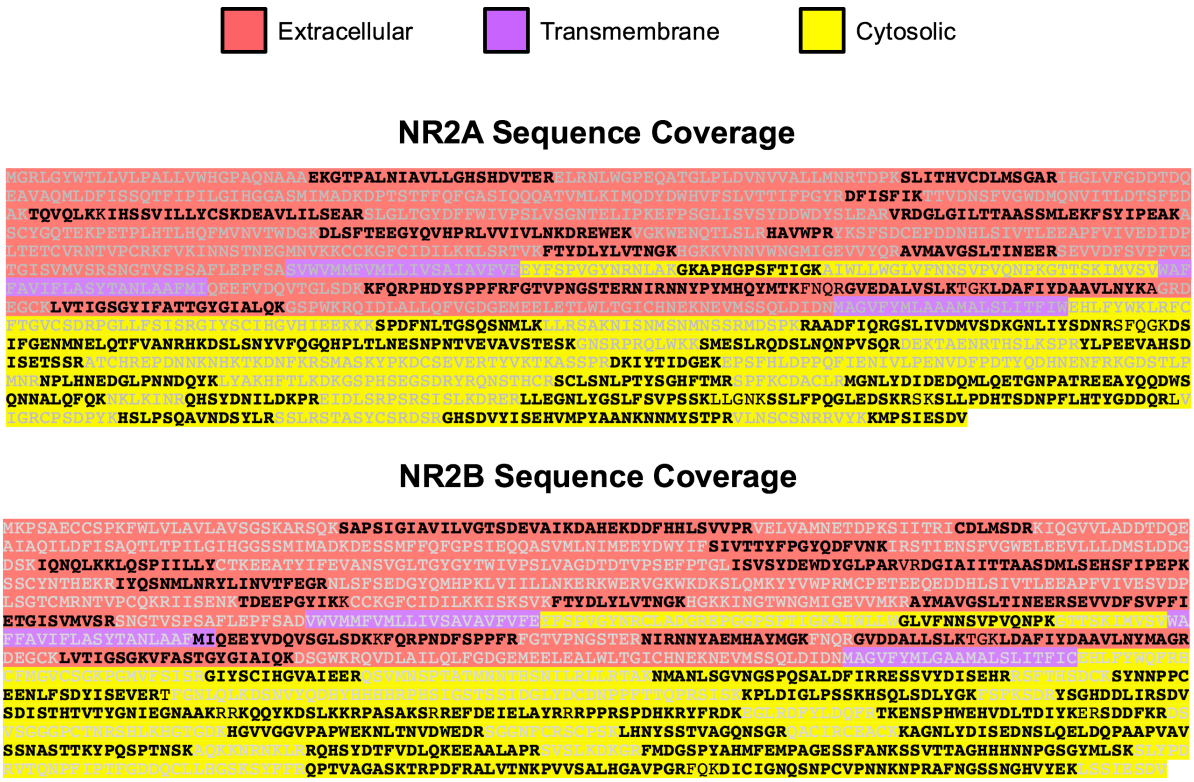

Figure 5.5 – Many peptides in the C-terminal domains of NR2A and NR2B were detected by mass spectrometry in WT and *Mecp2*-null mice at P30

The intracellular C-terminal tails of NR2A and NR2B contain numerous sites for post-translational modification. Bold lettering indicates sequence coverage.

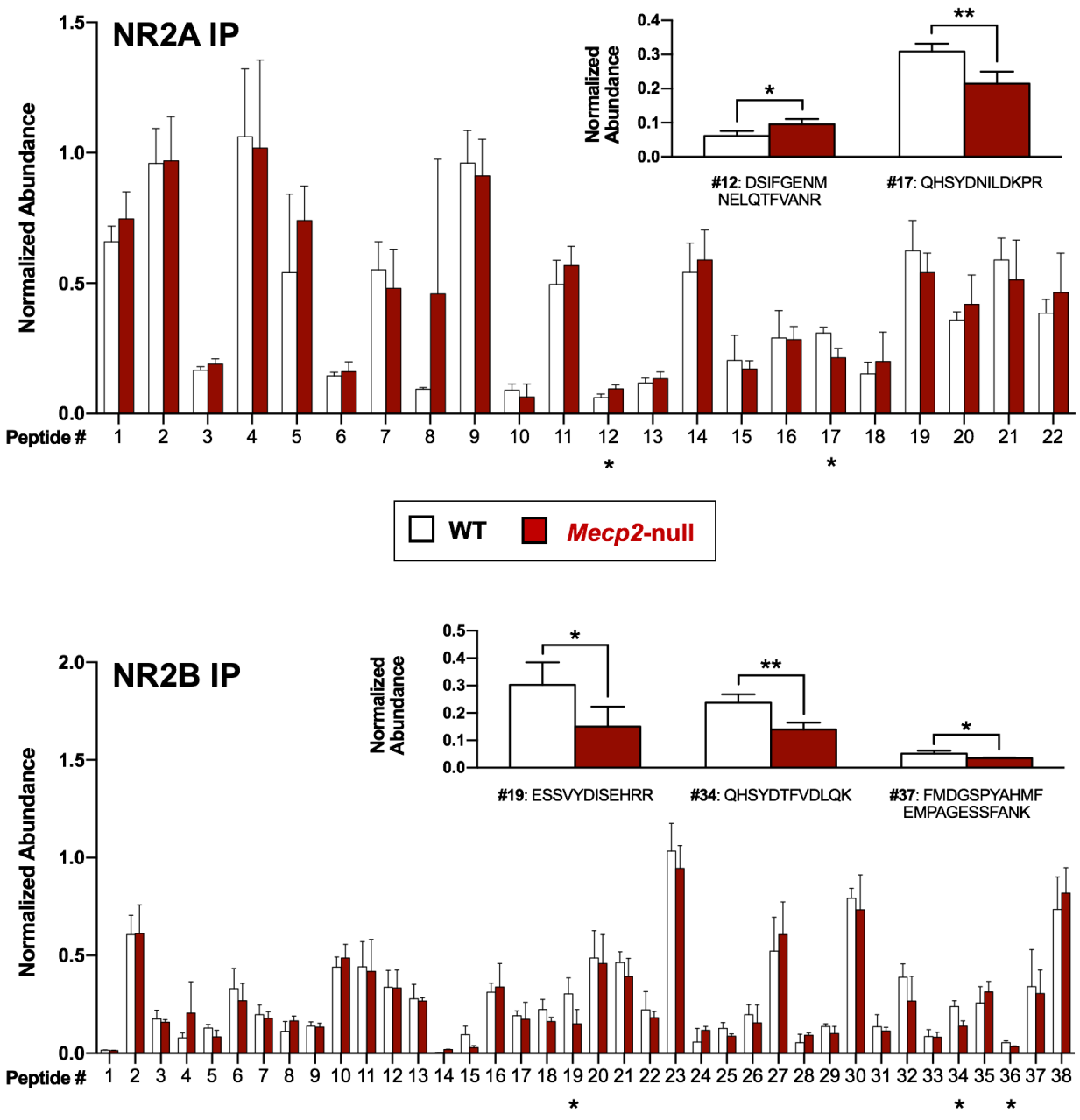

Figure 5.6 – At P30, a subset of NR2A and NR2B peptides were differentially modified in the visual cortex of *Mecp2*-null mice as measured by spectral counting

22 unmodified peptides of the NR2A protein and 38 unmodified peptides of the NR2B protein were detected by MS and quantified by spectral counting in both WT and *Mecp2*-null samples. 2 peptides from NR2A and 3 peptides from NR2B were differentially modified in WT and *Mecp2*-null mice (asterisk below number, and enlarged with sequence above). 6 Biological Repetitions, 2 Technical Repetitions, Mann-Whitney (* = $P \leq 0.05$, ** = $P \leq 0.01$).

plays a critical role regulating the trafficking of NMDARs to and from the post synaptic density (Sanz-Clemente et al., 2013). The spectral counting data demonstrated that *Mecp2*-null mice express reduced quantities of unmodified peptide #34: QHSYDTFVDLQK (Fig 5.6) To replicate this result with enhanced rigor, we compared the levels of peptide #34 from our samples to a known amount of a synthetic stable isotope labeled AQUA (Absolute QUAntification) peptide that possessed the same sequence as the S1303-containing unmodified endogenous peptide (Gerber et al., 2003). By comparing our experimental sample to a known internal standard, we used the AQUA peptide to confirm that the levels of unmodified peptide #34 on NR2B were reduced (Fig. 5.7a).

Ideally, we could use MS to directly detect the pS1303 phosphorylation on peptide #34, rather than extrapolate its presence based upon the absence of the unmodified peptide. However, the signal for this phospho-peptide was too weak to be consistently measured. Nevertheless, we had the capability to measure the extent of phosphorylation at this site with a phospho-specific antibody for NR2B-pS1303. When we performed this experiment with visual cortical lysates, we indeed found that S1303 is phosphorylated to a much higher degree in *Mecp2*-null mice than in WT mice (Fig. 5.7b). Other critical phosphorylation sites on NR2B that regulate NMDAR trafficking, such as Y1472 and S1480, were not impacted in *Mecp2*-null mice at P30 (Fig. 5.8) (Salter et al., 2009).

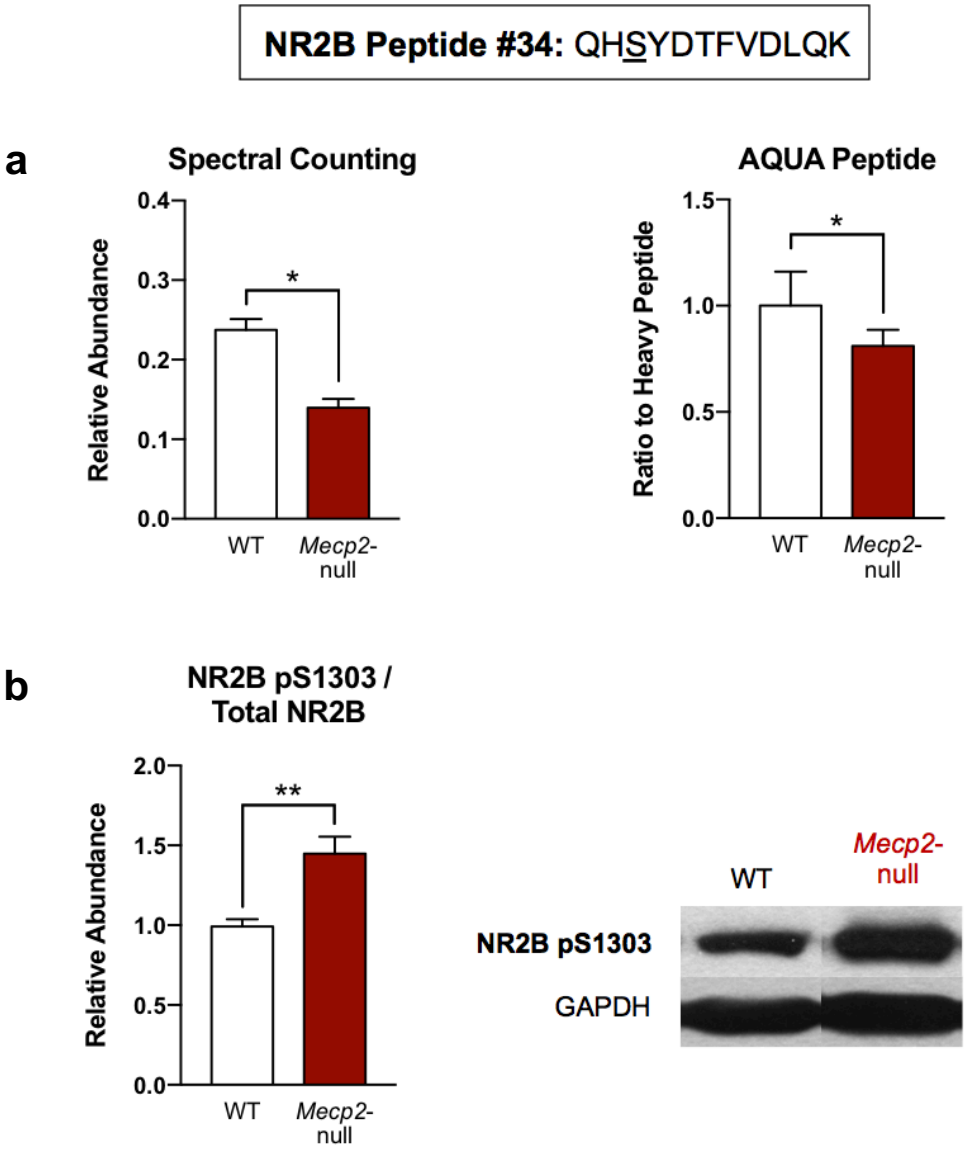

Figure 5.7 – S1303 phosphorylation on the NR2B subunit was augmented in *Mecp2*-null mice at P30

a. *Left*: the abundance of unmodified peptide #34 spectra was decreased two-fold in the Mecp2-*null* sample, indicating a greater extent of post-translational modification. 6 biological repetitions, 2 technical repetitions. *Right*: Similarly, AQUA peptide data demonstrated a significant reduction in the total amount of unmodified peptide. 3 biological samples, 2 technical repetitions, Mann-Whitney (* = $P \leq 0.05$).

b. Western blot data shows the ratio of pS1303-NR2B / Total NR2B was increased in *Mecp2*-null mice. 9 animals per group, Mann-Whitney (** = $P \leq 0.01$).

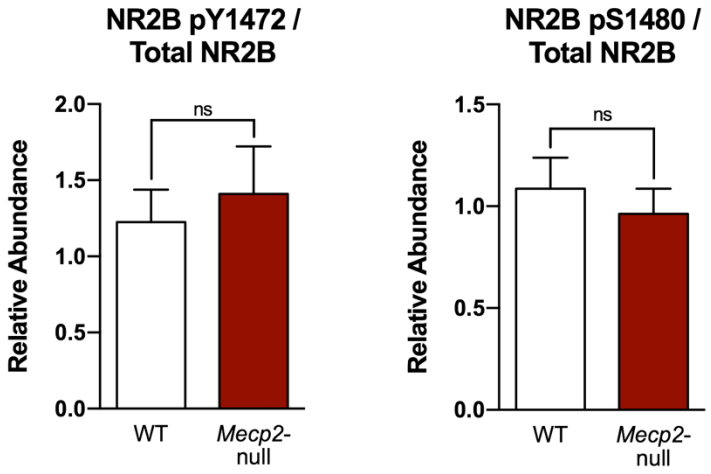

Figure 5.8 – In P30 *Mecp2*-null mice, phosphorylation is not altered at two other C-terminal residues involved with receptor trafficking

Western blot data did not demonstrate an increase in the ratio of pY1472 / Total NR2B nor pS1480 / Total NR2B in *Mecp2*-null mice at P30. 4 animals per group.

Phosphorylation of NR2B at S1303 is understood to promote synaptic maintenance of the NMDAR by repulsing the binding of CaMKII (Sanz-Clemente et al., 2010). Thus, in *Mecp2*-null mice, we'd expect more NR2B to be present at synapses in the visual cortex. To test for this possibility, we used array tomography to label visual cortical sections with NR2A/NR2B, PSD-95, and synaptophysin. In P30 *Mecp2*-null mice, we observed an increase in both NR2A and NR2B receptor subunits at synaptic sites (Fig. 5.9).

Discussion

Increased synaptic NR2A would be expected since the levels of NR2A protein are increased at P30 in *Mecp2*-null mice. However, NR2B protein levels appear equal between wild-type and *Mecp2*-null visual cortices, which hints that the aberrant over-expression of synaptic NR2B may be engendered by improper post-translational modification. In typical brain function, an NMDAR begins the process of lateral diffusion and internalization when CaMKII binds both NR2B and casein kinase 2 (CK2) (Sanz-Clemente et al., 2013). Creation of this tri-molecular complex allows casein kinase 2 to phosphorylate NR2B-S1480, a modification which abrogates the NMDAR's association with synaptic MAGUK proteins and promotes clathrin-mediated endocytosis through Y1472's endocytic motif (Fig. 5.10) (Prybylowski et al., 2005).

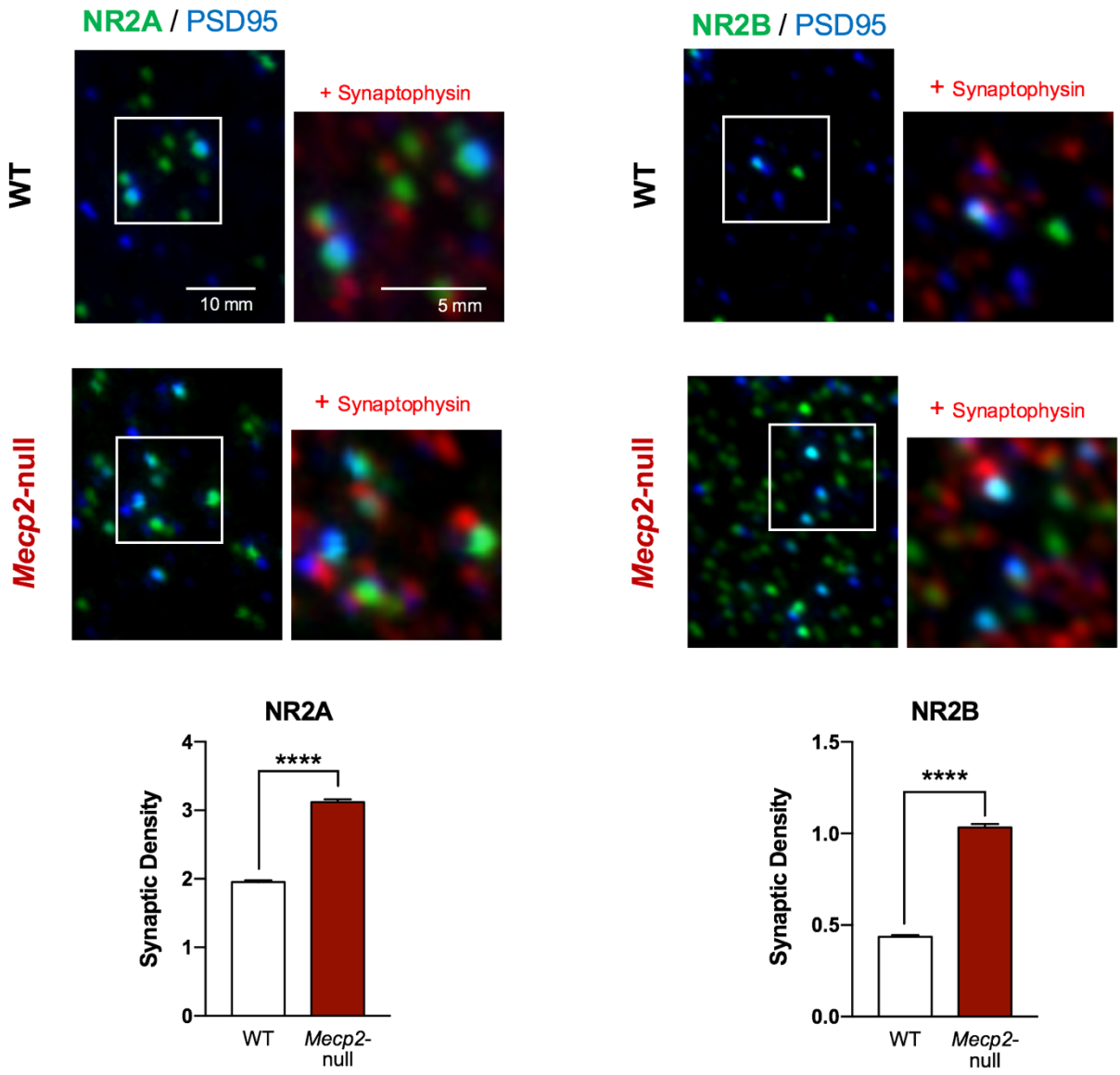

Figure 5.9 – *Mecp2* deficiency alters NMDAR subunit composition at visual cortical synapses at P30

Upper: representative array tomography sections from visual cortex stained for NR2A (left) and NR2B (right) for co-localization with PSD-95 (blue, post-synaptic marker) and synaptophysin (red, pre-synaptic marker) in wild-type (top row) and *Mecp2*-null (bottom row) mice at P30.

Lower: Bar graphs show quantification of the NR2A (left) and NR2B (right) synaptic density in layer 2/3 visual cortex of WT and *Mecp2*-null mice. Mann-Whitney (**** = $P \leq 0.0001$)

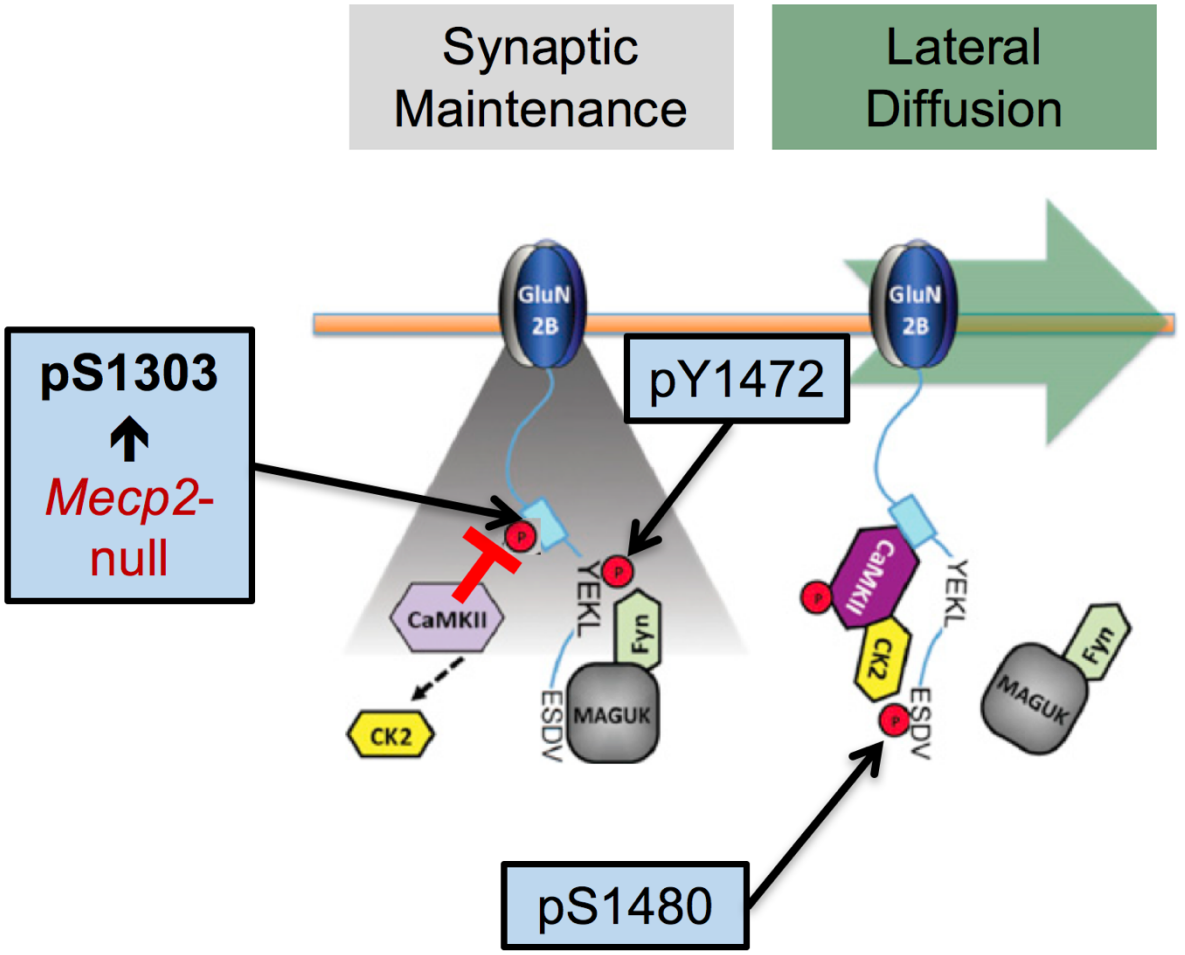

Figure 5.10 – A model for NR2B trafficking by post-translational modification

CaMKII initiates the endocytotic process by binding to the region of NR2B surrounding pS1303. Once bound, CaMKII recruits casein kinase 2 (CK2) in order to create a tri-molecular complex wherein CK2 gains the ability to phosphorylate S1480. After S1480 is modified, NR2B breaks away from MAGUKs and Fyn kinase, the latter responsible for phosphorylating Y1472. Once Y1472 loses its phosphorylation status, the YEKL endocytotic motif signals for internalization via the clathrin adaptor complex AP-2.

In *Mecp2*-null mice, it appears that high levels of pS1303 phosphorylation promote the synaptic maintenance of NR2B-containing NMDARs, and hinder lateral diffusion and recycling.

Adapted by permission from Elsevier: Cell Reports Vol. 3 (2013)

Interestingly, although we uncovered no abnormalities with phosphorylation at Y1472 or S1480, we did record increased phosphorylation at S1303. Phosphorylation of this serine blocks NR2B's association with CaMKII and the ensuing internalization of the entire receptor, which could reasonably lead to increased synaptic expression of NR2B. Further experiments are required, likely by site-directed mutagenesis of the S1303 residue, to fully assess the contribution that this phosphorylation site makes to RTT-afflicted synapses.

Contributions

This project was enacted through the joint efforts of the Fagiolini and Steen labs. Waltraud Mair operated the mass spectrometer and analyzed the raw data, especially with regards to the AQUA peptides. Hui Chen performed the spectral counting analyses. Annarita Patrizi performed and analyzed the array tomography experiments. All other experiments were designed by Alex Simon and Michela Fagiolini, and performed by Alex Simon.

Chapter 6

Discussion

Conclusions and future directions

Employing a well-established sensory modality, which is linked to higher cognitive function, our work suggests that—even in adulthood—certain aspects of cortical circuits can be recovered following global re-expression of MeCP2. Specifically, re-activating *Mecp2* in early adulthood recovers the levels of spontaneous and evoked activity in visual cortex at P105 as well as neuronal response reliability. In the LGN, re-introduction of MeCP2 prevents the anatomical de-segregation of eye-specific layers observed at P105 in *Mecp2*$^{stop/y}$ mice.

On the other hand, features such as PV hyperconnectivity and the aberrantly heightened orientation selectivity of V1 neurons failed to be corrected at P105 in Late Re-expression mice. Notably, neurons do not require visual experience to develop orientation selectivity; dark-rearing mice from P0-P30 does not result in a significant reduction in the OSI (Espinosa and Stryker, 2012; Wang et al., 2010). However, in order to maintain proper OSI, mammals must be exposed to external visual stimulation (Crair et al., 1998; Fagiolini et al., 1994). When dark-reared from birth, mice exhibit reduced orientation selectivity upon assessment at P60 (Crair et al., 1998; Fagiolini et al., 1994; N. Picard, unpublished data). Perhaps MeCP2 only becomes required during this activity-dependent period, which would explain why the orientation selectivity index of *Mecp2*$^{stop/y}$ mice was not significantly different from WT at the P30 baseline. One group has suggested that a critical plasticity period for orientation selectivity occurs between

4-7 weeks (Yoshida et al., 2012). Late Re-expression mice only begin to express MeCP2 protein towards the end of this window, which may explain why this receptive field property did not renormalize in our paradigm.

An alternative explanation for the persistence of orientation selectivity deficits in P105 Late Re-expression mice implicates PV cells. Although thalamocortical excitatory input usually establishes the orientation preference of V1 excitatory neurons, their orientation selectivity is sharpened by local, cortical inhibition (Liu et al., 2011). Indeed, optogenetic activation of inhibitory PV cells *in vivo* has been demonstrated *to* sharpen the orientation selectivity of nearby excitatory cells, and also enhance orientation discrimination in awake behaving mice (Lee et al., 2012). At P105, we find that PV cell hyperconnectivity endures in both *Mecp2*$^{stop/y}$ and Late Re-expression mice, along with increased orientation selectivity compared to WT mice. In support of this correlation, when PV hyperconnectivity is rescued in *Mecp2*-null mice in response to chronic low-dose ketamine treatment (Patrizi et al., 2015), orientation selectivity is renormalized as well (N. Picard, unpublished data). Yet, this interconnection falters when we consider that P30 *Mecp2*$^{stop/y}$ mice exhibit PV hyperconnectivity, but a normal OSI.

Our *Mecp2*$^{stop/y}$ x IRES-PV-Cre mice may provide another angle from which we can contemplate the relationship between MeCP2, PV neurons, and orientation selectivity. In contrast with Late-Re-expression mice, the OSI of *Mecp2*$^{stop/y}$ x IRES-PV-Cre V1 excitatory neurons is not significantly different from controls. Thus, it appears

that conditional expression of MeCP2 in 70% of PV cells by P30 is sufficient to prevent the disruption of OSI displayed in *Mecp2*$^{stop/y}$ mice at P105. The 100% cell-type specificity of the IRES-PV-Cre line reiterates the importance of MeCP2 function in PV cells during the visual critical period for effectively maintaining the proper orientation selectivity of excitatory neurons throughout adulthood.

While we focused on relatively straightforward parameters for analyzing excitatory neuronal function in this study, numerous options exist for future researchers who wish to better understand the impact of re-introducing MeCP2 into sensory systems. One feature of visual processing which demands further investigation in RTT mice is binocular matching. Shortly after eye opening (~P15), neurons in the binocular zone of V1 respond to stimulation from both eyes; however, the orientation preference of the neuron differs depending on which eye receives the stimulus. Subsequently, during the critical period, visual experience corrects this mismatch so that binocular neurons become tuned to the same orientation from both eyes (Wang et al., 2010). Proper binocular matching underlies the formation of coherent visual perceptions.

Mecp2-null mice demonstrate deficient binocular matching when recorded at P35 (Krishnan et al., 2015). Afterwards, in adulthood, these inappropriately wired binocular neurons are considered to be permanently mismatched (Espinosa and Stryker, 2012). What effect would MeCP2 exert on improper binocular matching were it not re-activated until early adulthood, similar to the Late Re-expression mouse?

Diminished plasticity following the critical period would suggest that MeCP2 lacks the capability to—in adulthood alone—establish appropriate binocular matching, but the outcome should be determined empirically.

Other features of visual processing such as temporal frequency sensitivity and contrast sensitivity also warrant examination. Although not previously examined in *Mecp2*-deficient mice, it's well understood how these features typically develop in visual cortex, and vary by cortical layer (Gao et al., 2010; Niell and Stryker, 2008; Prusky and Douglas, 2004; Prusky et al., 2004). Measuring these parameters provides the opportunity to uncover novel deficits in RTT mice vision, and also to assess their potential for recovery in Late Re-expression mice.

By performing VEP recordings and testing mice in the optomotor chamber, we concluded that Late Re-expression animals exhibited significantly increased visual acuity compared to *Mecp2*$^{stop/y}$ mice. However, we did not confirm that these corrections resulted in improved perception in freely behaving mice. One possibility for obtaining a corroborative assessment of visual perception involves training mice for a computer-based discrimination task. In this test, a low-spatial frequency grating appears randomly on one of two monitors located at the wide end of an arena containing shallow water. Trained to swim towards the monitors, the mice choose the side with the grating in order to escape onto a submerged platform (Prusky et al., 2000). A comparable visual-discrimination task may also be performed through the use

of a touchscreen platform (Oomen et al., 2013). In this manner, we can disentangle whether we're recovering a basic response to a visual stimulus or rather enabling an improved conscious perception of the external world. Answering this question would provide insights into which visual circuits are responsible for the observed rescue of visual function in Late Re-expression mice.

Moving forward, improvements should be implemented to our methodology for recording the activity of individual V1 neurons in response to visual stimulation. During our *in vivo* extracellular recordings, the number of V1 neurons we could monitor was limited by the 15 units on our electrode. Furthermore, our experimental mice were lightly anesthetized during our recordings, rather than fully awake and moving freely. Locomotor activity is known to dramatically amplify the visually-evoked firing rate (Niell and Stryker, 2010). New techniques utilizing both GCaMP6 (a fluorescent calcium indicator) and two-photon excitation microscopy allow researchers to measure the response properties of ensembles of neurons in visual cortex. In one field-of-view, it becomes possible to simultaneously analyze the evoked activity and orientation selectivity of > 400 cells (Wekselblatt et al., 2016). In addition, the neurons in these mice can be individually measured and tracked across multiple time points, unlike anesthetized mice that undergo a terminal surgery prior to recording.

These experiments, as well as those performed in Chapter 3, should be repeated in heterozygous female mice to confirm that *Mecp2* re-expression elicits the

same response in a situation where it was previously mosaically expressed, rather than globally absent as in *Mecp2*$^{stop/y}$ mice. Since female RTT mice develop symptoms far more heterogeneously than their male counterparts, the point where late re-expression of MeCP2 begins should be determined by a phenotypic score threshold, rather than a pre-determined age (Lang et al., 2014). Intriguingly, we were unable to successfully re-express MeCP2 in *Mecp2*$^{stop/y}$ x Cre-ER mice at P60-P70; the tamoxifen injections were too injurious to an already disabled mouse, and resulted in death. On the other hand, the more gradual regression of an *Mecp2*$^{stop/x}$ female would afford a larger time window, during which we can investigate the possibility for circuit recovery. For instance, *Mecp2* re-expression prevented the desegregation of eye-specific layers in Late Re-expression mouse (Fig. 3.21). However, in female mice, we would likely have the opportunity to wait until the eye-specific layers desegregated in the LGN, at which point we could inject tamoxifen and determine if re-wiring the retinal-thalamic circuit was possible.

Mechanisms of MeCP2 rescue

Upon re-introducing MeCP2 in early adulthood, we witnessed a remarkable recovery of function in the visual system. Yet, the mechanisms by which MeCP2 promotes that recovery are difficult to trace due to its sheer abundance in the nucleus and its global binding of methylated DNA (Kinde et al., 2015; Skene et al., 2010).

Unraveling the regulatory relationship between MeCP2 and specific genes of interest was first attempted by performing chromatin immunoprecipitation assays to report where MeCP2 bound to gene promoters *in vivo*. Many of the MeCP2-targeted promoters are related to genes associated with synaptic plasticity, inhibition, sensory function, and other neurological disorders (Gibson et al., 2010; Jordan et al., 2007; Leong et al., 2015; Urdinguio et al., 2008). Microarrays can also detect dysregulation of RNA transcript abundance in *Mecp2*-null mice, although the sheer quantity and variety of abnormally expressed transcripts precludes the formation of a cohesive mechanism that explains RTT phenotypes (Urdinguio et al., 2008).

While the level of PV intensity was normalized in Late Re-expression mice at P105, the number of connections those PV cells make onto pyramidal soma remained improperly augmented. Nevertheless, despite enduring PV hyperconnectivity, the evoked and spontaneous activity of the pyramidal neurons increased significantly. Understanding parvalbumin's role as a calcium buffer in these neurons may help us explain this effect.

Although data remains scarce on how exactly PV modulates neuronal firing, reports from the basal ganglia demonstrate that increased levels of PV reduce the intrinsic excitability of PV cells (Bischop et al., 2012; Orduz et al., 2013). These data provide a compensatory rationale for explaining why the PV cells of *Mecp2*$^{stop/y}$ mice make an augmented number of synapses on pyramidal cell soma. PV cells also make

local PV-to-PV connections in visual cortex (Gonzalez-Burgos and Lewis, 2008). If PV cells were hypo-inhibited by each other, this would result in a global hyper-inhibition. In the rescue, reducing PV intensity should theoretically re-normalize the firing rate of PV neurons. The re-establishment of proper E/I balance—despite hyperconnectivity of PV input onto pyramidal soma—may relate to MeCP2's key role in homeostatic synaptic scaling in response to cortical activity levels.

Glutamate receptors are widespread throughout the cortex and hold responsibility for dynamically mediating the post-synaptic excitation of neurons. Strikingly, MeCP2 has been reported to regulate the development and expression of these receptors (Mierau et al., 2014). MeCP2 phosphorylation at S421, which results in the increase in metabotropic glutamate receptor 5 (mGluR5), is required for appropriate synaptic scaling in mouse hippocampal neurons (Zhong et al., 2012). Additionally, when disrupted, MeCP2 dysregulates the induction of the immediately early gene, Arc (Su et al., 2012). An activity-regulated cytoskeleton-associated protein, Arc typically controls the synaptic scaling of AMPA receptors (Rial Verde et al., 2006; Shepherd et al., 2006). MeCP2 is most directly linked to the AMPA receptor subunit, GluR2, since it binds to the promoter of the GluR2 gene and recruits a repressor complex to inhibit transcription of subunit (Qiu et al., 2012). Since the vast majority of cortical AMPARs incorporate GluR2, MeCP2 can exercise significant influence on AMPARs present at the synapse (Lu et al., 2009; Shi et al., 2001).

Notably, de-silencing of *Mecp2* in early adulthood prevents the eventual de-segregation of eye-specific layers observed in LGN at P105 in *Mecp2*$^{stop/y}$ mice (Fig. 3.21). One explanation for this recovery may implicate cortex's recently uncovered role as a regulator of retinogeniculate refinement. Contrary to the traditional ''feedforward'' model of sensory pathway development from retina to thalamus to visual cortex, feedback from layer 6 has been demonstrated to influence the experience-dependent refinement of retinogeniculate projections (Thompson et al., 2016). Indeed, the thalamus and cortex interact bidirectionally to fine-tune visual circuitry during development. In *Mecp2*$^{stop/y}$ mice at P30, we observed that functional and anatomical and functional deficits were present in the cortex, while the status of the LGN appeared comparatively intact. In MeCP2-deficient mice, early cortical deficits could consequently be responsible for driving the anatomical desegregation that ensues in LGN. Experiments that allowed for cortex-specific expression of MeCP2 using either a Telencephalon-Cre x *Mecp2*$^{stop/y}$ mouse or by injecting AAV-Cre into the visual cortex of *Mecp2*$^{stop/y}$ mice would allow us to elucidate the contribution that an MeCP2-deficient cortex.

Recommendations for therapy

By activating a previously silenced gene, our MeCP2 re-expression studies in male mice represent the ideal treatment to rescue Rett syndrome. For human patients,

however, the strategy for delivering active *MECP2* to impacted neurons is far less straightforward. Most RTT patients are female, meaning that their neurons express MECP2 in heterozygous mosaic fashion. Currently, no method exists for directing gene therapy vectors specifically to MECP2-absent cells. Over-expression of MeCP2 in healthy neurons results in dysfunction equally severe to MeCP2 under-expression (Chao and Zoghbi, 2012). For this reason, no clinical trials in human patients have been designed that utilize AAV-mediated delivery of *MECP2*.

Since *MECP2* gene therapy is not currently feasible for Rett syndrome, alternative options for treatment instead focus on downstream targets. One avenue which has proven attractive involves the targeting of NMDARs. Indeed, treatment of *Mecp2*-deficient mice with the NMDAR antagonist, ketamine, improves RTT phenotypes and cortical processing (Kron et al., 2012; Patrizi et al., 2015). Concerns arise when translating this therapy to human patients since ketamine affects not only NMDARs, but also cholinergic, aminergic, and opioid systems (Sleigh et al., 2014). Moreover, the half-life of ketamine is only three hours, which spells challenges for keeping patients within the therapeutic window without inducing anesthesia or psychotomimesis (Clements et al., 1982). For this reason, scientists are investigating stereoisomers of ketamine that retain its beneficial pharmaceutical profile, but do not evoke psychotomimetic side effects (Yang et al., 2015).

In conclusion, contemporary Rett syndrome therapeutics are caught between the intractability of gene therapy and the staggering diversity of potential downstream targets. Thus far, subcutaneous injection of Recombinant Human Insulin Growth Factor 1 (rhIGF) represents the middle ground as a neurotrophic factor that promotes cell survival, plasticity, and synaptic strengthening (Tropea et al., 2009). In October 2016, Neuren Pharmaceuticals will finish their Phase 2 trial using trofenitide, a novel small molecule derived from IGF-1 that can formulated as an oral medication. Likewise, a team at Boston Children's Hospital has recently completed a Phase 2 trial using rhIGF (mescasermin). The primary endpoint of the latter study is assessment by the 50-point Rett Syndrome Behavioral Questionnaire. During and after the rhIGF treatment period, parents rate each item from the questionnaire on a three-point scale: 0 (not true), 1 (somewhat or sometimes true), or 2 (very true) (Mount et al., 2002). Examples of items include "seems frightened when there are sudden changes in own body position" and "uses eye gaze to convey feelings, needs, and wishes." When data from this clinical trial emerges, we'll receive the first hints regarding whether sensory systems, and the social interactions they enable, can be recovered in human RTT patients.

References

Amir, R.E., Van den Veyver, I.B., Wan, M., Tran, C.Q., Francke, U., Zoghbi, H.Y., 1999. Rett syndrome is caused by mutations in X-linked MECP2, encoding methyl-CpG-binding protein 2. Nat. Genet. 23, 185–188. doi:10.1038/13810

Armstrong, D.D., 2005. Can we relate MeCP2 deficiency to the structural and chemical abnormalities in the Rett brain?, in: Brain and Development. doi:10.1016/j.braindev.2004.10.009

Asaka, Y., Jugloff, D.G.M., Zhang, L., Eubanks, J.H., Fitzsimonds, R.M., 2006. Hippocampal synaptic plasticity is impaired in the Mecp2-null mouse model of Rett syndrome. Neurobiol. Dis. 21, 217–227. doi:10.1016/j.nbd.2005.07.005

Ballas, N., Lioy, D.T., Grunseich, C., Mandel, G., 2009. Non-cell autonomous influence of MeCP2-deficient glia on neuronal dendritic morphology. Nat. Neurosci. 12, 311–317. doi:10.1038/nn.2275

Ballestar, E., Yusufzai, T.M., Wolffe, A.P., 2000. Effects of rett syndrome mutations of the Methyl-CpG binding domain of the transcriptional repressor MeCP2 on selectivity for association with methylated DNA. Biochemistry 39, 7100–7106. doi:10.1021/bi0001271

Bauman, M.L., Kemper, T.L., Arin, D.M., 1995. Pervasive neuroanatomic abnormalities of the brain in three cases of Rett's syndrome. Neurology 45, 1581–1586. doi:10.1212/WNL.45.8.1581

Bedogni, F., Cobolli Gigli, C., Pozzi, D., Rossi, R.L., Scaramuzza, L., Rossetti, G., Pagani, M., Kilstrup-Nielsen, C., Matteoli, M., Landsberger, N., 2015. Defects During Mecp2 Null Embryonic Cortex Development Precede the Onset of Overt Neurological Symptoms. Cereb. Cortex 1–13. doi:10.1093/cercor/bhv078

Bischop, D.P., Orduz, D., Lambot, L., Schiffmann, S.N., Gall, D., 2012. Control of Neuronal Excitability by Calcium Binding Proteins: A New Mathematical Model for Striatal Fast-Spiking Interneurons. Front. Mol. Neurosci. 5, 1–9. doi:10.3389/fnmol.2012.00078

Blackman, M.P., Djukic, B., Nelson, S.B., Turrigiano, G.G., 2012. A Critical and Cell-Autonomous Role for MeCP2 in Synaptic Scaling Up. J. Neurosci. 32, 13529–13536. doi:10.1523/JNEUROSCI.3077-12.2012

Blue, M.E., Naidu, S., Johnston, M. V., 1999. Development of amino acid receptors in frontal cortex from girls with Rett syndrome. Ann. Neurol. 45, 541–545. doi:10.1002/1531-8249(199904)45:4<541::AID-ANA21>3.0.CO;2-2

Calfa, G., Percy, A.K., Pozzo-Miller, L., 2011. Experimental models of Rett syndrome based on Mecp2 dysfunction. Exp. Biol. Med. (Maywood). 236, 3–19. doi:10.1258/ebm.2010.010261

Cardoza, B., Clarke, A., Wilcox, J., Gibbon, F., Smith, P.E.M., Archer, H., Hryniewiecka-Jaworska, A., Kerr, M., 2011. Epilepsy in Rett syndrome: Association between phenotype and genotype, and implications for practice. Seizure 20, 646–649. doi:10.1016/j.seizure.2011.06.010

Carrasco, M.M., Razak, K. a, Pallas, S.L., 2005. Visual experience is necessary for maintenance but not development of receptive fields in superior colliculus. J. Neurophysiol. 94, 1962–1970. doi:10.1152/jn.00166.2005

Chahrour, M., Jung, S.Y., Shaw, C., Zhou, X., Wong, S.T.C., Qin, J., Zoghbi, H.Y., 2008. MeCP2, a key contributor to neurological disease, activates and represses transcription. Science (80-.). 320, 1224–1229.

Chahrour, M., Zoghbi, H.Y., 2007. The story of Rett syndrome: from clinic to neurobiology. Neuron 56, 422–437.

Chao, H.-T., Chen, H., Samaco, R.C., Xue, M., Chahrour, M., Yoo, J., Neul, J.L., Gong, S., Lu, H.-C., Heintz, N., Ekker, M., Rubenstein, J.L.R., Noebels, J.L., Rosenmund, C., Zoghbi, H.Y., 2010. Dysfunction in GABA signalling mediates autism-like stereotypies and Rett syndrome phenotypes. Nature 468, 263–269.

Chao, H.-T., Zoghbi, H.Y., 2012. MeCP2: only 100% will do. Nat. Neurosci. 15, 176–177. doi:10.1038/nn.3027

Chao, H.-T., Zoghbi, H.Y., Rosenmund, C., 2007. MeCP2 controls excitatory synaptic strength by regulating glutamatergic synapse number. Neuron 56, 58–65.

Chen, B.-S., Roche, K., 2007. Regulation of NMDA Receptors by Phosphorylation. Neuropharmacology 53, 362–368.

Chen, C., Regehr, W.G., 2000. Developmental remodeling of the retinogeniculate synapse. Neuron 28, 955–966. doi:10.1016/S0896-6273(00)00166-5

Chen, J., Yu, S., Fu, Y., Li, X., 2014. Synaptic proteins and receptors defects in autism spectrum disorders. Front. Cell. Neurosci. 8, 276. doi:10.3389/fncel.2014.00276

Chen, L., Chen, K., Lavery, L.A., Baker, S.A., Shaw, C.A., Li, W., Zoghbi, H.Y., 2015. MeCP2 binds to non-CG methylated DNA as neurons mature, influencing transcription and the timing of onset for Rett syndrome. Proc. Natl. Acad. Sci. 112, 201505909. doi:10.1073/pnas.1505909112

Cheng, T.L., Wang, Z., Liao, Q., Zhu, Y., Zhou, W.H., Xu, W., Qiu, Z., 2014. MeCP2 Suppresses Nuclear MicroRNA Processing and Dendritic Growth by Regulating the DGCR8/Drosha Complex. Dev. Cell 28, 547–560. doi:10.1016/j.devcel.2014.01.032

Cheval, H., Guy, J., Merusi, C., De Sousa, D., Selfridge, J., Bird, A., 2012. Postnatal inactivation reveals enhanced requirement for MeCP2 at distinct age windows. Hum. Mol. Genet. 21, 3806–3814. doi:10.1093/hmg/dds208

Cho, K.K.A., Khibnik, L., Philpot, B.D., Bear, M.F., 2009. The ratio of NR2A/B NMDA receptor subunits determines the qualities of ocular dominance plasticity in visual cortex. Proc. Natl. Acad. Sci. U. S. A. 106, 5377–5382.

Clements, J. a, Nimmo, W.S., Grant, I.S., 1982. Bioavailability, pharmacokinetics, and analgesic activity of ketamine in humans. J. Pharm. Sci. 71, 539–542. doi:10.1002/jps.2600710516

Coppus, A.M.W., 2013. People with intellectual disability: What do we know about adulthood and life expectancy? Dev. Disabil. Res. Rev. doi:10.1002/ddrr.1123

Crair, M.C., Gillespie, D.C., Stryker, M.P., 1998. The role of visual experience in the development of columns in cat visual cortex. Science (80-.). 279, 566–570. doi:10.1126/science.279.5350.566

Cruikshank, S.J., Lewis, T.J., Connors, B.W., 2007. Synaptic basis for intense thalamocortical activation of feedforward inhibitory cells in neocortex. Nat. Neurosci. 10, 462–8. doi:10.1038/nn1861

Cruz-Martín, A., El-Danaf, R.N., Osakada, F., Sriram, B., Dhande, O.S., Nguyen, P.L., Callaway, E.M., Ghosh, A., Huberman, A.D., 2014. A dedicated circuit links direction-selective retinal ganglion cells to the primary visual cortex. Nature 507, 358–61. doi:10.1038/nature12989

Dani, V.S., Nelson, S.B., 2009. Intact long-term potentiation but reduced connectivity between neocortical layer 5 pyramidal neurons in a mouse model of Rett syndrome. J. Neurosci. 29, 11263–70. doi:10.1523/JNEUROSCI.1019-09.2009

de Sousa Abreu, R., Penalva, L.O., Marcotte, E.M., Vogel, C., 2009. Global signatures of protein and mRNA expression levels. Mol. Biosyst. 5, 1512–1526. doi:10.1039/b908315d

Deaton, A.M., Bird, A., 2011. CpG islands and the regulation of transcription. Genes Dev. 25, 1010–22. doi:10.1101/gad.2037511

DeFelipe, J., Hendry, S.H., Jones, E.G., 1989. Visualization of chandelier cell axons by parvalbumin immunoreactivity in monkey cerebral cortex. Proc. Natl. Acad. Sci. U. S. A. 86, 2093–2097. doi:10.1073/pnas.86.6.2093

Dinstein, I., Heeger, D.J., Lorenzi, L., Minshew, N.J., Malach, R., Behrmann, M., 2012. Unreliable evoked responses in autism. Neuron 75, 981–91. doi:10.1016/j.neuron.2012.07.026

Du, F., Mandel, G., Nigam, A., Ballas, N., Shan, X., Felice, C.A., Nguyen, M.V.C., Robinson, J.K., 2012. MeCP2 Is Critical for Maintaining Mature Neuronal Networks and Global Brain Anatomy during Late Stages of Postnatal Brain Development and in the Mature Adult Brain. J. Neurosci. doi:10.1523/JNEUROSCI.1316-12.2012

Dumas, T.C., 2005. Developmental regulation of cognitive abilities: modified composition of a molecular switch turns on associative learning. Prog. Neurobiol. 76, 189–211.

Durand, S., Patrizi, A., Quast, K.B., Hachigian, L., Pavlyuk, R., Saxena, A., Carninci, P., Hensch, T.K., Fagiolini, M., 2012. NMDA Receptor Regulation Prevents Regression of Visual Cortical Function in the Absence of Mecp2. Neuron 76, 1078–1090. doi:10.1016/j.neuron.2012.12.004

Ebert, D.H., Gabel, H.W., Robinson, N.D., Kastan, N.R., Hu, L.S., Cohen, S., Navarro, A.J., Lyst, M.J., Ekiert, R., Bird, A.P., Greenberg, M.E., 2013. Activity-dependent phosphorylation of MeCP2 threonine 308 regulates interaction with NCoR. Nature 499, 341–5. doi:10.1038/nature12348

Espinosa, J.S., Stryker, M.P., 2012. Development and Plasticity of the Primary Visual Cortex. Neuron 75, 230–249. doi:10.1016/j.neuron.2012.06.009

Fagiolini, M., Hensch, T.K., 2000. Inhibitory threshold for critical-period activation in primary visual cortex. Nature 404, 183–186. doi:10.1038/35004582

Fagiolini, M., Katagiri, H., Miyamoto, H., Mori, H., Grant, S.G.N., Mishina, M., Hensch, T.K., 2003. Separable features of visual cortical plasticity revealed by N-methyl-D-aspartate receptor 2A signaling. Proc. Natl. Acad. Sci. U. S. A. 100, 2854–9. doi:10.1073/pnas.0536089100

Fagiolini, M., Pizzorusso, T., Berardi, N., Domenici, L., Maffei, L., 1994. Functional postnatal development of the rat primary visual cortex and the role of visual experience: Dark rearing and monocular deprivation. Vision Res. 34, 709–720. doi:10.1016/0042-6989(94)90210-0

Feldheim, D.A., O'Leary, D.D.M., 2010. Visual map development: bidirectional signaling, bifunctional guidance molecules, and competition. Cold Spring Harb. Perspect. Biol. doi:10.1101/cshperspect.a001768

Fish, K.N., Hoftman, G.D., Sheikh, W., Kitchens, M., Lewis, D.A., 2013. Parvalbumin-containing chandelier and basket cell boutons have distinctive modes of maturation in monkey prefrontal cortex. J Neurosci 33, 8352–8358. doi:10.1523/jneurosci.0306-13.2013

Gabel, H.W., Kinde, B., Stroud, H., Gilbert, C.S., Harmin, D.A., Kastan, N.R., Hemberg, M., Ebert, D.H., Greenberg, M.E., 2015. Disruption of DNA-methylation-dependent long gene repression in Rett syndrome. Nature 522, 89–93. doi:10.1038/nature14319

Gadalla, K.K.E., Bailey, M.E.S., Spike, R.C., Ross, P.D., Woodard, K.T., Kalburgi, S.N., Bachaboina, L., Deng, J. V, West, A.E., Samulski, R.J., Gray, S.J., Cobb, S.R., 2013. Improved survival and reduced phenotypic severity following AAV9/MECP2 gene transfer to neonatal and juvenile male Mecp2 knockout mice. Mol. Ther. 21, 18–30. doi:10.1038/mt.2012.200

Galarreta, M., Hestrin, S., 2002. Electrical and chemical synapses among parvalbumin fast-spiking GABAergic interneurons in adult mouse neocortex. Proc. Natl. Acad. Sci. U. S. A. 99, 12438–43. doi:10.1073/pnas.192159599

Gao, E., DeAngelis, G.C., Burkhalter, A., 2010. Parallel Input Channels to Mouse Primary Visual Cortex. J. Neurosci. 30, 5912–5926. doi:10.1523/JNEUROSCI.6456-09.2010

Garg, S.K., Lioy, D.T., Cheval, H., McGann, J.C., Bissonnette, J.M., Murtha, M.J., Foust, K.D., Kaspar, B.K., Bird, A., Mandel, G., 2013. Systemic Delivery of MeCP2 Rescues Behavioral and Cellular Deficits in Female Mouse Models of Rett Syndrome. J. Neurosci. 33, 13612–13620. doi:10.1523/JNEUROSCI.1854-13.2013

Gerber, S.A., Rush, J., Stemman, O., Kirschner, M.W., Gygi, S.P., 2003. Absolute quantification of proteins and phosphoproteins from cell lysates by tandem MS. Proc. Natl. Acad. Sci. U. S. A. 100, 6940–6945.

Gibson, J.H., Slobedman, B., K N, H., Williamson, S.L., Minchenko, D., El-Osta, A., Stern, J.L., Christodoulou, J., 2010. Downstream targets of methyl CpG binding protein 2 and their abnormal expression in the frontal cortex of the human Rett syndrome brain. BMC Neurosci. 11, 53. doi:10.1186/1471-2202-11-53

Godement, P., Salaün, J., Imbert, M., 1984. Prenatal and postnatal development of retinogeniculate and retinocollicular projections in the mouse. J. Comp. Neurol. 230, 552–575. doi:10.1002/cne.902300406

Goffin, D., Allen, M., Zhang, L., Amorim, M., Wang, I.-T.J., Reyes, A.-R.S., Mercado-Berton, A., Ong, C., Cohen, S., Hu, L., Blendy, J.A., Carlson, G.C., Siegel, S.J., Greenberg, M.E., Zhou, Z., 2011. Rett syndrome mutation MeCP2 T158A disrupts DNA binding, protein stability and ERP responses. Nat. Neurosci. 15, 274–283. doi:10.1038/nn.2997

Goffin, D., Brodkin, E.S., Blendy, J.A., Siegel, S.J., Zhou, Z., 2014. Cellular origins of auditory event-related potential deficits in Rett syndrome. Nat. Neurosci.

Gonzalez-Burgos, G., Lewis, D.A., 2008. GABA neurons and the mechanisms of network oscillations: Implications for understanding cortical dysfunction in schizophrenia. Schizophr. Bull. doi:10.1093/schbul/sbn070

Gordon, J.A., Stryker, M.P., 1996. Experience-dependent plasticity of binocular responses in the primary visual cortex of the mouse. J Neurosci 16, 3274–3286.

Griffen, T.C., Wang, L., Fontanini, A., Maffei, A., 2012. Developmental regulation of spatio-temporal patterns of cortical circuit activation. Front. Cell. Neurosci. 6, 65. doi:10.3389/fncel.2012.00065

Guy, J., Gan, J., Selfridge, J., Cobb, S., Bird, A., 2007. Reversal of neurological defects in a mouse model of Rett syndrome. Science 315, 1143–1147. doi:10.1126/science.1138389

Guy, J., Hendrich, B., Holmes, M., Martin, J.E., Bird, a, 2001. A mouse Mecp2-null mutation causes neurological symptoms that mimic Rett syndrome. Nat. Genet. 27, 322–6. doi:10.1038/85899

Hagberg, B., 2005. Rett Syndrome: Long-Term Clinical Follow-Up Experiences Over Four Decades. J. Child Neurol. 20, 722–727. doi:10.1177/08830738050200090401

Hagberg, B., Aicardi, J., Dias, K., Ramos, O., 1983. A progressive syndrome of autism, dementia, ataxia, and loss of purposeful hand use in girls: Rett's syndrome: report of 35 cases. Ann. Neurol. 14, 471–479. doi:10.1097/00001577-198901020-00018

Hayashi, S., McMahon, A.P., 2002. Efficient recombination in diverse tissues by a tamoxifen-inducible form of Cre: a tool for temporally regulated gene activation/inactivation in the mouse. Dev. Biol. 244, 305–318. doi:10.1006/dbio.2002.0597

Hensch, T.K., 2005a. Critical period mechanisms in developing visual cortex. Curr. Top. Dev. Biol. 69, 215–237.

Hensch, T.K., 2005b. Critical period plasticity in local cortical circuits. Nat. Rev. Neurosci. 6, 877–88. doi:10.1038/nrn1787

Hensch, T.K., 2004. Critical period regulation. Annu. Rev. Neurosci. 27, 549–579. doi:10.1146/annurev.neuro.27.070203.144327

Hensch, T.K., Fagiolini, M., 2005. Excitatory-inhibitory balance and critical period plasticity in developing visual cortex. Prog. Brain Res. 147, 115–124.

Hippenmeyer, S., Vrieseling, E., Sigrist, M., Portmann, T., Laengle, C., Ladle, D.R., Arber, S., 2005. A developmental switch in the response of DRG neurons to ETS transcription factor signaling. PLoS Biol. 3, 0878–0890. doi:10.1371/journal.pbio.0030159

Hooks, B.M., Chen, C., 2008. Vision triggers an experience-dependent sensitive period at the retinogeniculate synapse. J Neurosci 28, 4807–4817. doi:10.1523/jneurosci.4667-07.2008

Hooks, B.M., Chen, C., 2007. Critical periods in the visual system: changing views for a model of experience-dependent plasticity. Neuron 56, 312–326. doi:10.1016/j.neuron.2007.10.003

Hooks, B.M., Chen, C., 2006. Distinct roles for spontaneous and visual activity in remodeling of the retinogeniculate synapse. Neuron 52, 281–291. doi:10.1016/j.neuron.2006.07.007

Huang, Z.J., 2009. Activity-dependent development of inhibitory synapses and innervation pattern: role of GABA signalling and beyond. J. Physiol. 587, 1881–8. doi:10.1113/jphysiol.2008.168211

Hubel, D.H., Wiesel, T.N., 1962. Receptive fields, binocular interaction and functional architecture in the cat's visual cortex. J. Physiol. 160, 106–154.2. doi:10.1523/JNEUROSCI.1991-09.2009

Huberman, A.D., Feller, M.B., Chapman, B., 2008. Mechanisms Underlying Development of Visual Maps and Receptive Fields. Annu. Rev. Neurosci. 31, 479–509. doi:10.1146/annurev.neuro.31.060407.125533

Huberman, A.D., Wei, W., Elstrott, J., Stafford, B.K., Feller, M.B., Barres, B.A., 2009. Genetic Identification of an On-Off Direction- Selective Retinal Ganglion Cell Subtype Reveals??a Layer-Specific Subcortical Map of Posterior Motion. Neuron 62, 327–334. doi:10.1016/j.neuron.2009.04.014

Ito-Ishida, A., Ure, K., Chen, H., Swann, J.W., Zoghbi, H.Y., 2015. Loss of MeCP2 in Parvalbumin-and Somatostatin-Expressing Neurons in Mice Leads to Distinct Rett Syndrome-like Phenotypes. Neuron 88, 651–658. doi:10.1016/j.neuron.2015.10.029

Jellinger, K., Armstrong, D., Oghbi, H.., Percy, A.K., 1988. Neuropathology of Rett syndrome. Acta Neuropathol. 142–158.

Jones, P.L., Veenstra, G.J., Wade, P. a, Vermaak, D., Kass, S.U., Landsberger, N., Strouboulis, J., Wolffe, a P., 1998. Methylated DNA and MeCP2 recruit histone deacetylase to repress transcription. Nat. Genet. 19, 187–191. doi:10.1038/561

Jordan, C., Li, H.H., Kwan, H.C., Francke, U., 2007. Cerebellar gene expression profiles of mouse models for Rett syndrome reveal novel MeCP2 targets. BMC Med. Genet. 8, 36. doi:10.1186/1471-2350-8-36

Kang, E., Durand, S., LeBlanc, J.J., Hensch, T.K., Chen, C., Fagiolini, M., 2013. Visual acuity development and plasticity in the absence of sensory experience. J. Neurosci. 33, 17789–96. doi:10.1523/JNEUROSCI.1500-13.2013

Katagiri, H., Fagiolini, M., Hensch, T.K., 2007. Optimization of Somatic Inhibition at Critical Period Onset in Mouse Visual Cortex. Neuron 53, 805–812. doi:10.1016/j.neuron.2007.02.026

Katz, D.M., Bird, A., Coenraads, M., Gray, S.J., Menon, D.U., Philpot, B.D., Tarquinio, D.C., 2016. Rett Syndrome: Crossing the Threshold to Clinical Translation. Trends Neurosci. doi:10.1016/j.tins.2015.12.008

Kepecs, A., Fishell, G., 2014. Interneuron cell types are fit to function. Nature 505, 318–326. doi:10.1038/nature12983

Kilstrup-Nielsen, C., Rusconi, L., La Montanara, P., Ciceri, D., Bergo, A., Bedogni, F., Landsberger, N., 2012. What we know and would like to know about CDKL5 and its involvement in epileptic encephalopathy. Neural Plast. doi:10.1155/2012/728267

Kim, M.J., Dunah, A.W., Wang, Y.T., Sheng, M., 2005. Differential roles of NR2A- and NR2B-containing NMDA receptors in Ras-ERK signaling and AMPA receptor trafficking. Neuron 46, 745–60. doi:10.1016/j.neuron.2005.04.031

Kinde, B., Gabel, H.W., Gilbert, C.S., Griffith, E.C., Greenberg, M.E., 2015. Reading the unique DNA methylation landscape of the brain: Non-CpG methylation, hydroxymethylation, and MeCP2. Proc. Natl. Acad. Sci. U. S. A. 112, 6800–6. doi:10.1073/pnas.1411269112

Knudsen, E.I., 2004. Sensitive periods in the development of the brain and behavior. J. Cogn. Neurosci. 16, 1412–1425. doi:10.1162/0898929042304796

Ko, H., Cossell, L., Baragli, C., Antolik, J., Clopath, C., Hofer, S.B., Mrsic-Flogel, T.D., 2013. The emergence of functional microcircuits in visual cortex. Nature 496, 96–100. doi:10.1038/nature12015

Kobayashi, Y., Hensch, T.K., 2013. Germline recombination by conditional gene targeting with Parvalbumin-Cre lines. Front. Neural Circuits 7, 168. doi:10.3389/fncir.2013.00168

Kondo, S., Ohki, K., 2015. Laminar differences in the orientation selectivity of geniculate afferents in mouse primary visual cortex. Nat. Neurosci. 1–6. doi:10.1038/nn.4215

Krishnan, K., Wang, B., Lu, J., Wang, L., Maffei, A., Cang, J., 2015. MeCP2 regulates the timing of critical period plasticity that shapes functional connectivity in primary visual cortex. Proc. Natl. Acad. Sci. U. S. A. 112, 4782–4791. doi:10.1073/pnas.1506499112

Kron, M., Howell, C.J., Adams, I.T., Ransbottom, M., Christian, D., Ogier, M., Katz, D.M., 2012. Brain Activity Mapping in Mecp2 Mutant Mice Reveals Functional Deficits in Forebrain Circuits, Including Key Nodes in the Default Mode Network, that are Reversed with Ketamine Treatment. J. Neurosci.

Lang, M., Wither, R.G., Colic, S., Wu, C., Monnier, P.P., Bardakjian, B.L., Zhang, L., Eubanks, J.H., 2014. Rescue of behavioral and EEG deficits in male and female Mecp2-deficient mice by delayed Mecp2 gene reactivation. Hum. Mol. Genet. 23, 303–318. doi:10.1093/hmg/ddt421

LeBlanc, J.J., DeGregorio, G., Centofante, E., Vogel-Farley, V.K., Barnes, K., Kaufmann, W.E., Fagiolini, M., Nelson, C.A., 2015. Visual evoked potentials detect cortical processing deficits in Rett syndrome. Ann. Neurol. n/a–n/a. doi:10.1002/ana.24513

Lee, S., Kim, W., Ham, B.-J., Chen, W., Bear, M.F., Yoon, B.-J., 2008. Activity-dependent NR2B expression is mediated by MeCP2-dependent epigenetic regulation. Biochem. Biophys. Res. Commun. 377, 930–934.

Lee, S.-H., Kwan, A.C., Zhang, S., Phoumthipphavong, V., Flannery, J.G., Masmanidis, S.C., Taniguchi, H., Huang, Z.J., Zhang, F., Boyden, E.S., Deisseroth, K., Dan, Y., 2012. Activation of specific interneurons improves V1 feature selectivity and visual perception. Nature 488, 379–83. doi:10.1038/nature11312

Leong, W.Y., Lim, Z.H., Korzh, V., Pietri, T., Goh, E.L.K., 2015. Methyl-CpG Binding Protein 2 (Mecp2) Regulates Sensory Function Through Sema5b and Robo2. Front. Cell. Neurosci. 9, 1–12. doi:10.3389/fncel.2015.00481

Lewis, J.D., Meehan, R.R., Henzel, W.J., Maurer-Fogy, I., Jeppesen, P., Klein, F., Bird, A., 1992. Purification, sequence, and cellular localization of a novel chromosomal protein that binds to methylated DNA. Cell 69, 905–14. doi:10.1016/0092-8674(92)90610-O

Li, Y., Van Hooser, S.D., Mazurek, M., White, L.E., Fitzpatrick, D., 2008. Experience with moving visual stimuli drives the early development of cortical direction selectivity. Nature 456, 952–956. doi:10.1038/nature07417

Liao, W., Gandal, M.J., Ehrlichman, R.S., Siegel, S.J., Carlson, G.C., 2012. MeCP2+/- mouse model of RTT reproduces auditory phenotypes associated with Rett syndrome and replicate select EEG endophenotypes of autism spectrum disorder. Neurobiol. Dis. 46, 88–92. doi:10.1016/j.nbd.2011.12.048

Lidierth, M., 2009. sigTOOL: A MATLAB-based environment for sharing laboratory-developed software to analyze biological signals. J. Neurosci. Methods 178, 188–196. doi:10.1016/j.jneumeth.2008.11.004

Lioy, D.T., Garg, S.K., Monaghan, C.E., Raber, J., Foust, K.D., Kaspar, B.K., Hirrlinger, P.G., Kirchhoff, F., Bissonnette, J.M., Ballas, N., Mandel, G., 2011. A role for glia in the progression of Rett's syndrome. Nature 475, 497–500. doi:10.1038/nature10214

Liu, B. hua, Li, Y. tang, Ma, W. pei, Pan, C. jie, Zhang, L.I., Tao, H.W., 2011. Broad inhibition sharpens orientation selectivity by expanding input dynamic range in mouse simple cells. Neuron 71, 542–554. doi:10.1016/j.neuron.2011.06.017

Lombardi, L.M., Baker, S.A., Zoghbi, H.Y., 2015. MECP2 disorders: From the clinic to mice and back. J. Clin. Invest. doi:10.1172/JCI78167

Lonetti, G., Angelucci, A., Morando, L., Boggio, E.M., Giustetto, M., Pizzorusso, T., 2010. Early Environmental Enrichment Moderates the Behavioral and Synaptic Phenotype of MeCP2 Null Mice. Biol. Psychiatry 67, 657–665. doi:10.1016/j.biopsych.2009.12.022

Lu, W., Shi, Y., Jackson, A.C., Bjorgan, K., During, M.J., Sprengel, R., Seeburg, P.H., Nicoll, R.A., 2009. Subunit Composition of Synaptic AMPA Receptors Revealed by a Single-Cell Genetic Approach. Neuron 62, 254–268. doi:10.1016/j.neuron.2009.02.027

Lyst, M.J., Bird, A., 2015. Rett syndrome: a complex disorder with simple roots. Nat. Rev. Genet. 16, 1–13. doi:10.1038/nrg3897

Lyst, M.J., Ekiert, R., Ebert, D.H., Merusi, C., Nowak, J., Selfridge, J., Guy, J., Kastan, N.R., Robinson, N.D., de Lima Alves, F., Rappsilber, J., Greenberg, M.E., Bird, A., 2013. Rett syndrome mutations abolish the interaction of MeCP2 with the NCoR/SMRT co-repressor. Nat. Neurosci. 16, 898–902. doi:10.1038/nn.3434

Madisen, L., Zwingman, T.A., Sunkin, S.M., Oh, S.W., Zariwala, H.A., Gu, H., Ng, L.L., Palmiter, R.D., Hawrylycz, M.J., Jones, A.R., Lein, E.S., Zeng, H., 2010. A robust and high-throughput Cre reporting and characterization system for the whole mouse brain. Nat. Neurosci. 13, 133–140.

Markram, H., Toledo-Rodriguez, M., Wang, Y., Gupta, A., Silberberg, G., Wu, C., 2004. Interneurons of the neocortical inhibitory system. Nat. Rev. Neurosci. 5, 793–807. doi:10.1038/nrn1519

McGraw, C.M., Samaco, R.C., Zoghbi, H.Y., 2011. Adult neural function requires MeCP2. Science (80-.). 333, 186.

Medrihan, L., Tantalaki, E., Aramuni, G., Sargsyan, V., Dudanova, I., Missler, M., Zhang, W., 2008. Early defects of GABAergic synapses in the brain stem of a MeCP2 mouse model of Rett syndrome. J. Neurophysiol. 99, 112–121. doi:10.1152/jn.00826.2007

Meehan, R.R., Lewis, J.D., Bird, a P., 1992. Characterization of MeCP2, a vertebrate DNA binding protein with affinity for methylated DNA. Nucleic Acids Res. 20, 5085–92. doi:10.1093/nar/20.19.5085

Mierau, S.B., Patrizi, A., Hensch, T.K., Fagiolini, M., 2014. Cell-Specific Regulation of N-Methyl-D-Aspartate Receptor Maturation by Mecp2 in Cortical Circuits. Biol. Psychiatry. doi:10.1016/j.biopsych.2015.05.018

Mitchell, D.E., Mackinnon, S., 2002. The present and potential impact of research on animal models for clinical treatment of stimulus deprivation amblyopia. Clin. Exp. Optom. doi:10.1111/j.1444-0938.2002.tb03067.x

Mount, R.H., Charman, T., Hastings, R.P., Reilly, S., Cass, H., 2002. The Rett Syndrome Behaviour Questionnaire (RSBQ): Refining the behavioural phenotype of Rett syndrome. J. Child Psychol. Psychiatry Allied Discip. 43, 1099–1110. doi:10.1111/1469-7610.00236

Muir-Robinson, G., Hwang, B.J., Feller, M.B., 2002. Retinogeniculate axons undergo eye-specific segregation in the absence of eye-specific layers. J. Neurosci. 22, 5259–5264. doi:20026563

Nan, X., Campoy, F.J., Bird, A., 1997. MeCP2 is a transcriptional repressor with abundant binding sites in genomic chromatin. Cell 88, 471–481. doi:10.1016/S0092-8674(00)81887-5

Nan, X., Ng, H.H., Johnson, C.A., Laherty, C.D., Turner, B.M., Eisenman, R.N., Bird, A., 1998. Transcriptional repression by the methyl-CpG-binding protein MeCP2 involves a histone deacetylase complex. Nature 393, 386–389. doi:10.1038/30764

Neul, J.L., Fang, P., Barrish, J., Lane, J., Caeg, E.B., Smith, E.O., Zoghbi, H., Percy, A., Glaze, D.G., 2008. Specific mutations in Methyl-CpG-Binding Protein 2 confer different severity in Rett syndrome. Neurology 70, 1313–1321. doi:10.1212/01.wnl.0000291011.54508.aa

Neul, J.L., Kaufmann, W.E., Glaze, D.G., Christodoulou, J., Clarke, A.J., Bahi-Buisson, N., Leonard, H., Bailey, M.E.S., Schanen, N.C., Zappella, M., Renieri, A., Huppke, P., Percy, A.K., 2010. Rett syndrome: Revised diagnostic criteria and nomenclature. Ann. Neurol. 68, 944–950. doi:10.1002/ana.22124

Neul, J.L., Zoghbi, H.Y., 2004. Rett syndrome: a prototypical neurodevelopmental disorder. Neuroscientist 10, 118–28. doi:10.1177/1073858403260995

Niell, C.M., 2015. Cell types, circuits, and receptive fields in the mouse visual cortex. Annu. Rev. Neurosci. 38, 413–431. doi:10.1146/annurev-neuro-071714-033807

Niell, C.M., Stryker, M.P., 2010. Modulation of Visual Responses by Behavioral State in Mouse Visual Cortex. Neuron 65, 472–479. doi:10.1016/j.neuron.2010.01.033

Niell, C.M., Stryker, M.P., 2008. Highly selective receptive fields in mouse visual cortex. J. Neurosci. 28, 7520–7536. doi:10.1523/JNEUROSCI.0623-08.2008

Nomura, Y., Segawa, M., 2005. Natural history of Rett syndrome. J. Child Neurol. 20, 764–768. doi:10.1177/08830738050200091201

Noutel, J., Hong, Y.K., Leu, B., Kang, E., Chen, C., 2011. Experience-dependent retinogeniculate synapse remodeling is abnormal in MeCP2-deficient mice. Neuron 70, 35–42. doi:10.1016/j.neuron.2011.03.001

Oomen, C.A., Hvoslef-Eide, M., Heath, C.J., Mar, A.C., Horner, A.E., Bussey, T.J., Saksida, L.M., 2013. The touchscreen operant platform for testing working memory and pattern separation in rats and mice. Nat. Protoc. 8, 2006–21. doi:10.1038/nprot.2013.124

Orduz, D., Bischop, D.P., Schwaller, B., Schiffmann, S.N., Gall, D., 2013. Parvalbumin tunes spike-timing and efferent short-term plasticity in striatal fast spiking interneurons. J. Physiol. 591, 3215–32. doi:10.1113/jphysiol.2012.250795

Orefice, L.L., Zimmerman, A.L., Chirila, A.M., Sleboda, S.J., Head, J.P., Ginty, D.D., Orefice, L.L., Zimmerman, A.L., Chirila, A.M., Sleboda, S.J., Head, J.P., Ginty, D.D., 2016. Peripheral Mechanosensory Neuron Dysfunction Underlies Tactile and Behavioral Deficits in Mouse Models of ASDs Article Peripheral Mechanosensory Neuron Dysfunction Underlies Tactile and Behavioral Deficits in Mouse Models of ASDs. Cell 1–15. doi:10.1016/j.cell.2016.05.033

Paoletti, P., 2011. Molecular basis of NMDA receptor functional diversity. Eur. J. Neurosci. 33, 1351–1365. doi:10.1111/j.1460-9568.2011.07628.x

Patrizi, A., Picard, N., Simon, A.J., Gunner, G., Centofante, E., Andrews, N.A., Fagiolini, M., 2015. Chronic Administration of the N-Methyl-D-Aspartate Receptor Antagonist Ketamine Improves Rett Syndrome Phenotype. Biol. Psychiatry. doi:10.1016/j.biopsych.2015.08.018

Penn, a a, Riquelme, P. a, Feller, M.B., Shatz, C.J., 1998. Competition in retinogeniculate patterning driven by spontaneous activity. Science 279, 2108–2112. doi:10.1126/science.279.5359.2108

Petralia, R.S., Al-Hallaq, R.A., Wenthold, R.J., 2009. Biology of the NMDA Receptor, 1st ed. CRC Press, Boca Raton.

Piscopo, D.M., El-Danaf, R.N., Huberman, A.D., Niell, C.M., 2013. Diverse visual features encoded in mouse lateral geniculate nucleus. J. Neurosci. 33, 4642–4656. doi:10.1523/JNEUROSCI.5187-12.2013.Diverse

Popescu, M. V., Polley, D.B., 2010. Monaural Deprivation Disrupts Development of Binaural Selectivity in Auditory Midbrain and Cortex. Neuron 65, 718–731. doi:10.1016/j.neuron.2010.02.019

Pozzo-Miller, L., Pati, S., Percy, A.K., 2015. Rett Syndrome: Reaching for Clinical Trials. Neurotherapeutics. doi:10.1007/s13311-015-0353-y

Prusky, G.T., Alam, N.M., Beekman, S., Douglas, R.M., 2004. Rapid quantification of adult and developing mouse spatial vision using a virtual optomotor system. Invest. Ophthalmol. Vis. Sci. 45, 4611–4616. doi:10.1167/iovs.04-0541

Prusky, G.T., Douglas, R.M., 2004. Characterization of mouse cortical spatial vision, in: Vision Research. pp. 3411–3418. doi:10.1016/j.visres.2004.09.001

Prusky, G.T., West, P.W.R., Douglas, R.M., 2000. Behavioral assessment of visual acuity in mice and rats. Vision Res. 40, 2201–2209. doi:10.1016/S0042-6989(00)00081-X

Prybylowski, K., Chang, K., Sans, N., Kan, L., Vicini, S., Wenthold, R.J., 2005. The synaptic localization of NR2B-containing NMDA receptors is controlled by interactions with PDZ proteins and AP-2. Neuron 47, 845–857.

Qiu, Z., Sylwestrak, E.L., Lieberman, D.N., Zhang, Y., Liu, X.-Y.X.-Y., Ghosh, A., Qiu, Z., Liu, X.-Y.X.-Y., Lieberman, D.N., Ghosh, A., 2012. The Rett Syndrome Protein MeCP2 Regulates Synaptic Scaling. J. Neurosci. 32, 989–994. doi:10.1523/JNEUROSCI.0175-11.2012

Quinlan, E.M., Philpot, B.D., Huganir, R.L., Bear, M.F., 1999. Rapid, experience-dependent expression of synaptic NMDA receptors in visual cortex in vivo. Nat. Neurosci. 2, 352–357. doi:10.1038/7263

Raveendran, R., Devi Suma Priya, S., Mayadevi, M., Steephan, M., Santhoshkumar, T.R., Cheriyan, J., Sanalkumar, R., Pradeep, K.K., James, J., Omkumar, R. V, 2009. Phosphorylation status of the NR2B subunit of NMDA receptor regulates its interaction with calcium/calmodulin-dependent protein kinase II. J. Neurochem. 110, 92–105.

Rial Verde, E.M., Lee-Osbourne, J., Worley, P., Malinow, R., Cline, H., 2006. Increased Expression of the Immediate-Early Gene Arc/Arg3.1 Reduces AMPA Receptor-Mediated Synaptic Transmission. Neuron 52, 461–474. doi:10.1016/j.neuron.2006.09.031

Robinson, L., Guy, J., McKay, L., Brockett, E., Spike, R.C., Selfridge, J., De Sousa, D., Merusi, C., Riedel, G., Bird, A., Cobb, S.R., 2012. Morphological and functional reversal of phenotypes in a mouse model of Rett syndrome. Brain 135, 2699–710. doi:10.1093/brain/aws096

Salter, M.W., Dong, Y., Kalia, L. V, Liu, X.J., Pitcher, G., 2009. Regulation of NMDA Receptors by Kinases and Phosphatases. Biol. NMDA Recept. 1–18. doi:NBK5288 [bookaccession]

Sanz-Clemente, A., Gray, J.A., Ogilvie, K.A., Nicoll, R.A., Roche, K.W., 2013. Activated CaMKII Couples GluN2B and Casein Kinase 2 to Control Synaptic NMDA Receptors. Cell Rep. 3, 607–614. doi:10.1016/j.celrep.2013.02.011

Sanz-Clemente, A., Matta, J. a, Isaac, J.T.R., Roche, K.W., 2010. Casein kinase 2 regulates the NR2 subunit composition of synaptic NMDA receptors. Neuron 67, 984–96. doi:10.1016/j.neuron.2010.08.011

Schwaller, B., Meyer, M., Schiffmann, S., 2002. "New" functions for "old" proteins: the role of the calcium-binding proteins calbindin D-28k, calretinin and parvalbumin, in cerebellar physiology. Studies with knockout mice. Cerebellum 1, 241–258. doi:10.1080/147342202320883551

Shepherd, G.M.G., Katz, D.M., 2011. Synaptic microcircuit dysfunction in genetic models of neurodevelopmental disorders: Focus on Mecp2 and Met. Curr. Opin. Neurobiol. doi:10.1016/j.conb.2011.06.006

Shepherd, J.D., Rumbaugh, G., Wu, J., Chowdhury, S., Plath, N., Kuhl, D., Huganir, R.L., Worley, P.F., 2006. Arc/Arg3.1 Mediates Homeostatic Synaptic Scaling of AMPA Receptors. Neuron 52, 475–484. doi:10.1016/j.neuron.2006.08.034

Shi, S.H., Hayashi, Y., Esteban, J.A., Malinow, R., 2001. Subunit-specific rules governing AMPA receptor trafficking to synapses in hippocampal pyramidal neurons. Cell 105, 331–343. doi:10.1016/S0092-8674(01)00321-X

Skene, P.J., Illingworth, R.S., Webb, S., Kerr, A.R.W., James, K.D., Turner, D.J., Andrews, R., Bird, A.P., 2010. Neuronal MeCP2 Is Expressed at Near Histone-Octamer Levels and Globally Alters the Chromatin State. Mol. Cell 37, 457–468. doi:10.1016/j.molcel.2010.01.030

Sleigh, J., Harvey, M., Voss, L., Denny, B., 2014. Ketamine - more mechanisms of action than just NMDA blockade. Trends Anaesth. Crit. Care. doi:10.1016/j.tacc.2014.03.002

Somogyi, P., Tamás, G., Lujan, R., Buhl, E.H., 1998. Salient features of synaptic organisation in the cerebral cortex1Published on the World Wide Web on 3 March 1998.1. Brain Res. Rev. 26, 113–135. doi:10.1016/S0165-0173(97)00061-1

Steen, H., Jebanathirajah, J.A., Springer, M., Kirschner, M.W., 2005. Stable isotope-free relative and absolute quantitation of protein phosphorylation stoichiometry by MS. Proc. Natl. Acad. Sci. U. S. A. 102, 3948–3953.

Su, D., Cha, Y.M., West, A.E., 2012. Mutation of Mecp2 alters transcriptional regulation of select immediate-early genes. Epigenetics 7, 146–154. doi:10.4161/epi.7.2.18907

Subramaniam, B., Naidu, S., Reiss, A.L., 1997. Neuroanatomy in Rett syndrome: cerebral cortex and posterior fossa. Neurology 48, 399–407. doi:10.1212/WNL.48.2.399

Sugino, K., Hempel, C.M., Okaty, B.W., Arnson, H.A., Kato, S., Dani, V.S., Nelson, S.B., 2014. Cell-type-specific repression by methyl-CpG-binding protein 2 is biased toward long genes. J. Neurosci. 34, 12877–12883. doi:10.1523/JNEUROSCI.2674-14.2014

Tarquinio, D.C., Hou, W., Neul, J.L., Kaufmann, W.E., Glaze, D.G., Motil, K.J., Skinner, S.A., Lee, H.S., Percy, A.K., 2015. The Changing Face of Survival in Rett Syndrome and MECP2-Related Disorders. Pediatr. Neurol. 53, 402–411. doi:10.1016/j.pediatrneurol.2015.06.003

Thompson, A., Picard, N., Min, L., Fagiolini, F., Chen, C., 2016. Cortical Feedback Regulates Feedforward Retinogeniculate Refinement. Neuron 91, 1–13. doi:10.1016/j.neuron.2016.07.040

Tomassy GS, Morello N, Calcagno E, G.M., 2014. Developmental Abnormalities Of Cortical Interneurons Precede Symptoms Onset In A Mouse Model Of Rett Syndrome. J Neurochem.

Torborg, C.L., Feller, M.B., 2004. Unbiased analysis of bulk axonal segregation patterns. J. Neurosci. Methods 135, 17–26. doi:10.1016/j.jneumeth.2003.11.019

Tropea, D., Giacometti, E., Wilson, N.R., Beard, C., McCurry, C., Fu, D.D., Flannery, R., Jaenisch, R., Sur, M., 2009. Partial reversal of Rett Syndrome-like symptoms in MeCP2 mutant mice. Proc. Natl. Acad. Sci. U. S. A. 106, 2029–2034. doi:10.1073/pnas.0812394106

Urdinguio, R.G., Lopez-Serra, L., Lopez-Nieva, P., Alaminos, M., Diaz-Uriarte, R., Fernandez, A.F., Esteller, M., 2008. Mecp2-null mice provide new neuronal targets for rett syndrome. PLoS One 3. doi:10.1371/journal.pone.0003669

Vanhoutte, P., Bading, H., 2003. Opposing roles of synaptic and extrasynaptic NMDA receptors in neuronal calcium signalling and BDNF gene regulation. Curr. Opin. Neurobiol. 13, 366–371. doi:10.1016/S0959-4388(03)00073-4

Vicini, S., Wang, J.F., Li, J.H., Zhu, W.J., Wang, Y.H., Luo, J.H., Wolfe, B.B., Grayson, D.R., 1998. Functional and pharmacological differences between recombinant N-methyl-D-aspartate receptors. J. Neurophysiol. 79, 555–566.

Wan, M., Lee, S.S., Zhang, X., Houwink-Manville, I., Song, H.R., Amir, R.E., Budden, S., Naidu, S., Pereira, J.L., Lo, I.F., Zoghbi, H.Y., Schanen, N.C., Francke, U., 1999. Rett syndrome and beyond: recurrent spontaneous and familial MECP2 mutations at CpG hotspots. Am. J. Hum. Genet. 65, 1520–9. doi:10.1086/302690

Wang, B.S., Sarnaik, R., Cang, J., 2010. Critical Period Plasticity Matches Binocular Orientation Preference in the Visual Cortex. Neuron 65, 246–256. doi:10.1016/j.neuron.2010.01.002

Wang, Y., Dye, C.A., Sohal, V., Long, J.E., Estrada, R.C., Roztocil, T., Lufkin, T., Deisseroth, K., Baraban, S.C., Rubenstein, J.L.R., 2010. Dlx5 and Dlx6 regulate the development of parvalbumin-expressing cortical interneurons. J. Neurosci. 30, 5334–5345. doi:10.1523/JNEUROSCI.5963-09.2010

Wekselblatt, J.B., Flister, E.D., Piscopo, D.M., Niell, C.M., 2016. Large-scale imaging of cortical dynamics during sensory perception and behavior. J. Neurophysiol. jn.01056.2015. doi:10.1152/jn.01056.2015

Winterer, G., Ziller, M., Dorn, H., Frick, K., Mulert, C., Wuebben, Y., Herrmann, W.M., Coppola, R., 2000. Schizophrenia: Reduced signal-to-noise ratio and impaired phase-locking during information processing. Clin. Neurophysiol. 111, 837–849. doi:10.1016/S1388-2457(99)00322-3

Wu, H.Y., Hsu, F.C., Gleichman, A.J., Baconguis, I., Coulter, D.A., Lynch, D.R., 2007. Fyn-mediated phosphorylation of NR2B Tyr-1336 controls calpain-mediated NR2B cleavage in neurons and heterologous systems. J. Biol. Chem. 282, 20075–20087. doi:10.1074/jbc.M700624200

Yang, C., Shirayama, Y., Zhang, J., Ren, Q., Yao, W., Ma, M., Dong, C., Hashimoto, K., 2015. R-ketamine: a rapid-onset and sustained antidepressant without psychotomimetic side effects. Transl. Psychiatry 5, e632. doi:10.1038/tp.2015.136

Yoshida, T., Ozawa, K., Tanaka, S., 2012. Sensitivity profile for orientation selectivity in the visual cortex of goggle-reared mice. PLoS One 7. doi:10.1371/journal.pone.0040630

Young, J.I., Hong, E.P., Castle, J.C., Crespo-Barreto, J., Bowman, A.B., Rose, M.F., Kang, D., Richman, R., Johnson, J.M., Berget, S., Zoghbi, H.Y., 2005. Regulation of RNA splicing by the methylation-dependent transcriptional repressor methyl-CpG binding protein 2. Proc. Natl. Acad. Sci. U. S. A. 102, 17551–8. doi:10.1073/pnas.0507856102

Zhao, X., Chen, H., Liu, X., Cang, J., 2013. Orientation-selective responses in the mouse lateral geniculate nucleus. J. Neurosci. 33, 12751–12763. doi:10.1523/JNEUROSCI.0095-13.2013

Zhao, Y.-T., Goffin, D., Johnson, B.S., Zhou, Z., 2013. Loss of MeCP2 function is associated with distinct gene expression changes in the striatum. Neurobiol. Dis. 59, 257–266. doi:10.1016/j.nbd.2013.08.001

Zhong, X., Li, H., Chang, Q., 2012. MeCP2 Phosphorylation Is Required for Modulating Synaptic Scaling through mGluR5. J. Neurosci. doi:10.1523/JNEUROSCI.2784-12.2012